Direct geomechanical inversion from geodetic data

A new method for a regularised direct inversion to geomechanical parameters using measurements from optical leveling campaigns

R.E. Broeksma

Technische Universiteit Delft

TU Delft

Direct geomechanical inversion from geodetic data

A new method for a regularised direct inversion to geomechanical parameters using measurements from optical leveling campaigns

by

R.E. Broeksma

to obtain the degree of Master of Science
at the Delft University of Technology,
to be defended publicly on Monday March 30th, 2020 at 9:30 AM.

Student number:	4238516	
Project duration:	May 2, 2019 – March 30, 2020	
Thesis committee:	Prof. Dr. Ir. R.F. Hanssen,	TU Delft, supervisor
	Dr. Ir. F.J. van Leijen,	TU Delft
	Dr. Ir. F.C. Vossepoel,	TU Delft

TU Delft

Abstract

Subsidence of the ground surface, caused by hydrocarbon production, compaction of soft ground layers or other subsidence causes, is a timely topic in the Netherlands. Geodetic measurements of the surface can help us improve our knowledge of the subsurface; this process is called geomechanical inversion. Improved knowledge on the subsurface is needed for example to improve deformation predictions and to safeguard subsurface and surface infrastructure.

Related works in this domain use derivatives of geodetic measurements as input for their inversion methodologies, but not the measurements themselves. Performing geomechanical inversion with derivatives of geodetic measurements introduces correlations in the covariance matrix of the data, making error propagation into the geomechanical estimates more complex. Defining a direct relationship between measurements and geomechanical estimates and subsequently inverting this relationship, makes the error propagation less complex. This thesis presents a new methodology that can be used to estimate reservoir geomechanical parameters through direct inversion using measurements from optical leveling campaigns. In the context of this thesis, a direct inversion is an inversion of a linear relationship between data and measurements.

In this thesis, we propose and test a workflow for the estimation of a simplified set of geomechanical parameters. Part of the workflow is an extensive testing procedure of the geodetic data. A Geertsma nucleus-of-strain model is used to express a source parameter term in function of optical leveling measurements. This source parameter term is a lumped term and consists of a volume term, a pressure term, and several elastic rock parameter terms. This system is inverted using a Tikhonov regularization with a spatial penalty term. The methodology is applied to optical leveling data from a case study (the Norg and Roden gas fields in the northern Netherlands) and shows promising results. The RMS between modeled and measured subsidence for the most promising parameterization is 3.0 mm.

The proposed methodology leads to geomechanical estimates with formal quality description, that could improve geomechanical models and subsequently leads to a better understanding of the subsurface and better subsidence predictions. The geomechanical parameter that is estimated is lumped and without additional information, it is impossible to differentiate between individual compaction parameter terms. Feeding the problem more information might also relax the need for regularization but can lead to the introduction of bias. We believe that the framework proposed in this work can be a good starting point for further research that uses geodetic measurements directly as input for a geomechanical inversion.

Acknowledgements

I would like to thank the Royal Dutch Shell for allowing me to conduct this research under their guidance. Especially I want to thank my two mentors at Shell: Raoul Quadvlieg and Kees Hindriks. They offered me daily guidance and answered all my questions regarding respective geodesic and geomechanical related topics.

I would also like to thank Gini Ketelaar and Hermann Baehr from the geomatics department at the NAM for providing me with a leveling dataset and the software tools for processing of the dataset. Gini and Hermann have been kind enough to receive me at the NAM in Assen and spend a day explaining the data and software tools needed for this research. Also at later moments during my research, they have taken the time to help me with all the questions I had.

Last but not least I would like to thank my supervisors at the TU Delft: Ramon Hanssen, Freek van Leijen and Femke Vossepoel, for the discussions, their reviews, and support during the writing of this thesis.

R.E. Broeksma
Delft, March 2020

Contents

List of Figures

1 Introduction

1.1. Motivation and background

The aim of this research is to assess whether optical leveling measurements can be used to optimally derive information about geomechanical subsurface processes with a direct geomechanical inversion. The main advantage of this method is that the errors of the geodetic measurements can be directly propagated into the geomechanical parameter estimates. The focus of the research is on surface deformation induced by hydrocarbon production. Hydrocarbon production decreases pore pressures in the subsurface, changing the subsurface stress fields. This leads to reservoir compaction, which is subsequently imprinted as subsidence at the surface. Geodetic survey campaigns, such as optical leveling campaigns, are organized to estimate the amount of subsidence. Geodetic estimates can subsequently be used to estimate geomechanical parameters of the subsurface; this process is called inverse geomechanical modeling [70].

Monitoring surface deformation is important to safeguard infrastructure and building integrity and to assess the land's height with respect to the sea level. Additionally, estimates of surface deformation are used to evaluate the predictions of expected deformation patterns. If the estimated deformation is different than expected, it may lead to new insights of knowledge on the subsurface and may lead to mitigating measures in e.g. hydrocarbon production schemes.

Subsidence, heave and lateral movements of the ground are all forms of surface deformation. Surface deformation typically takes place at all scales and can be caused by natural and human factors, other than hydrocarbon extraction. Recent examples of deformation processes in the Netherlands include peat compaction in the Rhine-Meuse Delta [69], local ground displacements due to a subway construction in Amsterdam (North-South subway line) [30], a migrating cavity leading to foundation failure under a shopping mall in Heerlen in 2011 [10] and subsidence due to gas extraction in the Groningen area [75] and the Wadden Sea [18].

To get insight into surface deformation, the surface can be monitored with various geodetic measurement techniques, such as optical leveling, GPS and InSAR. These measuring techniques reflect height differences at specified moments over time. The main aim of geodetic measurement campaigns is to use the estimated spatial height differences to derive surface deformations over time. After survey campaigns are organized, iterative hypothesis testing is applied to a functional model and the resulting deformation estimations are expressed in either grid or at measurement point level.

To predict the amount of subsidence, geomechanical models are used [15]. These models predict the response of the subsurface to changes, e.g. to changes in the pressure distribution due to hydrocarbon production. The changes in the subsurface, such as volume compaction, can subsequently be translated to deformation at the surface. Subsurface properties and production data are typically taken as input and subsequently, the subsidence is predicted that results due to the hydrocarbon production or liquid injection in the subsurface. To validate the predictions of the geomechanical models, often surface deformation data is used. Inverse geomechanical modeling reverses this process: estimates of deformation at the surface are used to estimate geomechanical subsurface properties.

For inverse geomechanical modeling, surface deformation data is thus used to estimate parameters of the geomechanical models. In this process, the geodetic data is used as input for inverse geomechanical modeling. Inverse theory tries to estimate model parameters from physical measurements [3]. This thesis uses linear inverse theory to estimate subsurface parameters directly from measurements of surface displacement. The so-called forward model consists of a geomechanical model, that evaluates surface deformation in function of subsurface parameters, such as subsurface volume compaction coefficients. The subsurface parameters are then estimated by inverting the forward model, using the geodetic deformation data as input. With inverse modeling, the uncertainty of the geodetic measurements propagates into the estimated geomechanical parameters, resulting in the estimated geomechanical parameters carrying an uncertainty. If decisions are to be made based on these estimated parameters (e.g. decisions about the development plan of a gas field or the integrity of infrastructure), it is important to be aware of how large this uncertainty is. Therefore, a formal and correct description of the errors should be given after geomechanical inversion. The flow diagram in Figure 1.1 visualizes a workflow currently often used in geomechanical inversion. The main disadvantage of this workflow is the need for formal error propagation during all steps. The uncertainty structure of raw leveling measurements is relatively simple, but after the geodetic inversion to subsidence estimates, correlations are introduced. These correlations make the error propagation during the geomechanical inversion more complex.

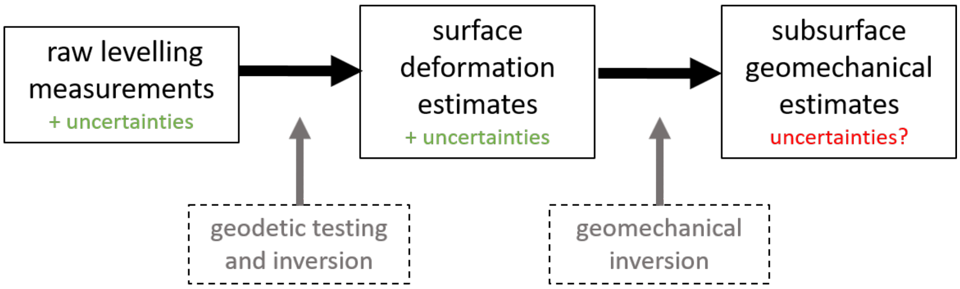

Figure 1.1: Currently often applied workflow for geomechanical inversion. First, geodetic measurements are tested and then used to estimate deformation, with a geodetic inversion method. Error propagation during this step is usually done properly, often leading to full covariance matrix. The deformation estimates are in the next step used as input for a geomechanical inversion. Error propagation in this step is often omitted or carried out incorrectly.

The goal of this thesis is to develop a new method that uses geodetic optical leveling data directly to estimate geomechanical parameters, and thereby to provide a formal and correct description of the error propagation for this geomechanical inversion. To achieve that goal, a new workflow is proposed that includes a geodetic testing procedure and a regularised inversion. To demonstrate the capabilities of the new workflow, the methodology will be applied to a case study.

The case study focuses on surface deformation caused by two gas fields, one near Norg and one near Roden (both in the Netherlands), an area that has shown surface deformation over the past 30+ years. The location of both gas fields is indicated on the map in Figure 1.3. The gas production leads to pressure decline in the subsurface, which caused subsidence. A timeline for both fields can be found in Figure 1.2. The Norg gas field was discovered in 1965 and produced from 1983 until 1995. The nearby Roden gas field was discovered in 1970, production started in 1976 and ended in 2003. The Roden field is currently abandoned. The Norg gas field is since 1997 a gas storage location [48]. This means that each year gas is injected in the summer period, this gas is produced during colder months. The NAM has been (and is) closely monitoring the amount of subsidence at these fields and therefore a large optical leveling dataset of these fields is available. This research focuses on data measured between 1975 and 1993, which is the period before the gas storage at the Norg location began. In 2000 the NAM wrote a report in which the estimated in 1997 was estimated to be 10 cm since 1975, at the deepest point of the subsidence bowl [44], see Figure 1.4.

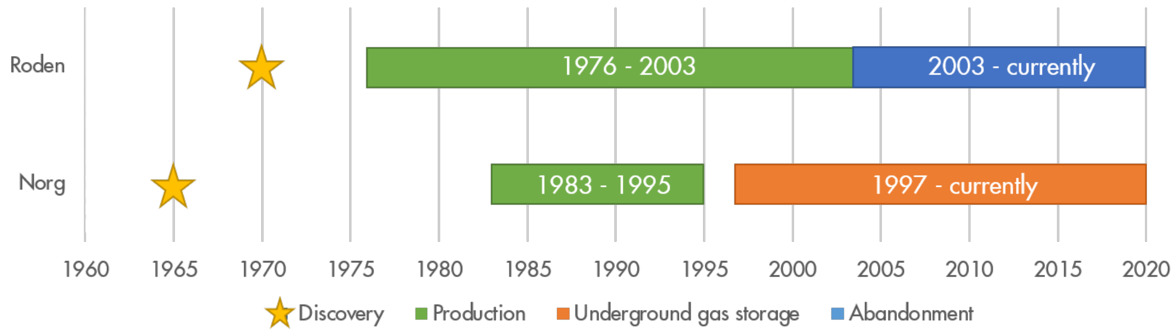

Figure 1.2: Timeline for Roden and Norg gas fields.

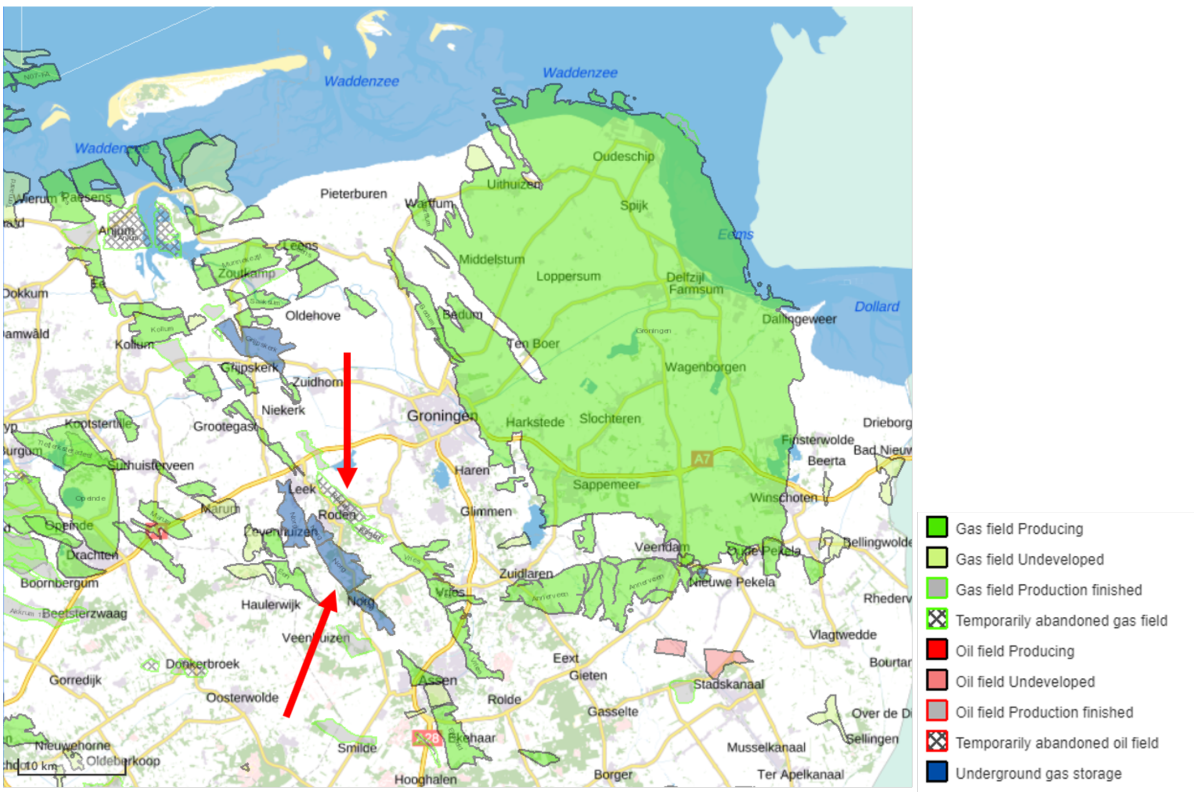

Figure 1.3: Hydrocarbon fields in the North Netherlands, case study Norg field and Roden field are indicated with red arrows. In 1995, the Norg field has been turned into a gas storage location and in 1995 the Roden field was abandoned (adapted from NLOG [50])

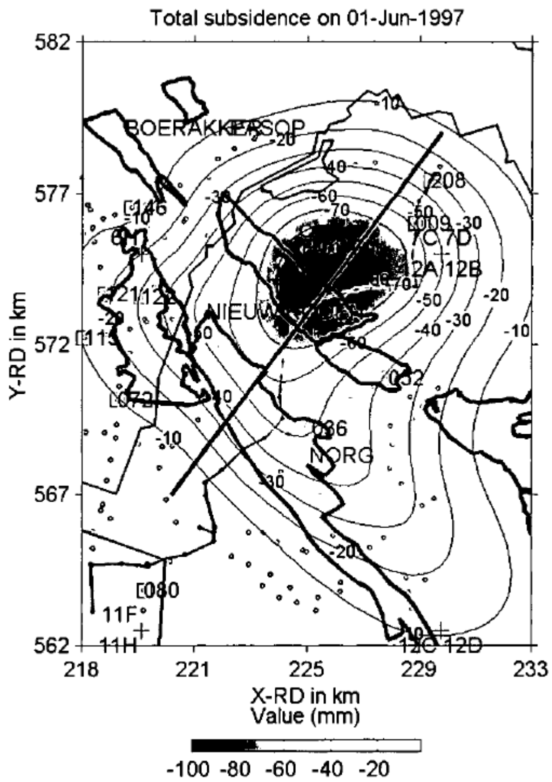

Figure 1.4: The amount of subsidence in 1997 above the Norg and Roden fields since 1975, as estimated by the NAM in an analysis by Quadvlieg [55].

1.2. Current methods

Inversion of surface estimation to estimate subsurface parameters has been a topic of research for many years, with the research on the Lacq gas field (France) from 1992 being one of the first researches in this area [61] [37], where a relation between seismic events, subsidence and reservoir pressure drop was found. In more current research, either direct inverse modeling techniques or data assimilation techniques are used. Some methods use actual geodetic measurements or double-differenced geodetic measurements as input, whereas other methods use deformation estimates. Some works implement formal error propagation, whereas others omit error propagation. Here, a summary of a few relevant current works related to this thesis is given. Fokker and van Thienen-Visser [17] performed an inversion of double-differenced measurements from optical leveling to estimate compaction parameters, improving an existing compaction model of the Groningen Gas Field. NAM [46] used a model ensemble in their Long Term Subsidence Study Part Two (LTS-2) of the Dutch Wadden Sea, where parameter values for the compaction and influence function are estimated, by confronting model members to geodetic data and calculating weights of each specific model member. Hanssen et al. [30] performed an inversion of radar and leveling data, using a Mogi source model and estimating a source strength, related to the volumetric strain of a gas field near Alkmaar. Chapter 4 will further elaborate on these and other studies that perform a geomechanical inversion with geodetic data.

1.3. Objectives and research questions

The main objective of this work is to develop a method in which information about geomechanical subsurface processes is directly estimated from geodetic measurements, using a linear inversion, with formal proper error propagation. This means that the survey observations should be directly written in function of geomechanical parameters, defining a forward model. Subsequently, this forward model is inverted using a regularized Tikhonov inversion, to get an estimation of the geomechanical parameters. After the inversion, a correct description of the uncertainties of the geomechanical parameters is defined. Part of the process is a geodetic testing procedure, to detect outliers in the data and to compute model imperfections.

This thesis is carried out in collaboration with Shell. At Shell, geodetic data is used as input in different stages of the hydrocarbon production. Measurement surveys are carried out and deformation, with corresponding uncertainties, is estimated, after hypothesis testing. The estimated deformation is used to comply with legislation, to improve the knowledge on the deforming surface, possibly lead to mitigation measures and to steer deformation predictions. Subsequently, the deformation estimates are handed over to a geomechanical team, either in measurement point level or at interpolated grid level. These deformation estimates carry an uncertainty structure with correlations. The geomechanical team uses these deformation estimates (instead of the original geodetic survey observations) for geomechanical inversions or validations of their geomechanical predictions. This is a two-step process, in which the stochastic description of the survey observations is often misinterpreted or even omitted in the final geomechanical estimates. Therefore, the goal of this thesis is to develop a method where simple geomechanical parameters are written directly in function of survey observations, and to propagate precision and correlation of the deformation measurements appropriately into the estimated parameters.

This leads to the principal research question:

To what extent can results from optical leveling campaigns be used as input for a direct inversion to estimate a simplified set of geomechanical parameters?

First, it is important to have a clear definition of what a “direct inversion to estimate a simplified set of geomechanical parameters” means. In this thesis, a direct inversion is defined as the process in which geomechanical parameters are directly estimated from geodetic input data, so a direct relationship between geodetic data and geomechanical parameters is defined. This direct relationship limits the amount and complexity of possible geomechanical parameters to be estimated, hence the definition of “a simplified set of geomechanical parameters”. This thesis focuses on optical leveling data, taking into account characteristics typical for this kind of survey data. Further research is encouraged to extend the proposed methodologies to other geodetic surveying techniques.

The principal research question is subdivided into the following sub-questions:

1. *What are the current methods used for geomechanical inversion?*

   Geomechanical inversion can be performed in many ways, all with advantages and disadvantages. By studying previous researches and their ways of working, we can identify advantages and disadvantages and use this information in designing a new workflow. By studying current research we can also identify gaps in current research. For this assessment, focus will lay on what kind of input data is used and what the amount of processing of this data is, what kind of inversion methodology is used, how uncertainty is quantified and whether and how this uncertainty is propagated into the estimates, and on what prior information is used in the inversion methodology.

2. *How are geomechanical parameters directly expressed in terms of geodetic leveling measurements?*

   To define a relationship between geomechanical parameters and geodetic leveling measurement, a geomechanical model is needed. This model needs to be rewritten, such that geomechanical parameters are defined in function of optical leveling measurements. It is important to be aware of what kind of parameters can be estimated with the proposed inversion and whether additional information is needed to estimate specific parameters.

3. *Why and how can the optical leveling measurements be geodetically tested, before being used as input for the geomechanical inversion?*

   Geodetic measurements carry uncertainty, which consists of measurement noise and idealization noise, which are all deformation signals other than the deformation signal of interest. Geodetic data-sets should also be tested for outliers. What kind of errors are expected in the optical leveling data, how can these errors be detected and how can we deal with these errors? A geodetic testing procedure will be assessed and a geodetic software program will be tested.

4. *How could a direct geomechanical inversion, with correct uncertainty handling and uncertainty propagation, look like*?

   This thesis will propose a methodology for a direct geomechanical inversion of geodetic data. Part of this inversion is the propagation of data uncertainties into parameter estimate uncertainties.

5. H*ow does the proposed inversion methodology and error propagation perform on actual geodetic measurements?*

   The methodology will be applied to data from a case study: the Norg and Roden field. Optical leveling data from this case study will be tested, processed and used as input for an inversion. Different parameterizations will be tested.

6. *What are the limitations of a direct linear geomechanical inversion?*

   A direct geomechanical inversion does have advantages, but there are also several limitations to the proposed methodology. These limitations can be adressed in future research.

1.4. Outline

This thesis is divided into seven chapters. Chapter 2 starts with the theory behind subsidence, geomechanical models that link subsidence to subsurface compaction and elaborates on how to measure subsidence. Chapter 3 discusses inversion theory combined with regularization. Chapter 4 gives an overview of other researches done in this area. Chapters 5 discusses the developed methodology and describes the experiments and case study. In Chapter 6 the results of the experiments are given. A conclusion is drawn in chapter 7, followed by recommendations for future research. Additional figures are provided in the Appendices.

2 Subsidence

Subsidence is the gradual settling or sudden sinking of the ground surface, not restricted to a specific time or area [52]. Other forms of ground movement are lateral movements and uplift or heave. Subsidence is perhaps the most well-known form of land movement and is often in the Netherlands in the news concerning hydrocarbon production in Groningen and compaction of peat and clay areas in the western part of the country [49]. Causes of land movement include both natural and anthropogenic causes, acting at different time-scales and spatial extents. In this chapter, the causes of subsidence will be discussed. The chapter subsequently gives an introduction to geomechanics of ground deformation with the theory of elasticity and poroelasticity. The link between subsidence and reservoir parameters is described with a geomechanical forward model. The nucleus-of-strain theory is described, with a focus on Geertsma's model [21] [22]. The chapter ends with the theory behind measuring subsidence, an explanation of optical leveling and on how leveling measurements can be tested and processed using the SuRe software [31].

2.1. Causes of subsidence

Subsidence can be caused by both natural and anthropogenic causes. This section gives an overview of possible subsidence causes, subdivided into natural and anthropogenic causes.

Kooi et al. [33] describe three major natural contributions to long-term vertical land movements in the Netherlands: (1) compaction, (2) postglacial isostasy and (3) tectonics. The Netherlands is located at the end of major rivers, which have been depositing sediments since the beginning of the Cenozoic. The weight of the deposited sediments causes compaction of underlying sediments, leading to subsidence. Changes in surface load are not only caused by the deposition of sediments, but also by deglaciation of land ice. During the last glacial cycle, the melting of glaciers in Scandinavia and Scotland has led to a reduction of surface load [35], which induces surface deformation. The third contribution to vertical land movement is tectonic activity, which is most active in the Roer Valley Graben in Southern Netherlands. Kooi et al. [33] attempted to quantify the different contributions to the vertical land movement, see Figure 2.1. This figure shows that the long-term natural causes are each maximally in the order of $\pm$ 0.1 mm/yr. On the shorter term, peat compaction and oxidation, caused by loading and drainage, are important contributors to subsidence [69]. The amount and rate of subsidence due to peat compaction and oxidation is variable in time and space and depends mainly on overburden weight, depth, groundwater table, time since loading and organic-matter content of the peat. Compaction grades can vary from $\sim$10% up to $\sim$75% of the peat layer, depending on the mentioned factors.

Fokker et al. [18] describe the main anthropogenic subsurface activities affecting the ground surface level in the Netherlands: hydrocarbon production, solution mining of salt, mining of coal, gas storage, geothermal exploitation, and groundwater exploitation. All subsurface activities influence different time scales and spatial extents. This research focuses on vertical deformation caused by hydrocarbon extraction.

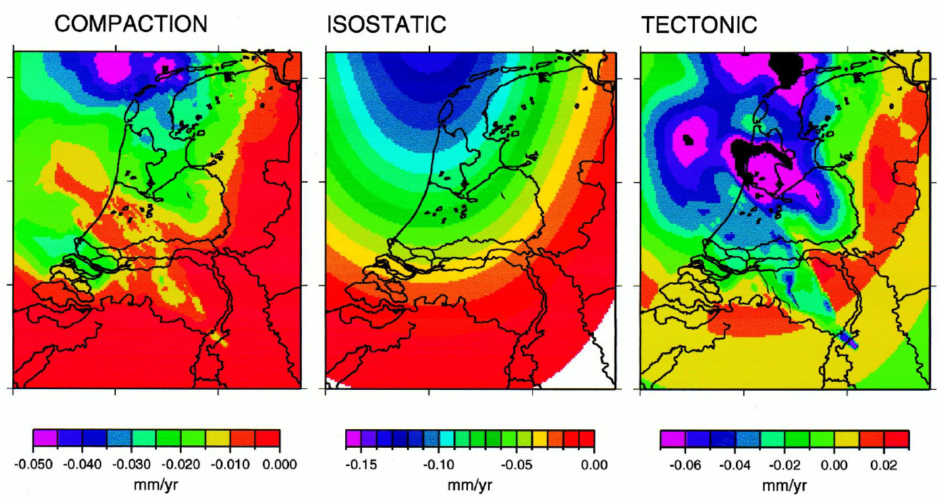

Figure 2.1: Separation of natural contributions to vertical land movement (2.5 Ma-present), constructed by 3D backstripping of Cenozoic stratigraphy of the Netherlands and the southern North sea basin (from Kooi et al. [33]).

Hydrocarbon production generally induces a decline in fluid pressure in the subsurface, also known as pore pressure. The reduced pore pressure increases the so-called effective stress field in the subsurface, causing the rock itself to shrink, which in turn leads to compaction of the reservoir [15]. Reservoir compaction leads to surface subsidence and lateral movements at the surface (see Figure 2.2). Expansion of a reservoir, due to fluid injection, such as gas storage or steam or water injection, has an opposite effect: increased subsurface fluid pressure leads to reservoir expansion and thus uplift of the surface [63].

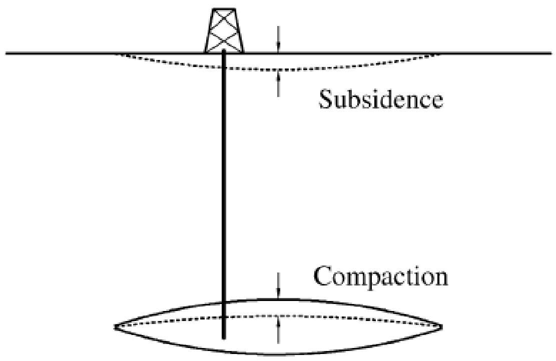

Figure 2.2: Reservoir compaction leading to subsidence (from Fjaer et al. [15]).

2.2. Geomechanics of subsidence

Geomechanics is the study of the interaction between rock, stresses, pressure and temperatures [59]. With the theory of geomechanics, deformation at the surface can be related to subsurface volume strain. This section describes the theory and equations behind elasticity and poroelasticity, used in forward geomechanical models. When hydrocarbons are produced from geological formations, the stress fields in the subsurface change and effective stress increases, leading to reservoir compaction and displacements at reservoir and surface level. To predict surface deformation from fluid extraction and injection, multiple geomechanical models exist. This section gives an equation for reservoir compaction, where the compaction coefficient C_m will be introduced. Reservoir compaction is followed by a brief description of common nucleus-of-strain methods, that are frequently used in the oil and gas industry to relate reservoir compaction to subsidence. The analytical Mogi model [41] and Geertsma model [21] [22] are highlighted and compared.

2.2.1. Elasticity and poroelasticity

The foundation for all geomechanics is elasticity: the ability of materials to resist and recover from deformation produced by forces [15]. Two principal concepts in the theory of elasticity are stress and strain. In a linearly elastic material, deformation is reversible and stress and strain are linearly proportional [82]

$$\sigma = \frac{F_n}{A}, \tag{2.1}$$

where stress σ is defined as the force F_n acting normal through a cross-section with area A. The orientation of the cross-section relative to the direction of the force is important in the definition of stress. If the force is normal to the cross-section, we talk about normal stress. Shear stress is defined as

$$\tau = \frac{F_p}{A}, \tag{2.2}$$

where the shear stress τ is coming from the force component parallel to cross-section F_p. Usually, shear stresses are defined with two subscripts (e.g. τ_{xy}). The first subscript relates to the surface the force is acting on, and the second subscript describes the direction of the force. All normal and shear stresses can be described with a stress tensor, which gives a complete description of the stress state at a point

$$\begin{pmatrix} \sigma_x & \tau_{xy} & \tau_{xz} \\ \tau_{yx} & \sigma_y & \tau_{yz} \\ \tau_{zx} & \tau_{zy} & \sigma_z \end{pmatrix}. \tag{2.3}$$

The stress components in 2D are visualized in Figure 2.3.

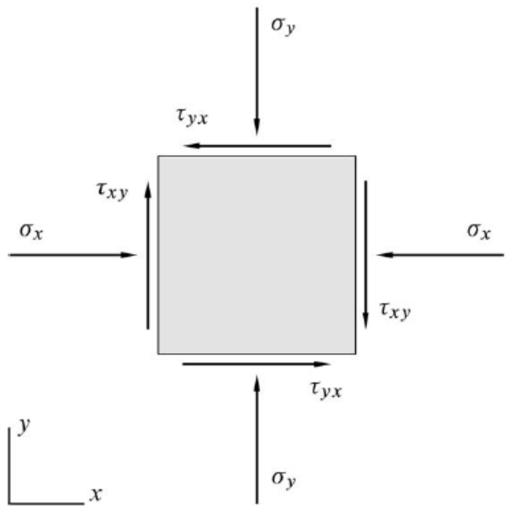

Figure 2.3: Normal (σ) and shear (τ) stresses in 2D (from Fjaer et al. [15]).

Strain is the relative deformation that occurs when stress is applied to a body,

$$\varepsilon_x = \frac{\Delta x}{x}. \tag{2.4}$$

Strain in the normal direction ε_x is called elongation, shear strain Γ_{xy} is deformation in the same direction as shear stress τ_{xy}. Similar to Equation (2.3), strain at a certain point can be described by a tensor: the strain tensor

$$\begin{pmatrix} \varepsilon_x & \Gamma_{xy} & \Gamma_{xz} \\ \Gamma_{yx} & \varepsilon_y & \Gamma_{yz} \\ \Gamma_{zx} & \Gamma_{zy} & \varepsilon_z \end{pmatrix}. \tag{2.5}$$

Volumetric strain (i.e. the relative decrease in volume) is identical to the trace of the strain tensor [15]

$$\varepsilon_{\text{vol}} = \varepsilon_x + \varepsilon_y + \varepsilon_z. \tag{2.6}$$

The relation between stress σ_x and strain ε_x is described by Hooke's law

$$\varepsilon_x = \frac{1}{E}\sigma_x, \tag{2.7}$$

where the coefficient E is called Young's modulus: the sample's resistance against being compressed by uniaxial stress (i.e. the stiffness of the sample). Young's modulus is an elastic modulus, like the Poisson's ratio ν, which is a measure of lateral expansion relative to longitudinal contraction [15]

$$\nu = -\frac{\varepsilon_y}{\varepsilon_x}. \tag{2.8}$$

Other elastic moduli include Lamé's parameters λ and G, which are used to express the general stress-strain relationships for the description of isotropic, linear elastic materials. G is also known as the modulus of rigidity, which is a measure of the sample's resistance against shear deformation [15]. The relations between stress and strain in the theory of elasticity are given by

$$\sigma_x = (\lambda + 2G)\varepsilon_x + \lambda\varepsilon_y + \lambda\varepsilon_z, \tag{2.9}$$

$$\sigma_y = \lambda\varepsilon_x + (\lambda + 2G)\varepsilon_y + \lambda\varepsilon_z, \tag{2.10}$$

$$\sigma_z = \lambda\varepsilon_x + \lambda\varepsilon_y + (\lambda + 2G)\varepsilon_z, \tag{2.11}$$

$$\tau_{yz} = 2G\Gamma_{yz}, \tag{2.12}$$

$$\tau_{xz} = 2G\Gamma_{xz}, \tag{2.13}$$

$$\tau_{xy} = 2G\Gamma_{xy}. \tag{2.14}$$

The theory of linear elasticity assumes that there are linear relationships between the applied stresses and the resulting strains. For rocks, this linear assumption holds if the applied stresses are sufficiently small. However, at a certain pressure, the stress applied to rock can be so large that the rock starts to show permanent deformation. This type of deformation is called plastic deformation [82]. At even larger stresses, the rock will show failure. Figure 2.4 shows a typical laboratory stress-strain experiment with uniaxial deformation. The graph shows the amount of strain of certain applied stress, for a well-cemented rock. At the start of the experiment, when little stress is applied, there is a small amount of crack closure. The crack closure is followed by linear elastic behavior. Inelastic (plastic) deformation is seen at the highest stress levels, just before rock failure.

The elastic stress-strain relationships assume that rocks are homogeneous, solid materials. However, rocks do have void space, making them inhomogeneous on a microscopic scale. The presence of a freely moving fluid in a porous rock modifies its mechanical response. If we consider a homogeneous reservoir consisting of isotropic material, reservoir compaction can be calculated assuming linear poroelasticity [15]. Two mechanisms play a key role in the interaction between rock fluids and porous rocks: (1) an increase of pore pressure causes dilation of the rock and (2) compression of the rock causes a rise in pore pressure. Important in the theory of poroelasticity is the effective stress σ_p': the difference between external stresses and pore pressure, first described by Terzaghi [64] in 1923. Reservoir depletion leads to decreases in pore pressure, which induces an increase in effective stress and thus could lead to reservoir compaction. Biot [7] was the first in 1941 to describe the static and dynamic properties of elastic porous media [13]. He modified the stress-strain relationships by including pore pressure and additional elastic moduli to describe the mechanical response of a two-phase

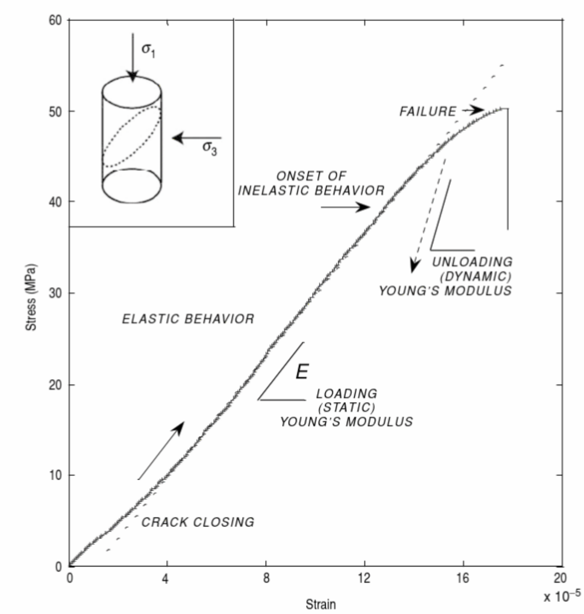

Figure 2.4: Typical laboratory stress-strain experiment with uniaxial deformation (from Zoback [82]).

medium. Important for the geomechanical models used in this thesis is the concept of Biot's poroelastic coefficient. Biot's coefficient a is used to describe which part of the total external stress on a porous rock is carried by the fluid, in case of total external stress acting on a rock

$$\sigma' = \sigma - ap_f, \tag{2.15}$$

with σ' being effective stress, σ the total stress on the rock, α the Biot's coefficient and p_f the fluid pore pressure. From a physical point of view, the solid framework carries the part σ' of the total external stress σ, while the remaining part αp_f is carried by the fluid. Biot's constant expresses the difference between the compressibility of the rock as a whole and that of rock particles

$$a = 1 - \frac{K}{K_s}, \tag{2.16}$$

where K is the bulk modulus of the rock matrix and K_s the bulk modulus of the rock grains. A more extensive description of the theory of poroelasticity including the theory behind the bulk modulus is outside the scope of this thesis, for more information see, e.g., Biot [8], Detournay and Cheng [13] or Wang [78].

2.2.2. Forward geomechanical model

Reservoir compaction can be calculated with a simple equation if some assumptions are made. Firstly, linear poroelasticity is assumed and a homogeneous reservoir consisting of isotropic rock. Secondly, the lateral extent of the reservoir is much larger than it's thickness so that the lateral strain can be ignored. This means that the reservoir is assumed to compact only in the vertical direction. And thirdly, the total vertical stress remains constant. Under these assumptions, the following compaction formula holds [15]

$$\frac{\Delta h}{h} = C_m a \Delta p_f. \tag{2.17}$$

In this equation, h is the vertical height of the reservoir, $\frac{\Delta h}{h}$ the change in reservoir thickness, a is Biot's poroelastic coefficient, Δp_f the change in pore pressure and C_m is called the compaction coefficient, which is given by

$$C_m = \frac{(1+\nu)(1-2\nu)}{E(1-\nu)}, \tag{2.18}$$

where E and ν are respectively Young's modulus and Poisson's ratio. The different parameters in equation (2.17) are usually derived from different types of sources [18]. The thickness of the reservoir is usually derived from seismic data and well data. Biot's poroelastic constant α is measured in a core-experiment, like the compaction coefficient C_m. However, the estimated compaction coefficient is often higher in experiments than the compaction coefficient found by the inversion of subsidence data. Δp_f (the change in pore pressure) is predicted with reservoir simulation models. These reservoir models can at a later stage be calibrated by using available field data, such as geodetic deformation data.

To link reservoir compaction to subsidence, the relation between reservoir compaction and deformation at the surface has to be defined. The "nucleus-of-strain" or "point dilatation source" methods are the frequently used concepts in the oil and gas industry to describe the subsidence due to fluid extraction. These methods use mathematical expressions to relate surface displacement to hydrostatic inflation or deflation of a small sphere (center of dilatation or nucleus of strain), buried in an elastic half-space. An elastic half-space is a first approximation of the earth and consists of one planar surface bounding a continuum that extends infinitely in all other directions [14]. The half-space is an isotropic linearly elastic solid: it is materially homogeneous and mechanically isotropic and it obeys Hooke's law (equation (2.7)). As mentioned earlier in this chapter rocks behave linear elastic within certain stress bounds (see Figure 2.4). Elastic half-space models do neglect many characteristics of the real Earth, but do provide a good approximation of surface deformation due to short-term phenomena in the shallow crust [14].

The most well-known nucleus-of-strain concept in the oil and gas industry is described by Geertsma [21] [22]. Geertsma was however not the first to come up with this concept, because the concept of nucleus-of-strain was introduced by Anderson [2]. In 1936, Anderson described displacement due to a point of dilatation in the neighborhood of a free plane surface, in the context of magma intrusions. Mindlin [39] (1936) and Mindlin and Cheng [40] (1950) used the concept of a nucleus-of-strain in the theory of thermoelasticity. Mogi [41] (1958) described volcano deformation using a nucleus-of-strain, the 'Mogi' point pressure source. The method uses an exact expression for the effects of a hydrostatically pressurized cavity in a uniform, isotropic elastic full-space. To convert to a half-space with a stress-free surface, an image of the original source is introduced into the full-space on the opposite side of the plane, to cancel out-of-plane shear stresses. The combined normal stress on the plane from the source and its image is then canceled by a similar distribution of opposing normal stress (see Figure 2.5).

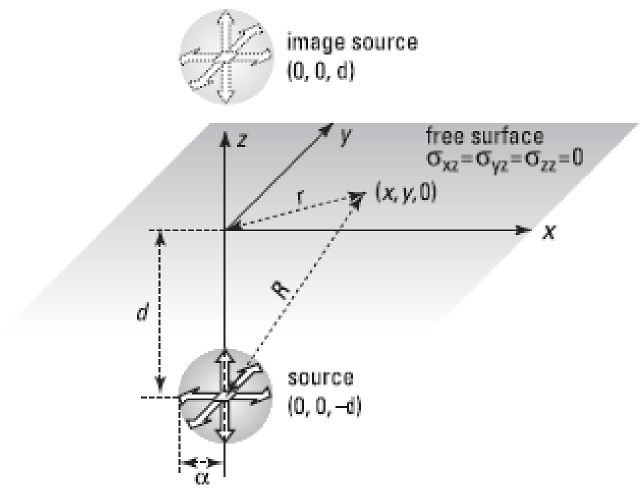

Figure 2.5: Coordinate system and geometric relationships used to derive surface deformation from an embedded point pressure source (from Dzurisin and Lisowski [14]).

The surface displacement in vertical z-direction (at $z = 0$) due to a Mogi source (a spherical cavity embedded in an elastic half-space, with its radius much smaller as its depth) is given by [14]

$$u_z = a^3 \Delta P \frac{(1-\nu)}{G} \frac{d}{R^3}, \tag{2.19}$$

where u_z is the displacement at surface point (x,y,0), $R = \sqrt{r^2 + d^2}$, a the radius of the source (see Figure 2.5) and ΔP the pressure change in the spherical source. G is the shear modulus of the half space and ν the Poisson's ratio. This model can also be defined for horizontal displacement, see e.g. Dzurisin and Lisowski [14]. For the Mogi model, individual contributions of different terms cannot be separated, meaning that a small pressure change in a small cavity can produce the same surface deformation as a large pressure change in a small cavity.

Geertsma [21] [22] used known solutions from thermoelasticics (Mindlin [39] and Mindlin and Cheng [40]) to arrive at an expression which expresses deformation as function of a compacting sphere. Geertsma also represents the subsurface by a homogeneous, isotropic, linear-elastic halfspace. Reservoir compaction is represented with many small compaction nuclei that have a small but finite volume V. A Green's function is used to calculate displacement for each nucleus. The influence of all nuclei is summed up to find the total subsidence due to the compacting reservoir. At the surface, vertical displacement in z direction due to a compacting nucleus is given by [15]

$$u_z = -\frac{C_m(1-\nu)}{\pi} V \alpha \Delta P \frac{d}{R^3}, \tag{2.20}$$

where:

C_m	Compaction coefficient
ν	Poissont's Ratio
α	Biot's coefficient
V	Volume of source
ΔP	Pressure change
d	Depth source
R	Distance to source

Integration of equation (2.20) over an arbitrary-shaped reservoir leads to subsidence at a certain point at the surface ($z = 0$) caused by hydrocarbon production induced by a decline in pore pressure in all reservoir sections. If the reservoir is subdivided into a finite sum of discrete contributions from n small elements ΔV, the integral is replaced by a finite sum [20]

$$u_z(x,y,0) = \sum_{n-1}^{N} \frac{C_{m,n}(1-\nu_n)}{\pi} a_n V_n \Delta P_n \frac{d_n}{((x-x_n)^2 + (y-y_n)^2 + d_n^2)^{3/2}}, \tag{2.21}$$

where x_n, y_n and z_n are the coordinates of the n-th reservoir volume with volume V_n, in which pore pressure is decreased by $\Delta p_{f,n}$, inducing a vertical displacement u_z at surface point (x,y). In 1974, Gambolati [20] used this method to predict subsidence due to hydrocarbon production in Groningen, by discretization of the Groningen reservoir volume, see Figure 2.6.

With equation (2.20) it is possible to compute subsidence for an arbitrarily-shaped reservoir by using numerical methods. Geertsma [22] developed equations for subsidence due a disk-shaped reservoir, by integrating over a reservoir. He expressed displacements and stresses in terms of integrals of Bessel functions. These Bessel functions are in turn epressed via elliptic integrals [15]. He developed tables of numerical values of the necessary integrals. For a more extensive description of these equations, see for example Fjaer et al. [15].

The theory by Geertsma was later further developed by van Opstal [74], who added a rigid basement to Geertsma's model. The NAM still uses Geertsma's en Opstal's nucleus of strain approach to transfer derived volume strains at reservoir level to surface subsidence [45]. The methodology is incorporated in Shell's 'SubCal' software.

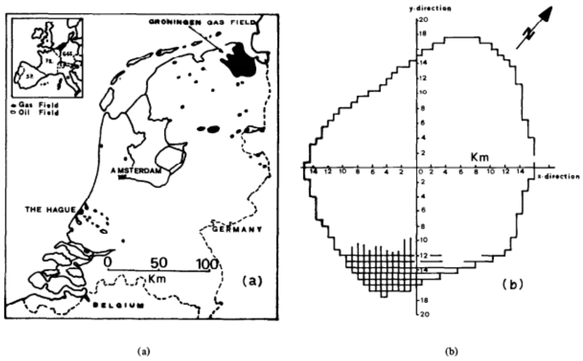

Figure 2.6: (a) location of Groningen reservoir. (b) discretization of Groningen reservoir by Gambolati [20].

Note that the nucleus-of-strain models by Mogi (2.19) and Geertsma (2.20) are quite similar. For a single point source, they both estimate vertical displacement as

$$u_z(x,y,0) = M\frac{d}{R^3}, \tag{2.22}$$

where M is a multiplication factor. The physical parameters involved in this multiplication factor depend on the application [76]: for volcanic activities, Mogi's model is used and M consists of the radius of the source, the pressure change, Poisson's ratio and the modulus of rigidity. For deformation due to gas extraction, M is a function of the compaction coefficient, Poisson's ratio, the volume of the nucleus, Biot's constant and the pressure drop. To integrate over the whole reservoir shape, a superposition of multiple point sources should be taken.

2.3. Measuring subsidence

To estimate the amount of subsidence, geodetic measurement campaigns are periodically organized. Typically, spatial height differences are measured and from these height measurements, an estimate of the amount of deformation is made. This section describes the difference between the deformation signal of interest and other signals in the measurements, known as idealization noise. The data used for this thesis is derived from optical leveling campaigns, a short description of the principles and uncertainties of this technique is given. After survey campaigns are executed, the data should be geodetically tested and processed, this can, for instance, be done by a software program called SuRe, which is described in this section.

2.3.1. Signal of interest

The definition of subsidence is the relative height change of a point over time relative to a reference point. Measuring subsidence can be done using naturally relative techniques, such as leveling or InSAR. Other techniques provide positions in a reference system (or "geodetic datum"), such as GNSS (Global Navigation Satellite Systems). It is important to be aware of what kind of signal the measurement technique measures: height, height differences between points (spatial changes), height changes for a certain point (temporal changes) or changes in height differences between points (spatio-temporal changes). Each technique has it's own platform (spaceborne, airborne or terrestrial) and measurement characteristics. These measurement characteristics consist of spatial density of measurements, spatial extent, geometric sensitivity, and precision [18]. The height parameter is different for different techniques. Leveling techniques measure spatial orthometric height differences. Orthometric height differences are height differences in the direction parallel to the local gravity acceleration vector and thus have physical meaning. Other techniques, such as GPS, define height differences geometrically relative to a reference system. For local subsidence, however, the differences between different height parameter definitions are usually negligible [18].

Some measurement techniques, like leveling, use pre-defined benchmarks to locate the measurements. This means that during every measurement campaign the same points are measured. The advantage of using benchmarks is that subsidence can directly be estimated from repeated geodetic measurements. Other techniques use natural reflection points, which result in a distribution of measurement points, such that subsidence estimation cannot be performed per point. In these cases, some form of interpolation is needed. Whether or not measurements are located at predefined points, it is important to be aware of the mechanical foundation of the benchmark or natural reflection point [76]. The subsidence measured at these points will reflect the subsidence of the foundation layer. The total subsidence at the surface is a sum of all processes in the subsurface. It depends thus on the foundation of the measurement points, for what kind of compaction effects a benchmark is sensitive. Figure 2.7 visualizes the effect of the use of two different founded benchmarks with different compaction processes.

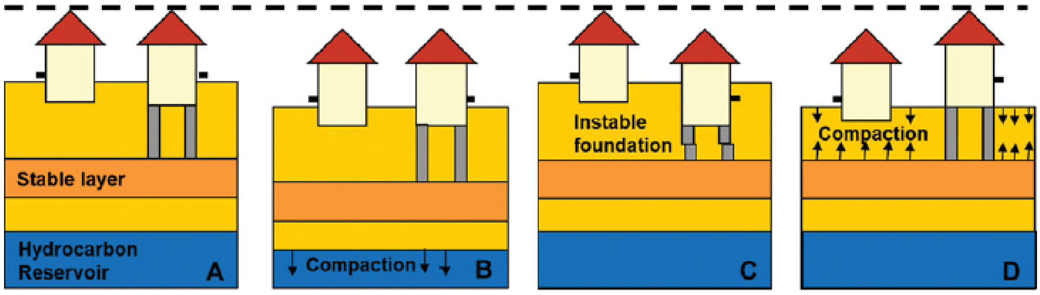

Figure 2.7: The effect of different compaction sources on benchmarks founded in different layers. (A) The original situation, benchmarks (black rectangles) located in house with no foundation on the right and house with foundation in deep stable layer on the left. (B) Compaction of the hydrocarbon layer, both benchmarks reflect the same subsurface motion. (C) Right house has an unstable foundation, such that a non-existing subsidence signal is measured. (D) Compaction of shallow layer is only reflected at the unfounded benchmark, not at deep founded benchmark (from Fokker et al. [18]).

A user of geodetic deformation data should be aware of his objective. Different subsidence regimes should be separated to find the effects of the subsidence regime of interest. The degree to which the measurement represents the actual signal of interest is called the idealization accuracy [18].

2.3.2. Optical leveling

The measurements of the surface of the Earth and its surface motions are called geodetic measurements. Geodetic measurements are obtained during geodetic surveys. There are many geodetic surveying methods, including leveling, GPS and InSAR. This thesis will only make use of optical leveling measurements, so a brief description of an optical leveling survey will be given here. For a more comprehensive description of the other various geodetic surveying methods, see for example Alberda and Ebbinge [1] or Torge and Müller [68].

Leveling measurements can be done both onshore and in rivers, lakes, and off-shore. Leveling in water bodies is called hydrostatic leveling. This thesis focuses on onshore leveling, also called geometric leveling, spirit leveling or differential leveling. This technique measures height differences, using horizontal lines of sight between points nearby. A leveling instrument is used together with two vertically standing leveling rods (Figure 2.8). The measured height difference is orthometric, so parallel to the local gravity acceleration vector. This is indicated with the equal gravity potential lines W_1 and W_2 in Figure 2.8. The height difference Δh between the rods is computed by subtracting the foresight reading (f) from the backsight reading (b)

$$\Delta h = b - f. \tag{2.23}$$

A section between two benchmarks is often too long to be measured with one measurement. Therefore, the section is broken up into smaller pieces along the path and a couple of measurements are performed consecutively, as depicted in Figure 2.9.

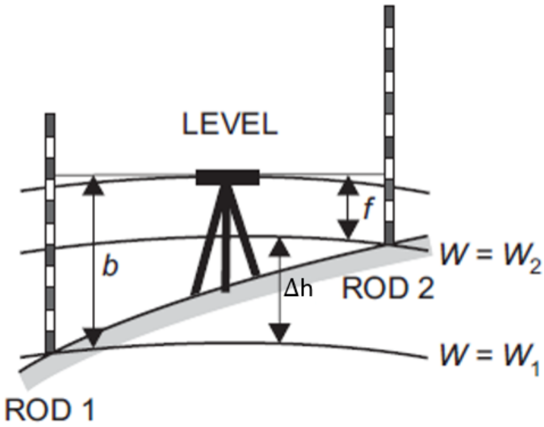

Figure 2.8: Leveling principle (from Torge and Müller [68]).

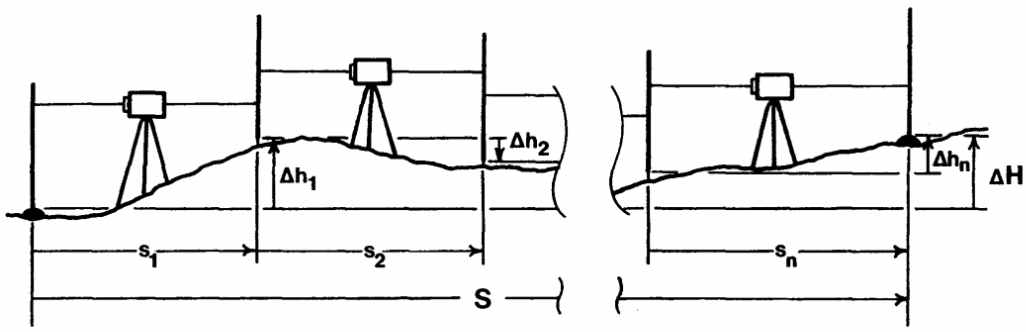

Figure 2.9: Leveling a complete section of length S using n measurements. Benchmarks are located at the start and end of the path (from Schomaker and Berry [60]).

2.3.3. Uncertainties

The random error of the measurements is called the measurement noise. The standard deviation for optical leveling (σ_{ol}) is linearly dependent on the length of the trajectory and is often approximated by

$$\sigma_{ol} = c_0 + c_1 \cdot \sqrt{l}, \tag{2.24}$$

where l is the length of the leveling trajectory in kilometer. For different survey campaigns other values for c_0 and c_1 are used, typical values for c_0 are within 0 and 2 mm [29], for c_1 between 0.64 and 1.29 mm/$\sqrt{\text{km}}$ [36]. The measured height differences in each leveling campaign are assumed to be uncorrelated.

The total measured subsidence is a sum of all deformation processes in the subsurface. Idealization noise is considered as deformation caused by other sources than the deformation signal of interest [72]. In the case of modeling subsidence induced by hydrocarbon production, deformation is caused by reservoir compaction and/or aquifer depletion. The main sources of idealization noise are other deformation regimes, which can be divided up into two groups. The first source of idealization noise consists of independent motion of individual benchmarks with respect to the foundation layer, due to for example structural instabilities, benchmark weight or pile friction. This autonomous deformation is assumed spatially uncorrelated, as construction settings differ per benchmark [57]. However, a temporal correlation is assumed, because deformation develops in time. The second source of idealization noise is shallow compaction of the Holocene layer beneath benchmarks, due to for example groundwater level variation or peat compaction. This type of idealization noise is assumed to have both spatial and temporal correlation. Idealization noise is unrelated to measurement noise [18].

There are thus two different classes of noise components: measurement noise and idealization noise. To represent the concept of idealization noise and measurement noise, the notation of van Leijen et al. [72] is followed. The deformation vector d can be decomposed in two components

$$\underline{d} = d_M + \underline{d}_I, \tag{2.25}$$

where d_M is the true and deterministic deformation signal of interest and $\underline{d}_I$ is the sum of all other deformation signals, here considered as idealization noise. The vector with geodetic observations is given by $\underline{y}$

$$\underline{y} = d + \underline{e} \tag{2.26}$$

where $\underline{e}$ are the random errors on the observations: the measurement noise. Combining Equations (2.25) and (2.26) leads to

$$\underline{y} = d_M + \underline{d}_I + \underline{e}. \tag{2.27}$$

From a geomechanical modeling perspective, the functional model relating the model parameters to the deformation due to hydrocarbon production will be: $G(m) = d_M$. The mathematical model for the parameter estimation will look like

$$E\{\underline{y}\} = d_M = G(m), \quad D\{\underline{y}\} = Q_{dI} + Q_e, \tag{2.28}$$

where Q_{dI} is the covariance matrix of the idealization noise and Q_e is the covariance matrix of the measurement noise.

2.3.4. Output level leveling data

Leveling data can be processed on different levels, it is important to be aware of the output level of a dataset. The overview of the output levels for leveling data proposed by Samiei-Esfehany and Bähr [57] is used for this thesis:

- **Level0:** Levelling campaign observation, that is height observations between benchmarks. This is the direct result of leveling campaigns.

- **Level1:** Adjusted heights per epoch or height differences per epoch with respect to a single reference benchmark.
- **Level2:** Double differenced heights with respect to a common reference benchmark and a common reference epoch. This is the result of taking the temporal differences of adjusted heights per epoch with respect to the height in a reference epoch.

2.4. Hypothesis testing

This thesis describes how model parameters are estimated from geodetic data, based on the principles of least squares estimation, combined with regularization. Determination of best values for unknown model parameters is based on observational data and possible a-priori information. To check the validity of the model and data, statistical hypothesis testing must be applied. Validation through probabilistic decision making aims to detect if the model is sufficiently consistent with the data, or whether there are better alternative models [66]. Finding the optimal parameterization of the unknowns is difficult in deformation analysis and the testing procedure is therefore important [76]. The validity of the null hypothesis is tested in the Detection, Identification and Adaptation (DIA) procedure as defined by Teunissen [65]. Multiple alternative hypotheses should be evaluated to determine the mathematical model that minimizes the least-square residuals with respect to the observations. With normally distributed data, all information about the quality of the estimator is contained in variance matrix $Q_{\hat{x}\hat{x}}$. This assumption only holds if the assumed mathematical model is valid. This section summarizes the mathematical framework of the adjustment and testing procedure.

Certain errors in the estimation problem do not affect the precision of the estimates, however, they do affect the size of the residuals and thus the consistency of design matrix A with observed data y. These errors are due to one of the following reasons [66]:

- outliers in the observed data y
- a systematic bias in the observed data y
- a wrong assumption for design matrix A
- a wrong assumption regarding Q_{yy}

The default model under the null-hypothesis, providing $\underline{x}_0$, is specified with the null hypothesis H_0

$$\begin{aligned} \underline{y} &\sim N_m(E(\underline{y}), Q_{yy}), \\ H_0 : E(\underline{y}) &= Ax, \\ \hat{e}_0 &= y - A\hat{x}_0. \end{aligned} \tag{2.29}$$

To detect whether something is wrong in the default mathematical model (the 'null hypothesis'), the overall model test is used. Estimates of the unknown parameters are obtained by the least-squares adjustment. The validity of the null hypothesis is tested in the detection step. The overall model test uses the weighted sum of squared residuals called the test statistic, which 'compresses' the residual vector $\hat{e}$ into a single quantity

$$\underline{T} = \underline{\hat{e_0}}^T Q_{yy}^{-1} \underline{\hat{e_0}}; \quad \text{reject } H_0 \text{ if } \underline{T} > K = \chi^2_\alpha(m-n, 0), \tag{2.30}$$

where $\underline{T}$ equals the test statistic, $\underline{\hat{e_0}}$ the residuals following from the null hypothesis, as described in equation (2.29) and $K = \chi^2_\alpha(m-n, 0)$ the critical value, belonging to a significance level α. If the observational data is normally distributed, the test statistic $\underline{T}$ follows a central χ^2-distribution [66]. The χ^2-distribution is characterized by the degrees of freedom of the inverse problem $(m-n)$, where m is the number of observations and n the number of unknown parameters. This test is only applicable in case of redundancy $(m > n)$ because the χ^2-distribution is only defined for degrees of freedom equal or larger than one.

The OMT should be rejected if the test statistic is larger than a certain critical value K. The critical value is obtained by defining a critical region. The critical region is derived by dividing the observation space, which represents all outcomes, into two parts: the critical region and its complement, the acceptance region. When the observations, as represented by the test statistic, happens to lie in the critical region, the null hypothesis is rejected. If the test statistic lies in the acceptance region, one accepts that the null-state reflects the state of the process in reality. This means that one assumes that there are no outliers, systematic biases or model errors. When the test statistic is rejected, alternative hypotheses with alternative models should be specified in the identification step, which may lead to an accepted OMT

$$H_a : \quad E\{\underline{y}\} = Ax + c_y \nabla, \tag{2.31}$$

where ∇ represents the model error and c_y the relation with the data, which can be multi-dimensional [76]. To detect single observation anomalies, such as outliers, a test called 'datasnooping' can be used [65]. For this test, c_y will have the shape

$$c_y = [0, 0, ..., 0, 1, 0, ...0]^T. \tag{2.32}$$

A-priori, it is often not known which functional model parameterizes the signal of interest best. To attempt to find the best model, multiple models of different dimensions can be specified. This means that for every model, n can vary. In the evaluation, it is then not straightforward to just take the model with the lowest test statistic. For that reason, de Heus et al. [11] introduced the test quotient: the ratio of test statistics and their critical values. The test quotient is found by dividing each test statistic by the appropriate χ^2 value. The hypothesis that should be rejected is the hypothesis with the largest test quotient

$$\underline{T}_i / \chi^2_\alpha(m - n_i) > \underline{T}_j / \chi^2_\alpha(m - n_j) \quad \forall j \neq i, \tag{2.33}$$

where $\underline{T}_i$ equals the test statistic following from alternative hypothesis H_a, i, with a critical value χ^2_α with $(m - n_i)$ degrees of freedom and a significance level α.

The final step is the adaptation step and involves the replacement of the null-hypothesis by the most likely alternative hypothesis. To test the validity of the alternative hypothesis, the DIA procedure is executed iteratively.

The DIA procedure is part of the software program that is being used for the geodetic testing of leveling data and iteratively estimating subsidence: SuRe. A description of SuRe will be given in the next section.

2.5. Processing of geodetic data with SuRe

Subsidence Residual Modelling (or SuRe) is a software package developed by Houtenbos [31] and is currently being used within the NAM to model subsidence. SuRe estimates subsidence by subtracting predicted spatial height differences from measured spatial height differences ("residuals"). The software package also screens the input data for measurement errors, point misidentifications, and abnormal vertical displacement rates. If errors in the input data are found, appropriate action is taken to minimize the quality loss of the solution. Eventually, the parameters of the variance model are re-tuned to the patterns of the residuals.

The mathematical framework behind SuRe can be summarized as

$$\underline{h}_{ij}^{t} = H_j^{t0} - H_i^{t0} + z_j^{t0,t} - z_i^{t0,t} + \underline{\delta h}_{ij}^{t} + \underline{\delta s}_j^{t} - \underline{\delta s}_i^{t} + \underline{\delta z}_j^{t0,t} - \underline{\delta z}_j^{t0,t}, \tag{2.34}$$

where:

$\underline{h}_{ij}^{t}$	the spatial height difference between points i and j at time t
H_j^{t0} and H_i^{t0}	initial heights
z	the functional model of subsidence due to gas extraction
$\underline{\delta h}$	measurement noise
$\underline{\delta s}$	autonomous movements of points or point/idealization noise
$\underline{\delta z}$	subsidence model imperfections

$\underline{\delta h}$, $\underline{\delta s}$ and $\underline{\delta z}$ are stochastically modelled components, which are estimated through variance component estimation [76]. Idealization noise is modelled with an empirical covariance function

$$\sigma^2_{s_i^t} = \sigma_s^2 |t - t_0|^{2p}, \quad \sigma_{s_i^t s_i^u} = \frac{1}{2}\sigma_s^2(|t - t_0|^{2p} - |t - u|^{2p} + |u - t_0|^{2p}), \tag{2.35}$$

where t and u are points in time, t_0 is the reference time, σ_s the standard deviation of autonomous benchmark displacement and p is the power of the empirical covariance function. This power is related to the smoothness of the benchmark displacement in time. A value of 1 implies a constant displacement rate, the lower the value of p the more the displacement rate can vary over short time intervals.

Houtenbos [31] describes the model imperfections that are due to uncertainties in the parameterization of the subsidence signal also by a covariance function

$$\sigma_{z_i^t z_j^u} = \frac{1}{2}\sigma_z^2(|t - t_0|^{2q} - |t - u|^{2q} + |u - t_0|^{2q})e^{-(l_{ij}/L)^2}, \tag{2.36}$$

where σ_z is the standard deviation of the predicted subsidence model, q the power of the model noise development with time, l_{ij} the distance between benchmarks i and j and L the residuals subsidence correlation length. A large value of L implies very smooth behavior, a low-value graininess of the subsidence residuals. The deeper the subsidence cause, the wider the associated the subsidence on the surface above will spread, thus leading to a larger L.

SuRe requires a process parameter file that controls the area of interest, the period of interest and possible project specifications. It also needs pre-defined noise parameters and a 3D subsidence prognosis. With the process parameter file, height observations are extracted from a database and the subsidence prognosis is subtracted from the height observations. Subsequently, the program tests and corrects for data and model errors, corrects noise parameters and computes initial benchmark heights. The flowchart in Figure 2.10 depicts the process of SuRe.

SuRe works in an iterative manner. First, points that are disconnected from the network are removed, because these points do not contribute to the solution and cause singularities. Then, a design matrix and variance matrix are constructed that are used in the least squares adjustment that is solved for the initial benchmark heights. During each iteration, 1D hypothesis testing is applied to identify points that cause the failure of the overall model test. After each iteration, the most likely cause of the overall model test failure is reported. Several 1D errors can be detected by SuRe, an overview with corresponding solution measures is given in Table 2.1.

Table 2.1: 1D Errors indicated by SuRe [31]).

1D Error description	Solution
Observation error	Observation is deleted
Benchmark misidentification error	Bypass affected benchmark
Benchmark disturbance	Benchmark history is split in 2 parts
Abnormally fast benchmark displacement	Increase of point noise standard deviation

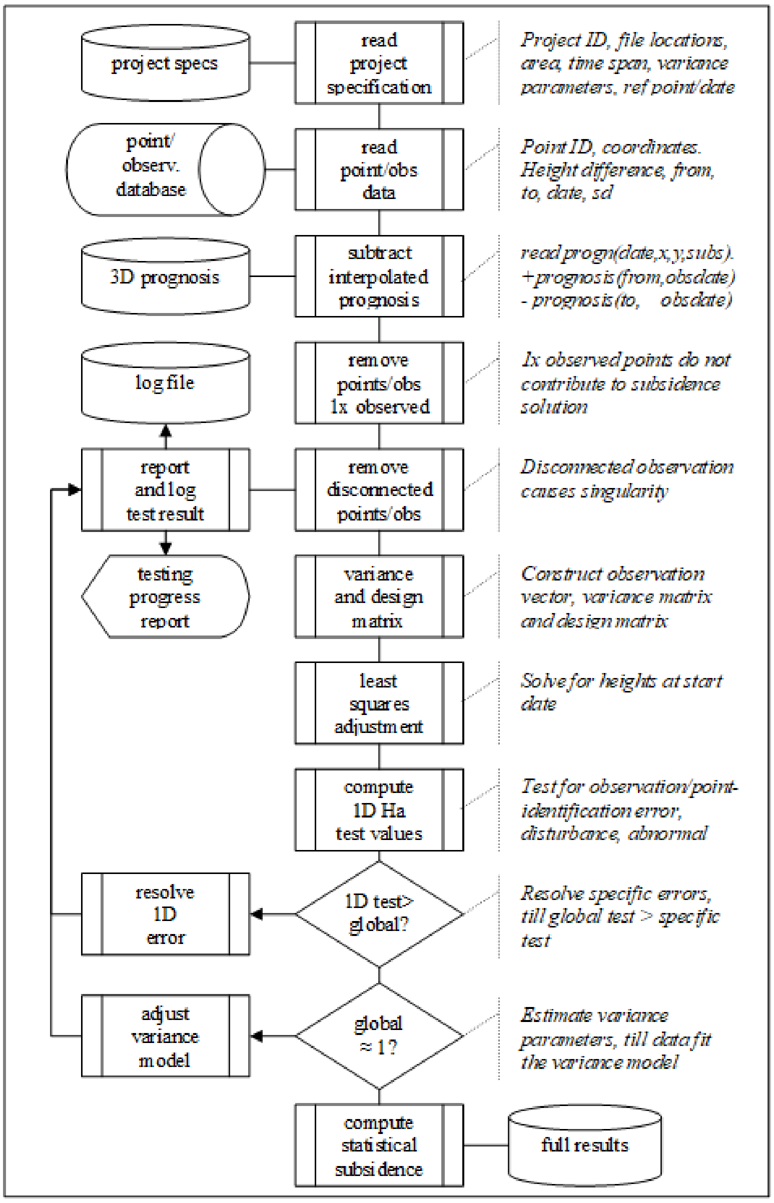

Figure 2.10: Overall process flow of SuRe (from Houtenbos [31])

At each iteration, the most likely cause of the failure of the overall model test is resolved. If eventually, the global test error is larger than all 1D errors, but yet not accepted, SuRe starts to tune the variance model. All variables in the variance model are adjusted until the data fits the variance model and all tests are accepted.

The input for the program is mentioned in the flowchart of Figure 2.10 and consists of a project specification file, in which the project is specified and time and area are specified. In this file, also values for the variance parameters that define the variance model are given:

- a factor for measurement noise standard deviation,
- the standard deviation of autonomous benchmark displacement (idealization noise),
- the power of autonomous benchmark displacement (2.35),
- the standard deviation of the prognosed subsidence model,
- the power of the prognosed subsidence model and,
- the correlation length of the prognosed subsidence model (2.36).

In the project specification file, one must also define a reference benchmark, it's reference height and a reference date. The last thing in the project specification file that should be defined is the test-criterion or significance level α (2.29). With control of the project specification file, SuRe fetches height differences from an internal database using an SQL statement.
The second input file the program needs is a 3D prognosis, which gives the approximate subsidence based on a subsidence model. Both a prognosis for a date before the first observation and a prognosis after the last observation should be given, such that the whole period of interest is covered. Using more prognosis grids at intermediate dates is possible. The prognosis grids should cover the entire area of interest and period of interest.

After the 1D and global tests are accepted, SuRe computes the estimated subsidence and gives full results. The program outputs three files containing all results. The first output file is a log file, listing the testing results per iteration. It gives for each iteration the outcome of the global test and the largest 1D test and gives the cause of the largest error, this is one of the 1D errors described in Table 2.1. Part of the report contains which benchmark or which measurement is flagged with a 1D error and at which time step(s). If all 1D errors are solved but the overall model is not yet accepted, the parameters of the variance model are adjusted to prevailing noise patterns. The outcomes of this variance model adjustment can also be found in this log file. The log file also contains a list of all benchmarks with their reference heights and estimated subsidence at the reporting date.
The second file that SuRe outputs is a subsidence grid at the reporting date that was stated in the project specification file. The layout of the file is similar to that of the subsidence prognosis grid. Together with the subsidence grid comes a grid with a standard deviation per subsidence estimate.
The third output file is a SuRe data file, in which a wide variety of data is given for further processing. This file contains the parameters of the variance model, information about all benchmarks and which benchmarks passed testing, all observations, and information about which observations passed testing.

2.6. Discussion and conclusion

Subsidence and other forms of ground deformation occur at all time scales and spatial scales. In the Netherlands, subsidence results from different deformation regimes, both with natural and anthropogenic causes. This thesis focuses on hydrocarbon production induced subsidence. To model the relation between hydrocarbon production and subsidence, a nucleus-of-strain model can be used, as defined by Mogi [41] or Geertsma [21]. Subsidence is estimated from measurements with different geodetic survey methods, each with its characteristics. When using geodetic survey data, one should be very well aware of the error sources in the data. These can be divided into two groups: measurement noise and idealization noise. Measurement noise is a characteristic of the measurement technique and idealization noise is the result of all other deformation signals than the signal of interest. When using geodetic data as input data for further computations, one should be aware of these error sources. Testing for errors can be done with the DIA-procedure, which can be integrated into software tools. SuRe is a software tool that, as part of its workflow, applies a geodetic testing procedure. SuRe needs a 3D subsidence prognosis and initial variance parameters to work, the influence of these input files should be investigated. SuRe is one of the possible options for geodetic testing, other tools may lead to different results.

3

Inversion theory and regularization

Menke [38] defines inverse theory as "an organized set of mathematical techniques for reducing data to obtain useful information about the physical world on the basis of inferences drawn from observations" (p.1). Inverse theory tries to estimate model parameters using observational data and a general principle or model. To be able to make a meaningful estimate of the model parameters, there should be some sort of relation between the data and the model. The contrary of an inverse problem is called a "forward problem". Forward theory makes a prediction of data, using a pre-defined model and model parameters. This chapter elaborates on direct linear inversions and Tikhonov regularization, a method of regularization for ill-conditioned systems.

3.1. Inversion of discrete linear systems

This research focuses on the inversion of a discrete linear system. This means that the inverse problem can be represented with an explicit linear equation

$$Ax = y, \qquad A \subseteq R^{m \times n}, \qquad x \subseteq R^n, \qquad y \subseteq R^m. \tag{3.1}$$

In equation (3.1), x is the vector of model parameters to be determined, y the vector with observation data and A the model matrix relating both. In discrete inverse theory, both the data vector y and the vector with model parameters x are discrete. Alternatively, a continuous inverse problem consists of estimating x, where the model and/or the data are functions of continuous variables. A continuous inverse problem can be converted to a discrete one, by approximating the function as a summation [3]. The simplest way of solving an inverse problem would be taking the inverse of A to directly convert the data vector into model parameters: $x = A^{-1}y$. This only leads to a unique solution if matrix A is invertible: it must be square and have full-rank. When the amount of observations is not equal to the amount unknown model parameters ($m \neq n$), this is not possible due to model and data uncertainties. A mathematical model is an idealized and simplified version of the real world. Therefore, it only gives a simplified approximation of reality, not describing the data perfectly. Data is a measured quantity and so there is the presence of errors or noise in the data vector. An inverse problem without an exact solution can be defined in terms of it's expectation

$$E\{\underline{y}\} = Ax, \tag{3.2}$$

which is equal to

$$\underline{y} = Ax + \underline{e}. \tag{3.3}$$

Observations y are realizations of a random variable: $\underline{y}$. Observations or measurements are made by imperfect instruments and under sub-optimal conditions. Observations are therefore always stochastic. A random variable is described by a probability density function (PDF). The uncertainty or precision of the observation vector y is described in covariance matrix Q_{yy}

$$D\{\underline{y}\} = Q_{yy}. \tag{3.4}$$

The random errors in the observations propagate into the estimated parameters. The probability density function (PDF) of the random vector $\underline{x} \subseteq R^n$ is described by $f_x(x)$ and $\underline{y} \subseteq R^m$ is written in function of $\underline{x}$: $\underline{y} = G(\underline{x})$, where $G : R^n \to R^m$. The PDF of $\underline{y}$ is given by [66]

$$D(\underline{y}) = D(G(\underline{x})) = \int_{R^n} [G(x) - \overline{y}][G(x) - \overline{y}]^T f_{\underline{x}}(x) dx, \tag{3.5}$$

with $\overline{y} = E\{G(\underline{x})\}$.

For the linear case, a simplification is obtained. If $\underline{y} = A\underline{x} + b$ and $A \subseteq R^{m \times n}$, error propagation follows the linear variance propagation law

$$D\{\underline{y}\} = Q_{yy} = AQ_{xx}A^T. \tag{3.6}$$

If the inverse problem has no exact solution, a solution should be found that approximates the exact solution as good as possible. A useful approximation is a model parameter estimate that minimizes the estimation error: the misfit between the estimated data and the observed data

$$\underline{\hat{e}} = \underline{y} - \underline{\hat{y}} = \underline{y} - A\underline{\hat{x}} \tag{3.7}$$

The best fitting solution is an estimate with certain model parameters, such that the smallest over-all error (the sum of squares of the individual errors) is achieved. For least squares this is done by minimizing the sum of squared residuals

$$||e|| = \sqrt{\sum_{i=1}^{m} e_i^2} = \sqrt{(e^T e)}, \tag{3.8}$$

where e is the estimation error or residual and m the total amount of observations. The corresponding $\hat{x}$ that minimizes this sum is called the least squares solution of the system of equations

$$\hat{x}_{LS} = \min_x \{||\underline{e}||^2\} = \min_x \{\underline{e}^T \underline{e}\} = \min_x \left\{(\underline{y} - Ax)^T (\underline{y} - Ax)\right\}. \tag{3.9}$$

The minimum of this function is found by taking it's first derivative to x and setting this equal to 0. Eventually this leads to the least squares estimator

$$\underline{\hat{x}}_{LS} = (A^T A)^{-1} A^T \underline{y}. \tag{3.10}$$

The uncertainty of the estimated model parameters follows after applying the linear error propagation law

$$D\{\underline{\hat{x}}_{LS}\} = Q_{\hat{x}\hat{x}} = (A^T Q_{yy}^{-1} A)^{-1}. \tag{3.11}$$

With ordinary least squares, each of the observations is treated on an equal basis [66]. If the accuracy of the measurements vary, such that the standard deviation of the individual observations is not equal, a methodology called weighted least squares can be used, that gives more weight to more accurate measurements. Instead of minimizing $\sum_{i=1}^{m} e^T e$, one should minimize the weighted sum of squares: $\sum_{i=1}^{m} e^T W e$, with weight matrix $W = \text{diag}(w_{11}, \ldots, w_{mm})$, $w_{ii} > 0, i = 1, \ldots, m$. Now, the estimated solution is found by minimizing [38]

$$\hat{x} = \min_x \{(y - Ax)^T W (y - Ax)\}. \tag{3.12}$$

Leading to the weighted least squares estimator

$$\underline{\hat{x}}_{WLS} = (A^T W A)^{-1} A^T W \underline{y}. \tag{3.13}$$

The dispersion of $\underline{\hat{x}}_{WLS}$ again follows from the linear error propagation laws

$$D\{\underline{\hat{x}}_{\text{WLS}}\} = Q_{\hat{x}\hat{x}} = (A^T W A)^{-1} A^T W Q_{yy} W A (A^T W A)^{-1}. \tag{3.14}$$

The best linear unbiased estimator (BLUE) is a special form of the weighted least-squares estimator (WLSE). BLUE is a special form of WLSE with the inverse covariance matrix of the data (Q_{yy}^{-1}) as weight matrix

$$\underline{\hat{x}} = (A^T Q_{yy}^{-1} A)^{-1} A^T Q_{yy}^{-1} \underline{y}. \tag{3.15}$$

BLUE is a linear unbiased estimator which has the smallest variance and therefore called “best” [66]. The covariance matrix of the estimated model parameters $\underline{\hat{x}}$ for BLUE is given by

$$D\{\underline{\hat{x}}_{BLUE}\} = Q_{\hat{x}\hat{x}} = (A^T Q_{yy}^{-1} A)^{-1}. \tag{3.16}$$

The quality of the estimators $\underline{\hat{y}}$ and $\underline{\hat{e}}$ for linear inversion is given by

$$D\{\underline{\hat{y}}\} = Q_{\hat{y}\hat{y}} = A Q_{\hat{x}\hat{x}} A^T. \tag{3.17}$$

$$D\{\underline{\hat{e}}\} = Q_{\hat{e}\hat{e}} = Q_{yy} - Q_{\hat{y}\hat{y}}. \tag{3.18}$$

The observation data vector y consists of m entries and the model parameter vector x of n unknowns: $y \in R^m$ and $x \in R^n$. Depending on the rank of the matrix, such a linear system may or may not have a solution (consistency), and this solution may or may not be unique. The rank of a matrix is the dimension of the vector space spanned by its columns. This corresponds to the maximal number of linearly independent columns. If rank$(A) = m$, consistency is guaranteed. A linear system may or may not be consistent if rank$(A) < m$. If rank$(A) = n$ (the columns of A are independent), a unique solution exists for the linear system. If rank$(A) < n$, the linear system is underdetermined, this means that there may be more than one solution. In this thesis, the linear system will be full of rank: rank$(A) = n$ and overdetermined: rank$(A) = n < m$. With such linear systems, least squares can be employed to select a best approximate solution [38].

3.2. Ill-conditioned problems

The majority of the inverse problems in geophysics are ill-posed [81]. This means that even if rank$(A) = n$, there is no reliable solution when using least squares estimation. Though the residuals are small, the solution is far off the exact solution. This means that small least-square residuals do not imply a good least-squares solution. Solving an ill-conditioned problem implies that more information should be added to the system. To get insight into the nature of an ill-conditioned problem, singular value decomposition can be used.

Singular Value Decomposition (SVD) of matrix A is the superior numerical method for analysis of discrete ill-posed problems [26]. Every matrix has a singular value decomposition [24]. SVD decomposes an m by n matrix A into three matrices U, Σ and V

$$A = U \Sigma V^T = \sum_{i=1}^{n} u_i \sigma_i v_i^T, \tag{3.19}$$

where

- U is an m by m orthogonal matrix, with columns forming the basis of the data space,
- Σ is an m by n diagonal matrix, with n entries called singular values,
- V is an n by n orthogonal matrix, with columns forming the basis of the model space.

The singular values along the diagonal of Σ are arranged in decreasing size: $\sigma_1 \geq \sigma_2 \geq ... \geq \sigma_n \geq 0$. The least square estimator $\hat{x}$ and the errors in the least-squares solution can also be expressed in terms of the singular value decomposition

$$\hat{x}_{LS} = \sum_{i=1}^{n} \frac{u_i^T y}{\sigma_i} v_i, \tag{3.20}$$

$$e_{\hat{x}} = \sum_{i=1}^{n} \frac{u_i^T e_y}{\sigma_i} v_i. \tag{3.21}$$

Equation (3.21) shows that perturbations or errors in the data vector cause perturbations in the least-squares solution. For exact data, without errors, $||u_i^T y||$ usually decreases with increasing i. However, this does not directly holds for $||u_i^T e_y||$, especially if the data errors have power at higher frequencies, corresponding to higher indices i. This means that the solution becomes very noisy with small singular values in the presence of data errors. This is caused by the amplification of high frequency data errors by small singular values [26]. Discrete ill-posed problems are characterized by singular values that decay gradually towards zero and do not show an obvious jump between nonzero and zero singular values [3].

3.3. Tikhonov regularization

Small singular values of the design matrix A cause the least squares solution to be useless, because the small singular values amplify data noise. To be able to still compute an estimate of the model parameters, one could make use of regularization. Regularization is a method that filters out the flawed components of the least squares solution, or in other words to filter out the contributions to the solution corresponding to the small singular values. This is done by introducing filter factors

$$\hat{x}_{reg} = \sum_{i=1}^{n} f_i \frac{u_i^T y}{\sigma_i} v_i, \tag{3.22}$$

where f_i are the filter factors. The filter factors differ for each regularization technique. The similarity between all regularization techniques is that as σ_i decreases, f_i must tend to zero, such that contributions to the solution from the smaller σ_i are filtered out [28]. Many regularization methods exist, for this thesis the Tikhonov regularization method is used.

Tikhonov regularization is a very widely applied regularization method and easily implemented for regularizing discrete ill-posed problems [3]. The method is developed by Tikhonov [67] in 1963. The key idea of Tikhonov regularization is to include an a priori assumption about the size and smoothness of the solution. Tikhonov regularization in its general form leads to the minimization problem

$$\underline{\hat{x}}_{L,\lambda} = \min_{x} \left\{ ||Ax - y||^2 + \lambda^2 ||Lx||^2 \right\}, \tag{3.23}$$

where regularization parameter λ controls the weight given to minimization of the regularization term $||Lx||$, relative to the minimization of the residual norm $||Ax - y||^2$. L is the regularization matrix, which gives preference to a particular solution with desirable properties. The Tikhonov solution $\hat{x}_{L,\lambda}$ is given by

$$\underline{\hat{x}}_{L,\lambda} = (A^T A + \lambda^2 L^T L)^{-1} A^T y. \tag{3.24}$$

Equations (3.23) and (3.24) hold for uncorrelated data with covariance matrix $Q_{yy} = \sigma_0 I_m$. If the covariance matrix of the data y is not equal to $\sigma_0 I_m$, the least squares residual should be scaled with the inverse of the covariance matrix [26]

$$\underline{\hat{x}}_{L,\lambda} = \min_{x} \left\{ Q_{yy}^{-1} ||Ax - y||^2 + \lambda^2 ||Lx||^2 \right\}, \tag{3.25}$$

with corresponding Tikhonov solution

$$\underline{\hat{x}}_{L,\lambda} = (A^T Q_{yy}^{-1} A + \lambda^2 L^T L)^{-1} A^T Q_{yy}^{-1} y. \tag{3.26}$$

Error propagation after linear inversion with Tikhonov regularization follows the covariance propagation law (equation (3.6)). The covariance matrix of the estimated parameters with Tikhonov regularization is found with [3]

$$
\begin{aligned}
\underline{\hat{x}}_{L,\lambda} &= By,\\
Q_{\underline{\hat{x}}_{L,\lambda}\underline{\hat{x}}_{L,\lambda}} &= BQ_{yy}B^T,\\
\text{with } B &= (A^T Q_{yy}^{-1} A + \lambda^2 L^T L)^{-1} A^T Q_{yy}^{-1}.
\end{aligned}
\tag{3.27}
$$

The choice of the regularization matrix decides on what kind of measure of x is minimized, expressed as Lx. The simplest choice of L would be the identity matrix $L_0 = I_n$, better known as zeroth-order Tikhonov regularization. For this type of regularization, the norm of the solution, $||Ix|| = ||x||$, is minimized. The filter factors for zeroth-order Tikhonov regularization look as

$$
f_i = \frac{s_i^2}{s_i^2 + \lambda^2},
\tag{3.28}
$$

where s_i is the ith singular value following from SVD and λ is the regularization parameter. Employing the SVD of A, the regularized solution can be written as

$$
\hat{x}_{reg} = \sum_{i=1}^{n} \frac{s_i^2}{s_i^2 + \lambda^2} \frac{u_i^T y}{\sigma_i} v_i.
\tag{3.29}
$$

In many situations, one prefers minimization of another measure of x, such as the norm of the first or second derivative of x. Minimization of the first order derivative of x for a one-dimensional model leads to solutions that are relatively flat and can be achieved by using the L_1 regularization matrix

$$
L_1 = \begin{bmatrix}
-1 & 1 & & & & \\
 & -1 & & & & \\
 & & \ddots & \ddots & & \\
 & & & -1 & 1 & \\
 & & & & -1 & 1
\end{bmatrix} \subseteq R^{(n-1)\times n}.
\tag{3.30}
$$

Minimization of the second derivative can be achieved by using the second-order Tikhonov regularization matrix L_2 that penalizes solutions that are rough in the squared second derivative sense [3]

$$
L_2 = \begin{bmatrix}
1 & -2 & 1 & & & & \\
 & 1 & -2 & 1 & & & \\
 & & \ddots & \ddots & \ddots & & \\
 & & & 1 & -2 & 1 & \\
 & & & & 1 & -2 & 1
\end{bmatrix} \subseteq R^{(n-2)\times n},
\tag{3.31}
$$

where $L_2 x$ is a finite-difference approximation that is proportional to the second derivative of x. For higher-dimensional models, equations (3.30) and (3.31) are not appropriate. In such cases, another regularization matrix should be implemented using a finite-difference operator of appropriate dimensionality and form. See e.g. Besag et al. [5] or Ryan et al. [56] for examples of regularization with spatial neighbourhoods.

To solve and analyze a zeroth-order Tikhonov regularization problem, the SVD is used. For higher-order Tikhonov regularization problems where $L \neq I_n$, a generalized singular value decomposition (GSVD) of matrix pair (A, L) should be employed. The generalized eigenvalues of matrix pair are essentially the generalized eigenvalues of the matrix pair $(A^T A, L^T L)$ [26]. With the GSVD, the solution of 3.23 can again be expressed as a sum of filter factors, analogue to Equation (3.29). For a comprehensive derivation of the GSVD, see e.g. Hansen [26] or Menke [38].

The Tikhonov regularization parameter λ (equation (3.23)) decides how much regularization is needed, and thus governs the weight given to the minimization of the norm $||Lx||^2$. The larger the regularization parameter, the more regularization is applied and with a large λ, the solution becomes very smooth, but the residual norm $||y - Ax||$ becomes very large. If the regularization parameter approaches zero, $\lambda \to 0$, the residuals will become small but the solution will approach the least squares solution: $\hat{x_\lambda} \to \hat{x}_{LSQ}$. Therefore, an appropriate size of the regularization parameter should be chosen.

The L-curve is a graphic tool for analysis of discrete ill-posed problems and the role of the Tikhonov regularization parameter. It is a plot of the norm of the regularized solution $||x_{\lambda,L}||$ versus the corresponding residual norm: $||y - Ax_\lambda||$, see Figure 3.1. Hansen [27] describes the L-curve as "a trade-off curve between two quantities that both should be controlled" and he describes an algorithm for choosing the regularization parameter λ with the L-curve criterion. The optimal regularization parameter is found at the point in the L-curve with maximum curvature [27].

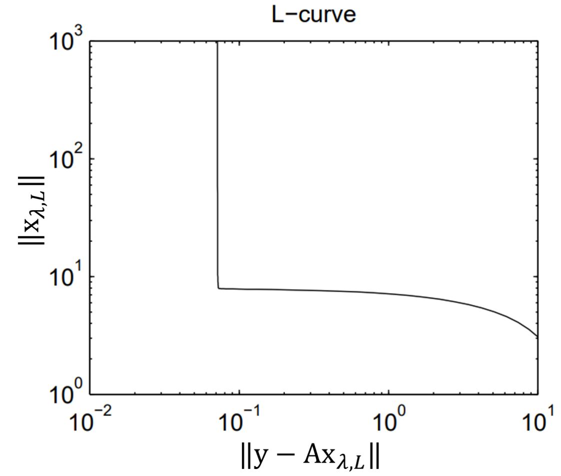

Figure 3.1: Typical L-curve (adapted from Hansen [27]).

Cross validation (CV) is an alternative method of selecting regularization parameter λ. The general idea behind CV is that the data is split and a part of the data is left out in the inversion. A set of candidate regularization parameters is defined. The best model for the measurements is the one that predicts each measurement (or subset of measurements) best as a function of the other measurements. For each candidate regularization parameter, the regularized least squares solution is computed with the reduced set of observations. The part of the data that is not used in the inversion, is later used to test the performance of the inversion for the candidate regularization parameter. The missing observation(s) are predicted using forward modelling. The root-mean-square (RMS) between "observed" and "predicted" is computed and the regularization parameter with the smallest RMS is chosen [34]. There are different ways of splitting up the dataset. With k-fold cross validation, the data is split up in k subsets and the inversion is performed on the other $k - 1$ subsets. This is done k times, each time leaving another subset out. An extreme form of k-fold CV is leave-one-out CV. For leave-one-out CV, each kth subset consists of 1 observation.

Generalized cross validation (GCV) is a form of leave-one-out CV and provides an objective methodology to choose the regularization parameter [25]. The GCV theorem finds the regularization parameter that minimizes the GCV functional

$$\min_{\lambda} = \frac{1}{m} \sum_{i=1}^{m} \left(\frac{y_i - \hat{y}_i(\lambda)}{1 - \bar{h}(\lambda)} \right)^2, \tag{3.32}$$

where m are the amount of measurements, y_i the ith measurement, $\hat{y}_i(\lambda)$ the prediction of y_i, computed with candidate regularization parameter λ and $\bar{h}(\lambda) = \frac{1}{m}\text{trace}(H)$. H is defined by [3]

$$H = A(A^T A + \lambda L)^{-1} A^T. \tag{3.33}$$

GCV can be very computationally expensive, since a number of regularized least-squares solutions should be computed to find a good regularization parameter.

4

Previous research

Production of hydrocarbons from the subsurface induces a pore pressure reduction. Due to this reservoir pressure depletion, the reservoir volume compacts and the surface above the reservoir subsides. This connection between reservoir compaction and subsidence is used in geomechanical modeling. Geomechanical models give estimations of subsidence in forward modeling, with the degree of compaction and other geomechanical parameters as input. For an elaborated description of geomechanical models connecting reservoir compaction and surface subsidence, see chapter 2. Inverse geomechanical modeling is used to obtain knowledge of geomechanical parameters from geodetic surface data. One of the first case studies of hydrocarbon induced subsidence and relations between reservoir parameters and subsidence data is performed on the Lacq gas field in the south of France. Maury et al. [37] concluded in his paper in 1992 that "monitoring subsidence and seismic events is a new and useful aid to understanding reservoir response to fluid withdrawal, the practical consequences with regard to safety and gas production, and a contribution to our knowledge of reservoir behavior over time.". In 1994, for the same case study, Segall et al. [61] related pressure reservoir drop to subsidence measurements. For Segall's study, it is, however, hard to judge the quality of the fit, since no quality description of the data is given.

More recent studies that focus on the relationship between reservoir behavior and subsidence measurements can roughly be divided into three groups: (1) methods that try to estimate geomechanical parameters using a data assimilation method, (2) methods that use subsidence estimates as a way of validating the goodness-of-fit of their subsurface models and (3) methods that use geodetic data as input for a direct inversion.

4.1. Data assimilation methods

Data assimilation is a group of methods that makes predictions of the state of a system, combining two sources of information: observation data and models that embody the physical laws governing the behavior of the system [80]. Both the observations and the physical model carry uncertainty, and these uncertainties should be included in the estimate of the state of the system [77]. Examples of systems are processes in the atmosphere, ocean, and land surface [80]. For geomechanical inversion, the system is the land surface and subsurface, modeled by a geomechanical model, which links surface deformation to reservoir compaction. The observation data consists of geodetic surface data. Various types of data assimilation techniques exist, currently Ensemble Kalman filters are popular data assimilation methods that are applied to a wide range of dynamical models [77]. Another popular group of data assimilation methods is particle filters [71]. This thesis will not go into detail on the theory behind these different data assimilation methods, for an extensive description see above mentioned papers.

LTS-II: The LTS-II study (Long Term Subsidence study part two) performed in 2017 by the NAM [46] aims to reduce the difference between the NAM-predicted subsidence and observed subsidence in the Ameland gas-field in the Netherlands. 58 reservoir pressure models were created, all history matched to available pressure and production data. Due to long production history and regular pressure measurements, the models are narrowly constrained and thus show little variation between the 58 models. Subsequently, for every pressure scenario, parameters of the geomechanical compaction model and the influence function were varied with a Monte Carlo simulation. For the compaction model, the Rate Type Compaction isotache Model (RTCiM) (Pruiksma et al. [54]) is used and for the influence function a modified Geertsma and van Opstal model [23]. The Monte Carlo procedure picks parameters for both the compaction model and the influence model. The combination of one reservoir model together with a set of parameters for both the influence function and the compaction model is called a subsidence model member, a group of subsidence members defines an ensemble. Each member is confronted with the geodetic data and a test statistic is computed, to define the probability and weight of the member. The geodetic data consists of double-differenced leveling and GPS techniques. The uncertainties of this data are described by a fully populated covariance matrix [72]. The final covariance matrix of the double differences does not only include measurement noise but also idealization noise: ”idealization noise is associated with deformation components in geodetic observations that are not related to the signal of interest.” (van Leijen et al. [72]). A formal outlier handling approach was applied to the data. This workflow identifies the most likely model factors (reservoir pressure model, parameter values for compaction model and influence function) and posterior probability distributions for the model data. The workflow of the LTS-II study is summarized in Figure 4.1. In Section 4.4, a closer look at the processing of the geodetic data will be given.

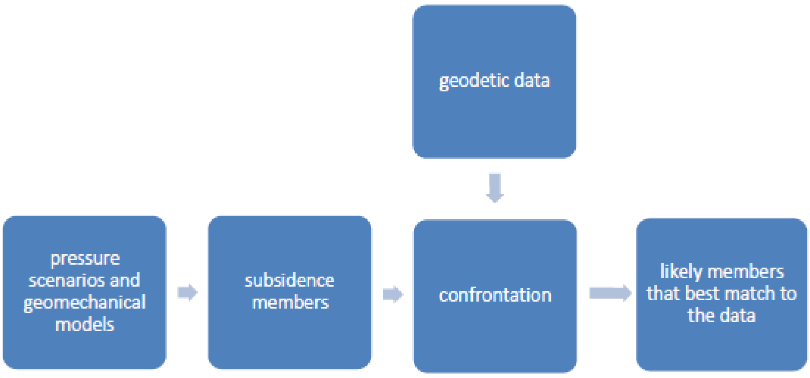

Figure 4.1: Main components of LTS-II workflow (from NAM [46])

Ensemble smoothing of land subsidence measurements for reservoir geomechanical characterization: Baù et al. [4] applied an ensemble smoother (ES) to provide improved estimates with reduced uncertainty of reservoir parameters. The ensemble smoother assimilates measurements of both horizontal and vertical surface displacement into geomechanical results. The ensemble smoother is a derivate of the classic Kalman filter [32]. The ES minimizes the variance of the estimation error, by merging the prior mathematical model with actual field data, to derive a corrected posterior estimate, making it a Bayesian data assimilation method. This method uses a Monte Carlo simulation to represent the model uncertainties by an ensemble of geomechanical parameters. The displacement ensemble and model parameters are simultaneously updated. The applicability of the ES is tested to provide reliable estimates of uncertain subsurface parameters. The effect on the geomechanical estimates of using increasing standard deviation values for the geodetic data is researched, as is the amount of geodetic measurements used. This paper applies the methodology on Geertsma’s analytical solution for a disk-shaped reservoir [22] on a synthetic data set. The authors make the remark that “the effectiveness of the ES data assimilation algorithm heavily relies on the correlation between reservoir parameters and surface displacement”. This means that the model should be able to explain all physics behind the processes causing surface displacement. Surface displacement is the summed effect of multiple components, such as hydrocarbon production, natural consolidation, surface loading, etc. Deformation components not related to the signal of interest is called “idealization noise”, as in the LTS-II study [46]. If this idealization noise is not modeled in the ES, the framework will provide fictitious parameters. Model uncertainty and bias are outside the scope of this paper.

4.2. Methods that use geodetic data as validation

Other studies use geodetic data primarily as a way of validating the outcomes of geomechanical models:

Winningsplan Groningen 2016: The NAM computes reservoir compaction in the Winningsplan 2016 [45] with two compaction models: the Time Decay Compaction model and the rate type compaction model (RTCiM). Input for these calculations is a top reservoir map, reservoir thickness, reservoir pressure, and porosity. The derived strains are transferred to surface subsidence using an influence function: semi-analytical approach, based on Geertsma [22] and Geertsma and van Opstal [23]. To calibrate the outcomes to the measured subsidence, the weighted root-mean-squared (RMS) value of the residuals between the surveyed and modeled subsidence at all benchmarks is determined. Both compaction models show a “reasonable to good” fit with the subsidence data, with the RTCiM being the best case model. The RTCiM model is subsequently used for subsidence forecasting with ongoing production.

History match of the Groningen field dynamic reservoir model to subsidence data and conventional subsurface data: Van Oeveren et al. [73] propose a new methodology of history-matching the Groningen field. The Groningen field dynamic reservoir model is usually history-matched to conventional data (pressure data and water influx data). This paper proposes an update of the existing history match, by including subsidence data. The Groningen field dynamic reservoir model is used to predict future subsidence, but calculated subsidence based on the results of the reservoir model resulted in notable mismatches to observed subsidence. Therefore, subsidence data can be used to constrain dynamic reservoir models, additional to pressure and water influx data. The subsidence data consists of the estimated displacements at benchmarks between 1972 and 2013 from satellite and leveling surveys, filtered for stable benchmarks. They estimate the measurement error over 1973-2013 to be in the order of 1 cm. The workflow consists of setting up variable uncertain model parameters, that likely impact the mismatch to the data. 1000 different models are formed, to make combinations of settings of the variable model parameters. The mismatch of the model output and the conventional history matching data plus the subsidence data is quantified with the RMS to each data set. Each time, the model with the lowest combined RMS is chosen and improved. This eventually resulted in a model that had a mismatch of ± 4cm to the subsidence data, which has a data uncertainty of ± 1cm. Figure 4.2 shows the results of the history matching. There are clear areal trends in the residuals from the subsidence match. The study assumes that all measured subsidence is due to reservoir compaction.

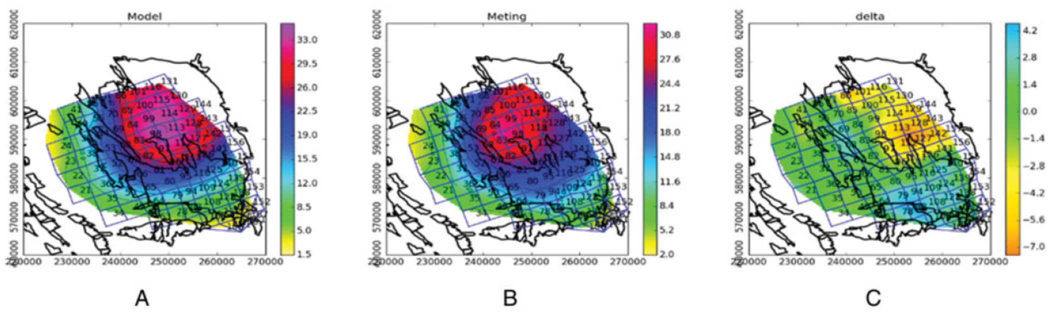

Figure 4.2: Results of history matching for subsidence estimates: (A) Modeled subsidence estimate, (B) measured subsidence, interpolated and (C) difference between (A) and (B) (from van Oeveren et al. [73]).

4.3. Direct inversion methods

The above-mentioned studies all use the geodetic data as a way to confront their geomechanical or reservoir models or to check the validity of the models. The data assimilation methods also use the geodetic data as input for estimating or improving geomechanical parameters. The third group of studies uses geodetic data as input to perform a direct geomechanical inversion.

Time-dependent inversion of surface subsidence due to dynamic reservoir compaction: Muntendam-Bos et al. [42] introduced a novel, time-dependent inversion scheme for resolving temporal reservoir pressure drop from surface subsidence observations in a single procedure. A prior reservoir pressure model is updated using geodetic observation data and the covariance matrix of the observations. The method uses both the prior covariance matrix and the data covariance matrix. This implicitly guarantees smoothness of the model estimate, while maintaining specific geological features. The inversion methodology is adopted from Tarantola [62], minimizing a cost function J:

$$J = \exp[-\frac{1}{2}(m - m_0)^T C_m^{-1}(m - m_0) - \frac{1}{2}(d - G(m))^T C_d^{-1}(d - G(m))] \tag{4.1}$$

This leads to the definition of the model estimates and it's covariance:

$$\begin{aligned} \hat{m} &= m_0 + C_m G^T (G C_m G^T + C_d)^{-1}(d - G_{m0}) \\ C_{\hat{m}} &= C_m - C_m G^T (G C_m G^T + C_d)^{-1} G C_m = (G^T C_d^{-1} G + C_m^{-1})^{-1} \end{aligned} \tag{4.2}$$

where m is the vector with adjustable model parameters, in this case, pressure drop, d the vector with observation data, G the forward model, m_0 the prior model, C_m the covariance matrix of the prior model and C_d the covariance matrix of the observational data. The estimate of the model parameter and its covariance are given by $\hat{m}$ and $C_{\hat{m}}$. The forward model is a linear, semi-analytic approach designed to account for layering by Fokker and Orlic [16]. The observation data is differenced, over different time steps, to ensure that available measured data is used optimally. The proposed methodology is applied to a synthetic data set.

Inversion of double-difference measurements from optical leveling for the Groningen gas field: Fokker and van Thienen-Visser [17] update an existing reservoir compaction model, by linearly inverting double-differenced leveling measurements. The followed methodology is on the basis similar to the inversion methodology proposed by Muntendam-Bos et al. [42]. The inversion exists of a conventional least-squares inversion, where the objective function J (equation (4.1)) is minimized. This study has formalized the definition of "double differences" and applied the methodology on real case study data, the Groningen gas field. Also, a smoothness constraint was added and the authors estimated an independent constant vertical velocity for each benchmark as an additional unknown parameter, to allow for movement not caused by depletion of the gas field. Eventually, the inversion returns an updated value for the compaction and values for autonomous movements of benchmarks. The quality of fit was calculated by $\chi^2 = \frac{1}{N}(G_m - d)^2/\sigma_d^2$, and improved from 8.8 to 5.9.

Validation of PSI results of Alkmaar and Amsterdam within the Terrafirma Validation Project: Hanssen et al. [30] compared deformation estimates from InSAR with in-situ measurements at two locations: a metro tunnel in Amsterdam and at gas fields in the vicinity of Alkmaar, both in the Netherlands. The in-situ measurements in Amsterdam consist of tachymetric observations, in Alkmaar leveling measurements are used. The Alkmaar case study is more interesting here since the deformation at that location is presumably caused by gas production. Correspondence of the leveling and InSAR measurements is analyzed in both the measurement space and in the parameter space, by their ability to estimate geomechanical source parameters. Mogi sources are placed in reservoir locations, the amount of sources depends on the reservoir size. The dimensions and depth are considered a priori knowledge. Leveling and InSAR data are inverted to derive source parameters. The data is inverted in Bayesian sense, the paper does not tell whether processed displacement data or raw measurement data is used. The data are considered uncorrelated and normally distributed, with $\sigma = 1$ mm for leveling data and $\sigma = 5$ mm for InSAR data.

Field-wide reservoir compressibility estimation through inversion of subsidence data above the Groningen gas field van Eijs and van der Wal [70] present a methodology to model compaction and subsidence, combining results from rock mechanics experiments and surface deformation measurements. A prior compaction grid was proposed, based on core plug experiments. During these experiments, porosity and compaction are measured on plugs and a trend line is fitted, defining the relation between porosity and compaction. This relation is then used to express the compaction coefficient on a spatial grid, covering the Groningen gas field. The compaction grid is used as prior input in an inversion scheme. Two penalties are used in the inversion process: (1) the difference between the inverted compaction coefficient C_m and the porosity derived C_m and (2) the residuals between modeled and measured subsidence. The forward model used is a time-decay compaction model, where decay times are varied. Eventually, the C_m with the lowest RMS is the time-decay model with a decay time of 5 years. The geomechanical model is a semi-analytical approach based on Geertsma [22] and Geertsma and van Opstal [23]. The input geodetic data are height differences at benchmark locations, relative to a stable benchmark. The reported height differences are not corrected for possible autonomous movement but present the total displacement at the surface. The study applies a conservative approach, meaning that all deformation is assumed to be a result of reservoir compaction. The paper is concluded with a discussion about the uncertainty description of the model and data, mentioning that the uncertainty description of both the model and data could be improved in further research.

Robust non-linear inversion for reservoir deformation from surface displacement data: Bisdom et al. [9] developed a workflow to derive geomechanical parameters, inverting surface displacements. The inverse solution of Geertsma's semi-analytical nucleus-of-strain model [22] is used together with a forward solution of a finite element model. The inversion workflow is an iterative procedure, see Figure 4.3.

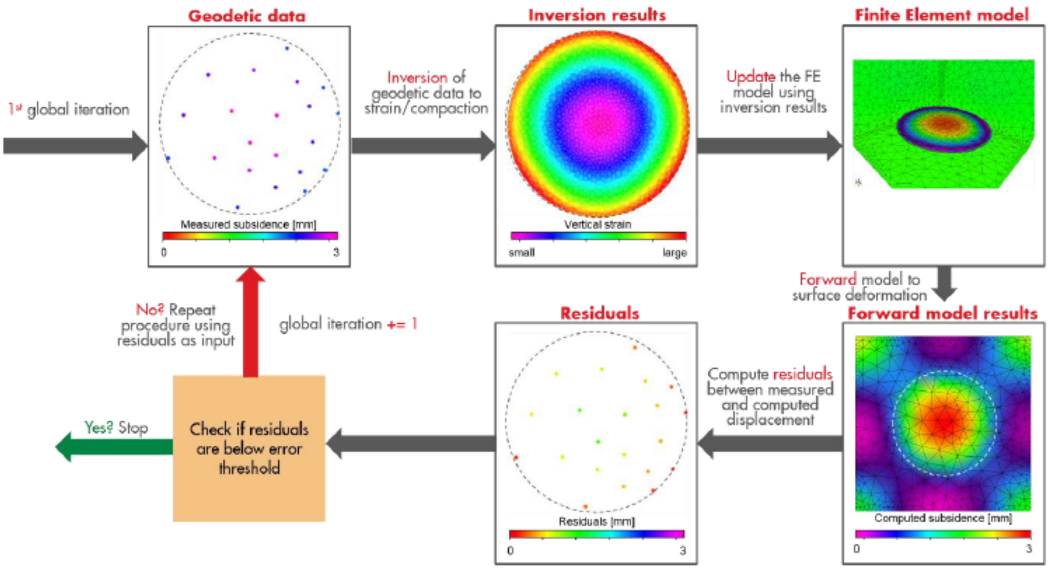

Figure 4.3: Inversion workflow as proposed by Bisdom et al. [9]. The workflow uses a Geertsma's nucleus-of-strain model, integrated with forward finite element models. The workflow is here applied to a synthetic dataset. Vertical surface displacement (top left) is inverted to reservoir strain or compaction (top middle). The updated reservoir compaction is used in a finite element model to forward-model surface displacement (down right). As long as the residual between modeled and measured displacement is above the acceptable threshold, the residual is inverted in iteration $n + 1$, repeating until the residual is below the threshold value (from Bisdom et al. [9])

The study makes use of estimated vertical displacement as input data. Uncertainty propagation has not been applied, because of the iterative nature of the workflow.

Regularised direct inversion to compaction in the Groningen reservoir using measurements from optical leveling campaigns: Bierman et al. [6] proposed a statistical methodology to estimate reservoir compaction through direct inversion using double-differenced measurements from optical leveling campaigns. This model does not use a prior compaction model to be not reliant on certain assumptions, as many of the other inversion studies do. Due to the absence of a prior model, regularization must be imposed to estimate compaction is different reservoir sections. regularization is achieved by imposing spatial smoothness on compaction estimates and by applying a non-negativity constraint.

The report does not talk about uncertainty of the used data, nor does it quantify measurement or idealisation noise. The uncertainty of the regularised compaction estimates has also not been given, nor is a methodology for assessing the error propagation given. This is mentioned as topic for future work.

4.4. Data-processing of LTS-II study

This section focuses on geodetic processing as performed for the LTS-II [46] study because this study gives an extensive description of the geodetic processing performed before measurements were used in the inversion. For other researches, this description usually misses. For the LTS-II study, both GPS and leveling data were prepared for subsidence modeling by the NAM with substantial support by Delft University of Technology [72]. Since the methodology proposed in this thesis works with leveling data, only LTS-II data processing from optical leveling campaigns will be described. For a description of processing and testing of the GPS data, see NAM [46] and Samiei-Esfehany and Bähr [57].

The leveling data consists of data from 26 optical leveling campaigns between 1986 and 2017. Hydrostatic leveling campaigns turned out to be too sparse for correct quality assessment, so these measurements were not used.

Samiei-Esfehany and Bähr [57] advised in 2015: "Use double differences with multiple reference epochs and points as an optimal interface between geodetic data and geomechanical modeling." In 2017, they revised this statement after more research to: "It can be concluded that the choice of the output level does not make a difference as long as the full covariance matrix is used.", which implies that no multiple reference epochs and points are needed, as long as the error propagation in processing steps is done adequately. So for the LTS-II research, spatio-temporal double-differences are used. This implies that changes in surface positions between two points in space and two epochs in time are used for the confrontation of measurements and subsidence model predictions. No assumption on a stable reference point is now necessary. A lot of double-differenced data in the LTS-II research has identical reference points and epochs and uncertainty is described by a full covariance matrix.
Measurement uncertainty was quantified with standard models, as described in section 2.3.3. Idealization noise is described by NAM [46] as "the displacements of the measurement points due to shallow movements like building settlement or soil compaction. Together with the measurement noise, it models the uncertainty of geodetic observations when used to quantify subsidence caused by (deep) reservoir compaction." The model that is used for the quantification of the idealization noise differentiates between 2 components:

- Temporal component: Shallow effects that are correlated in time but not in spatial extent,
- Spatio-temporal component: Shallow effects that are correlated in both space and time.

Idealization noise is estimated for each double-difference that is computed for the final analysis. Both idealization noise components are modeled by a five-parametric model described by Samiei-Esfehany and Bähr [57] [58]

$$\sigma_{DD}^2 = 2\sigma_t^2 \Delta t^{P_t} + 2\sigma_s^2 (1 - e^{-(\frac{\Delta d}{L}^2)} \Delta t^{P_s}, \tag{4.3}$$

where:

Δt	time difference,
Δd	spatial difference,
σ_t^2	the variance of the temporal component,
P_t	the power of the non-stationary signal associated with the temporal component,
σ_s^2	the variance of the spatio-temporal component,
P_s	the power of the non-stationary signal associated with the spatio-temporal component and,
L	correlation length.

The parameters of this idealization noise model were estimated with two datasets: (1) an onshore leveling dataset from an area where no gas production took place, to estimate both components, and

(2) an offshore leveling dataset, to calibrate the temporal component to relative intra-cluster movements.

Outlier handling was proposed in Samiei-Esfehany and Bähr [57] and implemented by van Leijen et al. [72]. Time series analysis is performed per benchmark of double-differences, with a common reference point and reference epoch. An a priori subsidence model is subtracted from the time series. A DIA-procedure is subsequently applied to the time series of the model residuals, to analyze for disturbances, identification errors and abnormal behavior, see Figure 4.4.

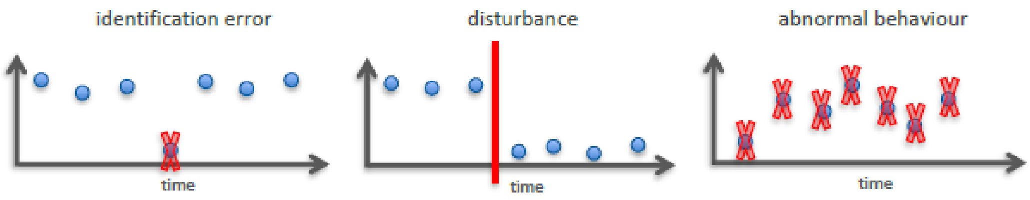

Figure 4.4: Alternative hypothesis to be tested in the LTS-II research with corresponding actions: identification errors are removed, at place of the disturbance, the timeseris is split in two and with abnormal behaviour, the entire time series is rejected (from NAM [46]).

The testing threshold in the DIA-procedure was largely increased because there were residual imperfections in the stochastic model and because of subsidence modeling imperfections and uncertainty. The consequence of this approach was that only obvious outliers were detected and the test statistic values for the confrontation of leveling observations and subsidence model predictions were far too high. To mitigate this, they tried additional outlier handling by visualizing time series and manually handling outliers. Even after this approach, test statistics were above the expected value, which can be an indication for a subsidence model mismatch, and it also became clear that remaining data outliers made a substantial contribution. To detect more outliers, they exploited the spatio-temporal smoothness of deformation signal caused by hydrocarbon production, by complementing the workflow with a spatio-temporal analysis of the geodetic observations. This is done by using a two-step approach: first, a zero deformation (a “null prognosis) is used to estimate a spatio-temporal correlated subsidence signal from the geodetic data. This estimation is then used as an approximation of the subsidence signal in a second run. The workflow of the outlier handling for the LTS-II study is visualized in Figure 4.5.

4.5. Discussion and conclusion

Research into geomechanical inversion can roughly be divided into three groups: (1) data assimilation methods, (2) methods that use geodetic data as validation and (3) direct inversion methods. These methods are characterized by the way the geodetic data is used as input into the inversion. For data assimilation methods, a confrontation between model states and geodetic data is done, to achieve a better estimation of the model state. Methods that use geodetic data as validation only use this data as a way of validating the outcomes of other physical models, so these methods do not use geodetic data actively. The third group, containing direct inversion method,is of most interest for this thesis. These methods use geodetic data as input data for an actual direct inversion. This means that the geomechanical estimates are usually in some form are expressed in function of geodetic data and that this system is inverted.

The input data and processing level for each methodology is different. Studies use either processed leveling, GPS or InSAR data. Bisdom et al. [9] and van Eijs and van der Wal [70] use surface displacement data at benchmark level. This means that geodetic data is used to estimate displacement at point level. Estimating displacements at point level introduces correlations in the covariance matrix of the data, and could possibly introduce biases, because a stable reference point has to be chosen. Other studies use geodetic data at other levels of processing, like NAM [46], Muntendam-Bos et al. [42], Fokker and van Thienen-Visser [17] and Bierman et al. [6], that use double differenced (spatio-temporal) leveling measurements.

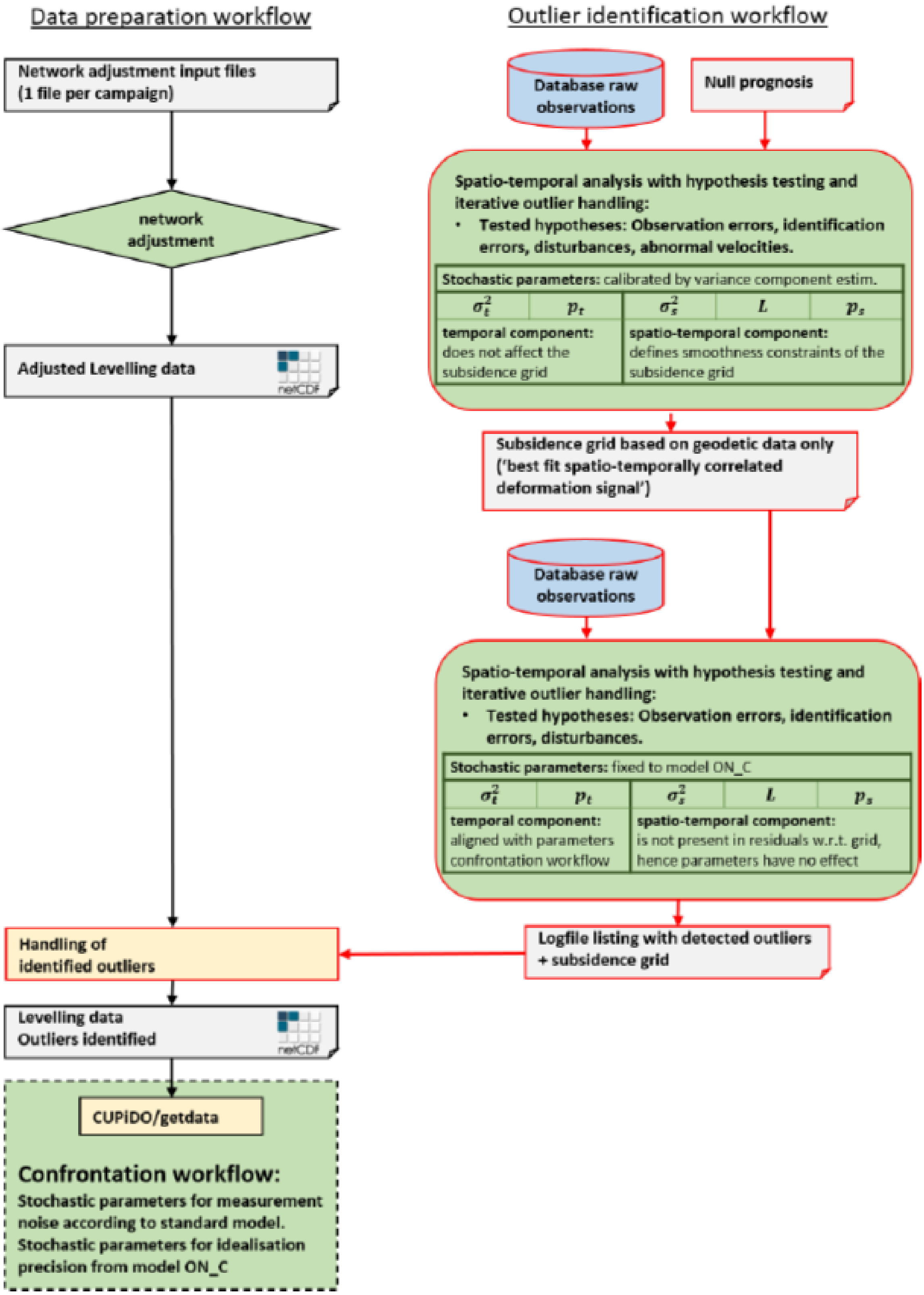

Figure 4.5: Outlier handling workflow for LTS-II (from NAM [46]).

Uncertainty quantification and error propagation is often not mentioned in previous research. Only NAM [46] mentions an extensive noise modeling and outlier handling and therefore a description of their workflow is disclosed in section 4.4. Muntendam-Bos et al. [42] and Fokker and van Thienen-Visser [17] estimate uncertainty of the model parameters, other works often acknowledge that uncertainty handling is part of future work.

The amount of information that is given to the inversion problems also differs per work. If we focus on the direct inversion methods, a few works update an existing physical model. Muntendam-Bos et al. [42] for example, updates a prior reservoir pressure model. Fokker and van Thienen-Visser [17] and van Eijs and van der Wal [70] update an existing reservoir compaction model. Other works don't use a prior model, like Bierman et al. [6], to not rely on certain assumptions (e.g. a prior reservoir compaction model). This however leads to the need of regularization.

The goal of this thesis is to develop a method in which geomechanical parameters are directly estimated from optical leveling measurements. This implies that the input data exists of non-differenced leveling data, which differs from all previous work mentioned above. With a direct inversion, error propagation is less complex and should be included. Uncertainty should be quantified, both measurement noise and idealization noise. Use of prior models does bring more information into the problem, but can also lead to reliance on wrong assumptions. If no prior assumptions on e.g. a compaction model are used, there might be a need for regularization.

5 Methodology

The goal of this thesis is to develop a methodology, which makes it possible to estimate geomechanical parameters directly from optical leveling measurements. The advantage of this direct relation between measurements and geomechanical parameters is the possibility to propagate geodetic uncertainties directly into geomechanical estimates. Currently, in Shell, the prevalent geomechanical inversion process takes three steps, see Figure 5.1. Optical leveling survey campaigns are organized and subsequently, a geodetic testing procedure is applied to the geodetic measurements by the SuRe software. SuRe adjusts measurements and adapts the design matrix and variance matrix accordingly to the outcome of the geodetic tests and delivers subsidence estimates as end-result. These subsidence estimates are used as input in the actual geomechanical inversion, performed by a geomechanical team. Estimation of subsidence (surface deformation) introduces correlated uncertainties, whereas the raw measurements are uncorrelated. The stochastic model for geodetic data that is currently deployed for geomechanical inversion is simplified and incomplete because it neglects correlations and only accounts for the uncertainty of the measurement itself.

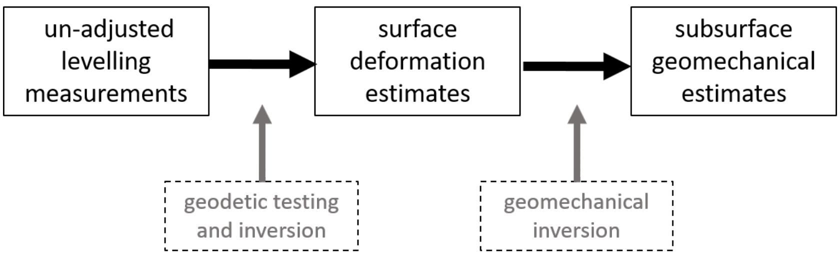

Figure 5.1: Current prevalent workflow for geomechanical inversion in Shell from geodetic data

The methodology proposed in this thesis removes the step in which surface deformation estimates are made, such that geomechanical parameters are directly estimated from geodetic measurements (see Figure 5.2). Geodetic testing is applied to the data, but no subsidence estimates are made. The extra information retrieved from the geodetic testing procedure is used to adjust the measurements. Error propagation for this process becomes less complex and computational heavy.

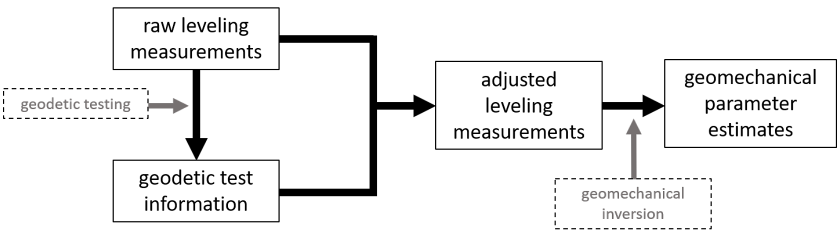

Figure 5.2: New proposed work flow for direct geomechanical inversion from geodetic data

The methodology is split into two parts: testing and processing of the data, to identify erroneous components in the data and to act on these outliers, and the actual inversion, where geomechanical parameters are estimated from the optical leveling measurements. Geodetic testing is performed with geodetic testing software currently used within Shell: SuRe. The geodetic department in Shell uses SuRe now predominantly to estimate subsidence, but for this thesis, SuRe will be used for the build-in geodetic testing procedures. After testing of the measurements, actual inversion takes place. The geomechanical parameterization used for this thesis is the Geertsma nucleus-of-strain model. The problem is ill-conditioned and thus regularization has to be applied.

5.1. Testing and processing of raw data

The first step of the new workflow is testing and subsequent processing of the raw leveling measurements of output level 0 (see Section 2.3.4 for an explanation of output levels). The input dataset consists of leveling measurements, which have not yet been adjusted. During each leveling campaign, the data has been tested for gross errors and if these are encountered, measurements were redone. The measurement noise for each measurement is considered known and is based on the length of the measured trajectory. Point noise for each measurement is added based on the adjusted variance model which is one of SuRe's output files. The point noise is computed with equation (2.35).

The data is not yet geodetically tested for any other outliers than gross measuring errors during the campaign. 4 types of outliers are considered: (1) observation errors, (2) benchmark identification errors, (3) benchmark disturbances and (4) abnormally fast benchmark displacement. With observation errors, an error in the measurement is encountered and the measurement is considered useless. A identification error is a measurement where another benchmark than indicated is measured. The data can still be used by bypassing the observation. If a measurement from benchmark A to B is done and from B to C and a identification error is encountered for benchmark B, a bypass can be made by combining the measurements of A and C. A disturbance error is an abrupt jump in the time series of a benchmark. This error can be solved by splitting the time series at the time of the jump. Figure 5.3 shows the concept of identification errors and disturbances. Abnormally fast behavior or idealization noise is indicated by a benchmark that behaves differently than expected, usually due to compaction of undeep layers or benchmark settling.

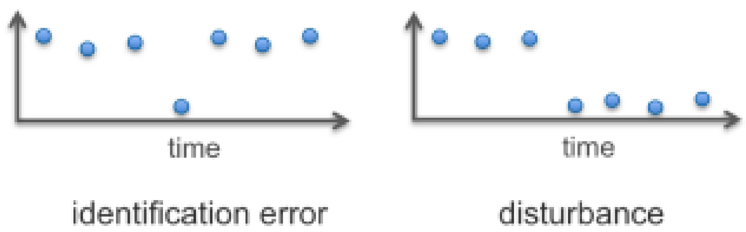

Figure 5.3: Concept of identication errors and disturbances in the timeseries of benchmark movement

To test the data for these outliers, the geodetic testing procedure of SuRe is applied. Part of the program is an extensive geodetic testing procedure, in which four 1D tests take place. The program tests respectively for observation errors, identification errors, benchmark disturbances, and abnormally fast benchmark movements. After each iteration, the program identifies the cause of the largest 1D error and solves the error appropriately by adjusting the observation(s), changing the variance model or deleting certain observations. For this methodology, SuRe is used only for the outcome of the geodetic testing procedure. One of the output files of SuRe is a log file with geodetic testing information per iteration. Based on this information, adjustments to the raw data and the uncertainty structure of the raw data are made:

- Observation error: the observation is deleted.
- identification error: a bypass is made.

- Disturbance: the time-series of the benchmark is split in two, by introducing a new benchmark.
- Abnormally fast displacement: the standard deviation of the measurement is adapted by adding a larger point noise standard deviation than for "normal" moving benchmarks. The idealization noise standard deviation of the abnormal fast-moving benchmark can also be found in SuRe's output files. By doing so, the measurement doesn't have to be rejected.

After the edits resulting from the testing procedure are done, the network is tested for disconnected network parts by testing if all benchmarks are connected with the reference benchmark.

SuRe is designed to make adjustments to the data, but these adjustments are not used for this workflow. The original height differences which also forms part of the input of SuRe are used as input for the geomechanical inversion together with the information given by SuRe.
As input, SuRe requires next to height differences a project file that states initial parameters for the variance model and a subsidence prognosis or subsidence model. This subsidence model is used to test the data against and the variance parameters are start parameters for the variance model. These parameters are later updated in the process, as is the subsidence model. To find out what the exact roles are of the subsidence prognosis and variance parameters on the results from SuRe, runs are done and the outcomes are compared, both on subsidence estimate level and flag level. The exact experiment set-up is described in Section 5.4.

5.2. Geomechanical inversion

The direct geomechanical inversion consists of a regularized least-squares inversion, weighted by the covariance matrix of the data. The forward geomechanical model is a Geertsma nucleus-of-strain model, with multiple nuclei to represent the reservoir. Vertical displacement of a point (x, y) on the surface due to multiple Geertsma nuclei is defined as (see also equation (2.21))

$$u_z^{t,t_0}(x,y,0) = \sum_{n=1}^{N} \frac{C_{m,n}(1-\nu_n)}{\pi} a_n V_n \Delta P_n^{t,t_0} \frac{d_n}{((x-x_n)^2+(y-y_n)^2+d_n^2)^{3/2}}, \tag{5.1}$$

where:

$u_z(x,y,0)$	Vertical displacement of a surface point with coordinates (x,y) between time t_0 and t,
$C_{m,n}$	Compaction coefficient of volume element V_n,
ν_n	Poissont's Ratio of volume element V_n,
a_n	Biot's coefficient of volume element V_n,
V_n	Volume of reservoir element represented by nucleus n,
$\Delta P_n^{t,t0}$	Pressure reduction in volume element V_n between time t_0 and t,
d_n	Depth of nucleus n,
x_n	x-coordinate of nucleus n,
y_n	y-coordinate of nucleus n.

This equation can be simplified by grouping terms $\Delta S_n = \frac{C_{m,n}(1-\nu_n)}{\pi} a_n V_n \Delta P_n$ and by grouping terms $R_n^3 = ((x-x_n)^2+(y-y_n)^2+d_n^2)^{3/2}$. Equation (5.1) simplifies to

$$u_z^{t,t_0}(x,y,0) = \sum_{n=1}^{N} \Delta S_n^{t,t_0} \frac{d_n}{R_n^3}, \tag{5.2}$$

where R_n is the distance from the surface point to the nucleus and $\Delta S_n^{t,t_0}$ is the change in the so-called "source term" between time t_0 and t. The source term is a lumped parameter term, that consists of

$$\Delta S_n^{t,t_0} = \frac{C_{m,n}(1-\nu_n)}{\pi} a_n V_n \Delta P_n^{t,t_0}. \tag{5.3}$$

The goal of the inversion is to use the leveling measurements as input and to give an estimate of each source term ΔS_n and corresponding uncertainties of the estimates.

The input data for this inversion does however not consist of vertical displacements of surface points but of differential leveling measurements h^t_{ij}, thus spatial height differences between points i and j at time t. To express these spatial height differences in function of Geertsma's nuclei, we have to introduce initial heights H^{t0}_i and H^{t0}_j to add a temporal difference to the equation. The data is "spatial differenced", which means that within each campaign the measured height of each benchmark is expressed as relative to the height of another benchmark and "temporal differenced", meaning that the difference between two campaigns of the measured relative height differences between benchmarks is estimated, by estimating an initial height. The equation relating spatial height differences to temporal height differences is as follows

$$E\{\underline{h}^t_{ij}\} = h^{t0,t}_j - h^{t0,t}_i + H^{t0}_j - H^{t0}_i, \tag{5.4}$$

where the spatial height difference h^t_{ij} is expressed as function of temporal height differences $h^{t0,t}_j$ and $h^{t0,t}_i$ by introduction of initial heights H^{t0}_j and H^{t0}_i. The temporal height differences are equal to the vertical displacement term u_z of equation (5.2). This means that now we can express the spatial height difference as function of Geertsma nuclei

$$E\{\underline{h}^t_{ij}\} = \sum_{n=1}^{N} \Delta S^{t,t0}_n \frac{d_n}{R^3_{n,j}} - \sum_{n=1}^{N} \Delta S^{t,t0}_n \frac{d_n}{R^3_{n,i}} + H^{t0}_j - H^{t0}_i. \tag{5.5}$$

The location, depth, and the number of nuclei are considered known, the source terms and the initial heights are unknowns. This equation can be further simplified to

$$E\{\underline{h}^t_{ij}\} = \sum_{n=1}^{N} \Delta S^{t,t0}_n \frac{d_n}{R^3_{n,j} - R^3_{n,i}} + H^{t0}_j - H^{t0}_i. \tag{5.6}$$

At the time of the measurements of the first survey campaign at t_0, subsidence is assumed to be 0 so the expectation of the measurements at $t0$ can be expressed only in terms of the initial heights

$$E\{\underline{h}^{t0}_{ij}\} = H^{t0}_j - H^{t0}_i. \tag{5.7}$$

When performing an inversion, one of the initial heights should be set to 0. All the other initial heights are then estimated relative to that benchmark height. Not setting one of the benchmark heights to 0 causes singularities in the inversion.

The linear system of equations $E\{\underline{y}\} = Ax$ incorporating equations (5.6) and (5.7) is different for each case. The design of A depends on how many measurements campaigns are used, which measurements are done during a campaign, and what kind of parameterization of the geomechanical model is used. An example of how the linear system of equations could look like is undermentioned in Equation (5.8). For this system, we have z measurement campaigns and j benchmarks. Each measurement campaign could consist of a different number of measurements, the only requirement is that each measurement from benchmark a to b should be executed at least during two measurement campaigns. Height differences observed once do not contribute to the final solution. For this example, the height difference between points 1 and 2 $h_{1,2}$ is measured during each campaign

$$E\left\{\begin{bmatrix} h_{1,2}^{t0} \\ \vdots \\ h_{i,j}^{t0} \\ h_{1,2}^{t1} \\ \vdots \\ h_{i,j}^{t2} \\ \vdots \\ h_{1,2}^{tz} \\ \vdots \\ h_{i,j}^{tz} \end{bmatrix}\right\} = \begin{bmatrix} 0 & \cdots & 0 & \cdots & 0 & \cdots & 0 & 1 & 0 & \cdots & 0 & 0 \\ \vdots & \ddots & \vdots & \ddots & \vdots & \ddots & \vdots & \vdots & \vdots & \ddots & \vdots & \vdots \\ 0 & \cdots & 0 & \cdots & 0 & \cdots & 0 & 1 & 0 & \cdots & 0 & 0 \\ \frac{d_1}{R_{1,2}^3 - R_{1,1}^3} & \cdots & \frac{d_N}{R_{N,2}^3 - R_{N,1}^3} & \cdots & 0 & \cdots & 0 & 1 & 0 & \cdots & 0 & 0 \\ \vdots & \ddots & \vdots & \ddots & \vdots & \ddots & \vdots & \vdots & \vdots & \cdots & \vdots & \vdots \\ \frac{d_1}{R_{1,j}^3 - R_{1,i}^3} & \cdots & \frac{d_N}{R_{N,j}^3 - R_{N,i}^3} & \cdots & 0 & \cdots & 0 & 0 & 0 & \cdots & -1 & 1 \\ \vdots & \ddots & \vdots & \ddots & \vdots & \ddots & \vdots & \vdots & \vdots & \cdots & \vdots & \vdots \\ 0 & \cdots & 0 & \cdots & \frac{d_1}{R_{1,2}^3 - R_{1,1}^3} & \cdots & \frac{d_N}{R_{N,2}^3 - R_{N,1}^3} & 1 & 0 & \cdots & 0 & 0 \\ \vdots & \ddots & \vdots & \ddots & \vdots & \ddots & \vdots & \vdots & \vdots & \cdots & \vdots & \vdots \\ 0 & \cdots & 0 & \cdots & \frac{d_1}{R_{1,j}^3 - R_{1,i}^3} & \cdots & \frac{d_N}{R_{N,j}^3 - R_{N,i}^3} & 0 & 0 & \cdots & -1 & 1 \end{bmatrix} \begin{bmatrix} \Delta S_1^{t1} \\ \vdots \\ \Delta S_N^{t1} \\ \vdots \\ \Delta S_1^{tz} \\ \vdots \\ \Delta S_N^{tz} \\ H_1^{t0} \\ \vdots \\ H_j^{t0} \end{bmatrix}. \quad (5.8)$$

The vector of estimators consists of system of equations (5.8) consists of terms for the source parameters (ΔS_x^{ty}) and initial benchmarks heights (H_z^{t0}). The measurement noise of the un-adjusted measurements is captured in its covariance matrix Q_e

$$Q_e = \begin{bmatrix} \sigma^2_{h_{1,2}^{t0}} & & 0 \\ & \ddots & \\ 0 & & \sigma^2_{h_{i,j}^{tz}} \end{bmatrix}, \quad (5.9)$$

The idealization noise, captured in Q_{dI} for each measurement is added to this, following equation (2.28). The idealization noise is computed with equation (2.35), with parameters found in SuRe's output file. For measurements with a abnormally fast displacement flag, a larger term for the standard deviation of autonomous benchmark displacement is used, this larger term is found in one of SuRe's output files. This system is inverted using regularized least-squares inversion as described in chapter 3.

Due to the ill-conditioned nature of the problem, Tikhonov regularization is applied by penalizing first-order spatial differences between estimates of compaction in neighboring reservoir blocks or sections. The larger the penalty on spatial differences the more the estimates of compaction in reservoir sections are restricted to vary smoothly over space.

For the Tikhonov regularization matrix, a first-order spatial neighborhood matrix is used. The exact design of L depends on the distribution of nuclei over the reservoir. Each nucleus represents a volume section of the reservoir. This thesis uses two different parameterizations: a centroid parameterization and a grid parameterization. For the centroid parameterization, the centroid or center of mass of each reservoir block is computed (assuming a constant reservoir thickness). The centroid of each reservoir block represents a Geertsma nucleus, see Figure 5.4. The centroid of each reservoir block is chosen because of the assumption that maximum deformation from each reservoir block is located at the center of the mass of the reservoir block. The depth of each nucleus is assumed to be the depth of the top of the reservoir at the centroid location.

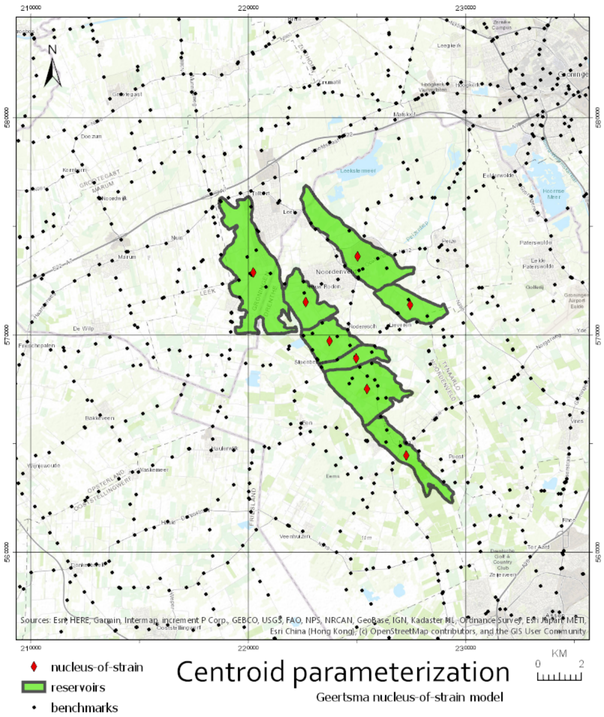

Figure 5.4: Centroid parameterization of Geertsma nucleus-of-strain model

For the centroid parameterization, the Tikhonov regularization matrix is designed such that large differences between source estimates of neighboring blocks are penalized. On the main diagonal a value that resembles minus the number of neighboring reservoir blocks is set. Each neighboring block gets a 1 on the off-diagonal. The rest of the off-diagonal values are 0. For the initial height estimates, the diagonal of that part of the L matrix consists of ones, because there is no spatial relationship between these points since they can be arbitrarily located at different heights. A "1" on the main diagonal means that the method will try to minimize the norm of that solution. The first 8 rows and columns and last rows and columns of the regularization matrix L for the centroid parameterization look like

$$L = \begin{array}{r} \Delta S^{t1}_{ROD1} \rightarrow \\ \Delta S^{t1}_{ROD2} \rightarrow \\ \Delta S^{t1}_{NOR1} \rightarrow \\ \Delta S^{t1}_{NOR2a} \rightarrow \\ \Delta S^{t1}_{NOR2b} \rightarrow \\ \Delta S^{t1}_{NOR2c} \rightarrow \\ \Delta S^{t1}_{NOR3} \rightarrow \\ \Delta S^{t1}_{NOR4} \rightarrow \\ \vdots \\ \vdots \\ H^{t0}_{i} \rightarrow \\ H^{t0}_{j} \rightarrow \end{array} \begin{bmatrix} -1 & 1 & 0 & & & \dots & & & & & 0 & 0 \\ 1 & -1 & 0 & & & \dots & & & & & 0 & 0 \\ 0 & 0 & -1 & 1 & & & & & & & & \\ & & 1 & -2 & 1 & & & & & & & \\ & & & 1 & -2 & 1 & & & & & & \\ \vdots & & & & 1 & -2 & 1 & & & & \vdots & \vdots \\ & & & & & 1 & -2 & 1 & & & & \\ & & & & & & 1 & -1 & & & & \\ & & & & & & & & \ddots & & & \\ & & & & & & & & & \ddots & & \\ 0 & & & & & \dots & & & & 0 & 1 & 0 \\ 0 & & & & & \dots & & & & 0 & 0 & 1 \end{bmatrix}. \tag{5.10}$$

The second parameterization consists of a grid set-up, with a pre-defined grid spacing. For this parameterization, L again is a spatial penalty matrix with now on the diagonal minus the number of neighbors in the Queen neighborhood of each of the neighboring reservoir sections. A value of 1 for each of the off-diagonal elements that represent a neighboring reservoir block is set. All other off-diagonal elements get a value of 0. An illustration of a Queen's neighborhood for a reservoir split up in 9 quadrants with the corresponding regularization L are given in Figure 5.5 and equation (5.11). The elements representing the initial heights again get a value of 1 on the diagonal. All other off-diagonal elements are 0.

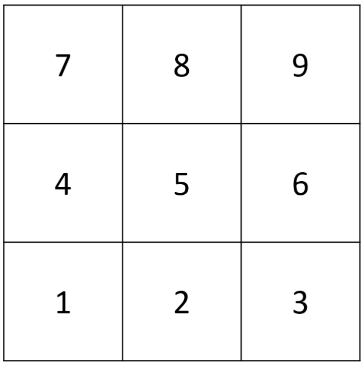

Figure 5.5: Illustration of a Queen's neighbourhood, which was used for defining the Tikhonov regularization matrix L (equation (5.11)). The Queen's neighbourhood is used for the grid parameterization.

$$L = \begin{bmatrix} -3 & 1 & 0 & 1 & 1 & 0 & 0 & 0 & 0 & \dots & 0 & 0 \\ 1 & -5 & 1 & 1 & 1 & 1 & 0 & 0 & 0 & & & \\ 0 & 1 & -2 & 0 & 0 & 1 & 0 & 0 & 0 & & & \\ 1 & 1 & 0 & -5 & 1 & 0 & 1 & 1 & 0 & & & \\ 1 & 1 & 1 & 1 & -8 & 1 & 1 & 1 & 1 & & \vdots & \vdots \\ 0 & 1 & 1 & 0 & 1 & -5 & 0 & 1 & 1 & & & \\ 0 & 0 & 0 & 1 & 1 & 0 & -3 & 1 & 0 & & & \\ 0 & 0 & 0 & 1 & 1 & 1 & 1 & -5 & 1 & & & \\ 0 & 0 & 0 & 0 & 1 & 1 & 0 & 1 & -3 & & & \\ \vdots & & & & & & & & & \ddots & & \\ 0 & & & & & \dots & & & & & 1 & \\ 0 & & & & & \dots & & & & & & 1 \end{bmatrix} \tag{5.11}$$

The optimal regularization parameter λ_{optim} is computed using cross-validation, by evaluating a range of candidate parameters. Recursively the parameter column $\hat{x}$ is estimated with a subset of all available measurements, after which the measure of the fit of the estimated measurements as predicted by the resulting model is evaluated to the measurements that have been omitted from the total data set. This is a form of k-fold cross-validation as described in Section 3.3. The following steps are used in the algorithm for cross-validation to find the optimal regularization parameter:

1. Partition the dataset of observations into k groups. For this thesis, a 4-fold CV scheme was used, which means that a grid was overlaid on the dataset partitioning the data in 4 subsets. The observations are assigned to a subset based on the midpoint of the measured trajectory. There are observations from all survey campaigns in each subset.

2. For each of the k subsets of the dataset and a range of candidate values for λ, the following steps are taken:

    (a) The dataset is split up in an testset y_{test} and a training set $y_{training}$. The design matrix is adapted accordingly to the training set ($A_{training}$).

    (b) The reduced training data set and adapted design matrix ($A_{training}$) are used to compute a regularized solution $\hat{y}$.

    (c) The sum of squared differences S_k between the predicted and observed observations from the test data set is computed ($S_k = ||y_{test} - \hat{y}||^2$).

3. Evaluate for which λ the sum of all squared differences $S_{tot} = \sum_k S_k$ is minimized, this is λ_{optim}.

4. Use λ_{optim} for the actual regularised inversion.

To check whether the model fits the data, an overall model test is performed as described in Section 2.4. If the OMT is not accepted, a w-test is applied to identify and delete the observations that cause this failure.

5.3. General description of the workflow

Testing and processing of raw data and a description of the geomechanical inversion process are given in previous sections. This section gives a brief overview of all steps that should be taken when using the proposed workflow:

1. Importing all raw leveling data from area and period of interest from the database.
2. Importing reservoir data:
   (a) Reservoir geometry: outlines reservoir blocks, top of reservoir data, reservoir thickness
   (b) Geographical center-points of reservoir blocks or center-points of grid division of reservoir
3. Geodetic testing with SuRe, saving geodetic test report and adjusted variance model.
4. Adding point noise to variance model of all measurements, based on Sure's adjusted variance model outcome.
5. Adjustment of raw measurements based on geodetic test report:
   (a) Observation error: observation is deleted.
   (b) identification error: bypassing the affected benchmark. If benchmark b is misidentified, the trajectories $a \rightarrow b$ and $b \rightarrow c$ are combined to a new observation $a \rightarrow c$. The uncertainty of the observation is adjusted accordingly.
   (c) Disturbance error: the time-series of the affected benchmark is split, the observations after the disturbance are assigned to a new benchmark.
   (d) Abnormal behaving benchmark: the uncertainty of the observation is increased by adding the estimated point noise. The point noise estimation is based on SuRe's adjusted variance model outcome.
6. Defining a reference benchmark that is measured during every measurement campaign. Removing all network parts that are disconnected from the reference benchmark.
7. Remove all measurements that have the same "from" and "to" coordinates.
8. Regularised inversion:
   (a) Defining a design matrix A and a regularization matrix L,
   (b) Compute regularization parameter λ with m-fold cross validation
   (c) Perform actual inversion
   (d) Check whether overall model tests gets accepted, otherwise redo inversion after w-test.
9. Interpretation of results
   (a) Forward model subsidence based on source strength estimates
   (b) Plot initial height estimates and visually compare them with the elevation model.

5.4. Experiments

To get insight into the used model, to research the outcomes of the geodetic testing procedure and to prove the feasibility of the proposed methodology, several experiments are designed. The experiments are split up in three parts:

1. Experiments with the Geertsma nucleus-of-strain methodology to see what the implications of the model are. Forward modeling is applied in which the depth of the source is changed, to assess the influence of the assumed depth on the source terms. Also, an assessment of the size of the subsidence bowl is made. Forward modeling is applied to the assumed parameterizations from the case study to find a rough approximation of the expected source strengths and amount of subsidence.
2. SuRe input sensitivity experiments to see what the influence of the input parameters on the outcome of the geodetic testing procedures and the final subsidence estimates is.
3. Inversion experiments, where the proposed workflow is applied to real geodetic data.

5.4.1. Geertsma nucleus-of-strain experiments

Goal: The goal of these experiments is to implement the used model into software and to assess the model with a couple of forward modeling experiments. The three subgoals of these experiments are:

1. To analyze the influence of the depth of the source on the expected subsidence and the size of the subsidence bowl. The size of the subsidence bowl is analyzed by computing at which distance $x_{u_{z,\text{fraction max}}}$ the vertical displacement u_z is a fraction of the maximum vertical displacement at the center of the bowl ($x = 0$), right above the source. This can be done with equation (5.12).

$$x_{u_{z,\text{fraction max}}} = \sqrt{\left(\frac{u_{z,x}}{u_{z,0}} \cdot dz^{-3}\right)^{-2/3} - dz^2}, \tag{5.12}$$

   with dz being the depth of the source and $u_{z,x}$ the displacement on location x. In the inversion workflow, the location and depth of the Geertsma are assumed known. With these experiments, an assessment of the influence of the depth of the sources is made.

2. To use the forward model to assess how large the source strengths are if certain assumptions regarding the parameters in the Geertsma model are made. The parameters are chosen based on reports by de Kloe et al. [12] and Nagelhout and Roest [43] and with the reservoir maps from NLOG [51], which can be found in Appendix A.

3. To forwardly model the amount of subsidence expected from the source strengths, estimated in experiment 2.

5.4.2. SuRe sensitivty experiments

Goal: The goal of these experiments is to see what influence the input parameters have on SuRe output, both on the test results and the final subsidence estimates. To assess the effect of each parameter, the software is ran multiple times, each time with different input settings. The outcomes are compared to the outcomes of a default setting. The SuRe input consists of:

- Prognosis grids, which serve as an approximate subsidence model. At least 2 subsidence grids are required, that must comprise the subsidence reference date and the range of observation dates. The grid northing and easting range must comprise the coordinates of all observations,

- A variance model, that gives initial values for the 5 variance model parameters used for the stochastic model,

- A test criterion, which specifies the significance of the 1D tests.

With this input, SuRe starts an analysis and finally gives full results. The SuRe output consists of:

- Subsidence estimate grids, with the amount of subsidence at the reporting date, relative to a reference date.

- Subsidence estimates at benchmark level, again with the amount of subsidence at the reporting date, relative to a reference date. These values are taken from the grid cells in which the benchmarks are located.

- Test results, which indicate which observations get flagged because they have led to the failure of a 1D test. This flag can be (1) an observation error, which indicates a failure in the observation, (2) a benchmark identification error, which means that the leveling beacon is inaccurately placed on the benchmark or another benchmark, (3) a benchmark disturbance and (4) abnormally fast benchmark displacement.

- A re-tuned variance model, where the parameters of the variance model are adapted to the prevailing noise patterns, such that the overall model test gets accepted.

To analyze the implications of the input on the SuRe output, several runs of the case study data with different input values are done and the output is analyzed. First, default values need to be established such that all outcomes can be compared with these default values. The default values are based on experience from the NAM. The default grids and parameters are summarized in Table 5.1. With 0-prognosis, a zero subsidence model is prepared that is used as a prognosis grid, at both a date before the first observation and a date after the last observation.

Table 5.1: Default parameters for SuRe sensitivity experiments.

Input	**Parameter**	**Value**
Prognosis grids	-	0-prognosis
Variance model	SD factor for measurement noise	1.00
	SD for autonomous displacement	0.33
	Power of autonomous displacement	0.75
	SD of prognosed subsidence model	2.7
	Power of prognosed subsidence model	0.75
	Correlation length of prognosed subsidence model	4000
Test criterion	α_0	0.001

The result of this default input is used to compare the results of runs with other input values. For each run, only 1 input value is changed, such that the influence of each input value on the output data can be analyzed, see Table 5.2. For the first run, the 0-prognosis grids are substituted for a geometrical subsidence estimation grid at each survey campaign date. This subsidence estimation is a model developed by Quadvlieg [55], details of this model are given in section 5.5.2. This model is assumed to give a more realistic subsidence model than the 0 prognosis. All input parameters of the variance model are increased and decreased relative to the default values, except for the factor of the standard deviation of the measurement noise, because this value is considered known. SuRe testing is finished with increasing and decreasing the test criterion α_0, to see what effect this has on the outcomes.

Table 5.2: Input set up SuRe tests

Prognosis grid	**Variance model**						**Test criterion**
	Meas. noise	Point noise		Model noise			
	S.D. factor	S.D. $[\frac{mm}{yr^P}]$	P [-]	S.D.$[\frac{mm}{yr^P}]$	P [-]	C.R. [m]	α_0 [-]
Geometric	1.0	0.33	0.75	2.7	0.75	4000	0.001
0	1.0	0.10	0.75	2.7	0.75	4000	0.001
0	1.0	1.0	0.75	2.7	0.75	4000	0.001
0	1.0	0.33	0.55	2.7	0.75	4000	0.001
0	1.0	0.33	0.95	2.7	0.75	4000	0.001
0	1.0	0.33	0.75	1.0	0.75	4000	0.001
0	1.0	0.33	0.75	5.0	0.75	4000	0.001
0	1.0	0.33	0.75	2.7	0.55	4000	0.001
0	1.0	0.33	0.75	2.7	0.95	4000	0.001
0	1.0	0.33	0.75	2.7	0.75	3000	0.001
0	1.0	0.33	0.75	2.7	0.75	5000	0.001
0	1.0	0.33	0.75	2.7	0.75	4000	0.0001
0	1.0	0.33	0.75	2.7	0.75	4000	0.01

To compare the outcome of a SuRe run with certain input parameters with the outcome of the SuRe run with default parameters, the RMSE is computed. For two subsidence grids of size $M \times N$, the RMSE can be computed as

$$\text{RMSE} = \sqrt{\frac{1}{MN}\sum_{m=1}^{M}\sum_{n=1}^{N}(u_1(m,n) - u_2(m,n))^2}, \tag{5.13}$$

where u is the amount of subsidence at a grid cell with coordinates (m, n). SuRe can give more than 1 output grid, it can give output grids with subsidence at every requested reference date. The RMSE can not only be computed to compare individual grids at 1 reference date, but also to compare all outcome grids if more reference dates are used

$$\text{RMSE} = \sqrt{\frac{1}{MNZ}\sum_{z=1}^{Z}\sum_{m=1}^{M}\sum_{n=1}^{N}(u_1(m,n,z) - u_2(m,n,z))^2}, \tag{5.14}$$

where Z is the total amount of output grids (and thus reference dates). Benchmark subsidence is extracted from the grid subsidence estimates. Therefore, no tests on benchmark subsidence estimates are done.

5.4.3. Inversion experiments

Goal: the goal of the inversion experiment is to assess if the proposed methodology works on a case study. The proposed steps in the workflow will be applied on optical leveling data from the Norg and Roden field, to see the effects of data testing, processing, and regularisation. Finally, the results for different parameterizations are compared. The tested parameterizations are:

- Centroid parameterization: 1 nucleus represents every reservoir block,
- Three nuclei in Norg reservoir. two in Roden,
- One nucleus in each reservoir,
- A grid parameterization, where both reservoirs are filled with a grid with a 1 kilometer spacing.

For each parameterization, the estimated source parameters will be given, together with uncertainty. These estimates will be used in a forward model to compute subsidence. The RMSE (root-mean-square-error) for each inversion is given, as is the amount of rejected obseravations (after the w-test) and the test statistic with critical value.

5.5. Case study: Norg and Roden

The methodology developed in this thesis is applied to a dataset with optical leveling measurements from multiple geodetic surveys from an area in the vicinity of two gas fields in the Northern Netherlands. The fields are called the Norg field and the Roden field. The location of the Norg gas field and the Roden gas field can be found in Figure 5.6. Some key numbers of the fields are summarized in Table 5.3. The Roden field was produced for 27 years starting in 1976, whereas production of the Norg field started in 1983 and lasted for 12 years. The Roden field is currently abandoned and the Norg field has been turned into an underground gas storage [48].

5.5.1. Geology

The north-eastern part of the Netherlands is structurally dominated by an NW-SE trending pull-apart system which has been formed by a complex interplay of wrench tectonics [19]. The geological structures of the Norg field and Roden field are dominated by two major fault systems, which are associated with the tectonic wrench system: NW-SE faults and NE-SW faults are present at the reservoir level. As shown in Figure 5.7, natural gas in the Norg field was structurally trapped by a large normal fault, which bounds the NE-dipping reservoir [43]. Due to tectonic activity, numerous faults of different types are present in the reservoir. The Norg field has been subdivided into 4 blocks, with block 2 forming the

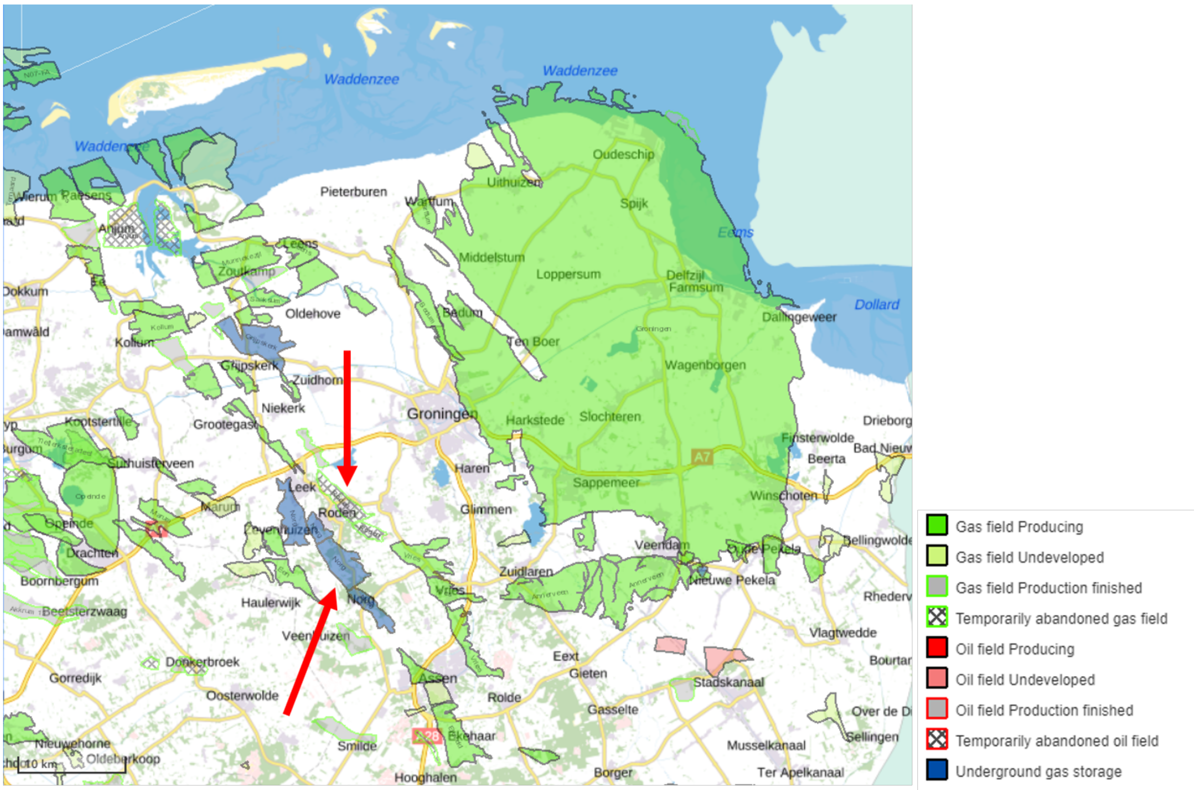

Figure 5.6: Location of Norg and Roden field with respect to other gas field in the northern Netherlands (adapted from NLOG [50]).

Table 5.3: Key numbers Norg and Roden fields (all derived from NLOG [51]).

	Roden	**Norg**
discovery	1970	1965
start production	1976	1983
end production	2003	1995
number of wells	3	13
average reservoir height	165 m	140 m
approximate area	10 km^2	30 km^2
current status (2019)	temporarily abandoned	underground gas storage
depth top reservoir	$\pm$ 2875 - 3025	$\pm$ 2700 - 2850
gas water contact	3021 m	block 1-3: 2847 m block 4: 2860 m

main part of the field (Figure A.1). SW-NE trending extensional faults form the boundaries of the blocks. These faults are not sealing and all blocks are in pressure communication. This has been inferred by similar pressure depletion encountered at wells at different blocks and by the similar GWC and gas compositions [44]. The Roden field has been subdivided by a non-sealing fault into two blocks, see figure A.2.

The Norg and Roden reservoirs are both made up of the Upper Rotliegend group, subdivided into the Slochteren sandstone and Lower ten Boer formations. These formations consist of fine to coarse sandstone deposits with local conglomerates. The lowermost reservoir unit is a few meters thick and consists of the Lower Slochteren Member and consists of fluvial and/or fan conglomerate deposits. This unit shows relatively low porosity. The Lower ten Boer unit makes up the largest part of the reservoir thickness and has a considerably higher porosity and permeability [43]. On top of the Rotliegend, we find the Zechstein Group: a sequence consisting of evaporites and carbonates with some thin intercalations of claystone of about 360 meters thick [44]. This layer acts as a caprock.

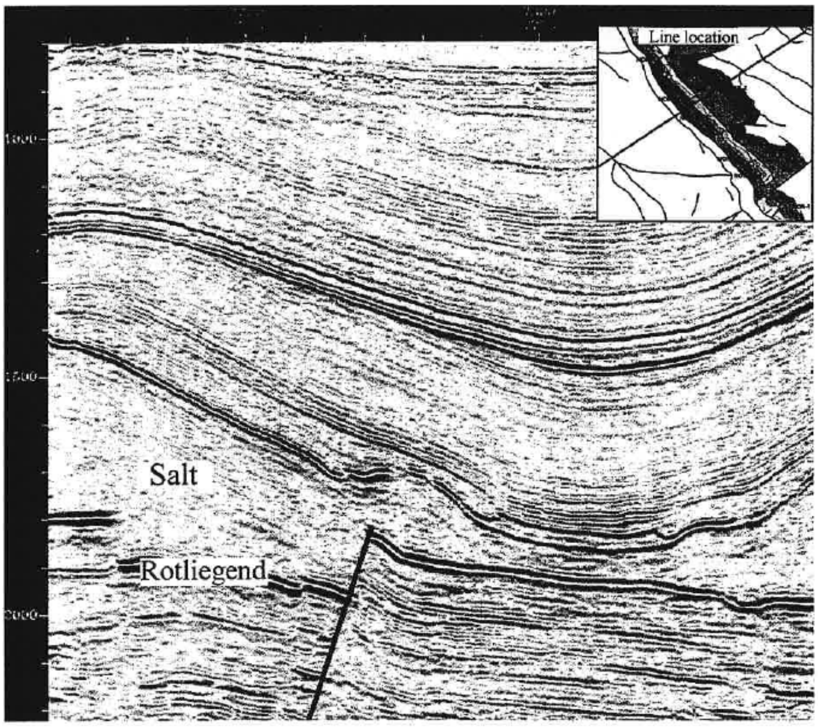

Figure 5.7: Seismic section of Norg. Depth is indicated by two-way traveltime (msec). The reservoir is located to the right side of the indicated fault, underneath the salt layer (from Nagelhout and Roest [43]).

The shallow subsurface in the vicinity of the Norg and Roden field consists mainly of sand, as can be seen in Figure 5.8, where soil data from the WUR [79] (Wageningen University Research) is visualized with reservoir outlines and all measured benchmark locations. The majority of the 886 benchmarks are founded in sandy soil. Mainly in the north-eastern part of the research area, benchmarks are founded in peat or clay. In the upper north-east corner, all benchmarks are located in the build-up area of the city of Groningen.

5.5.2. Production and subsidence

Historic pressure data for Norg (Figure 5.9) underlines the years given in Table 5.3. It can be observed that production in Norg started in 1983 and stopped in 1995. During the production period, the pore pressure dropped from 325 bar to 185 bar. This figure also illustrates that pressure does not differ much between wells located at different blocks. The wells mentioned in this figure can be found on the map in Appendix A.

Production of the Roden field commenced in 1976 and continued until 2003 when production stopped. Measurements were done at the three Roden wells and are visualized in Figure 5.10. From 1986 the

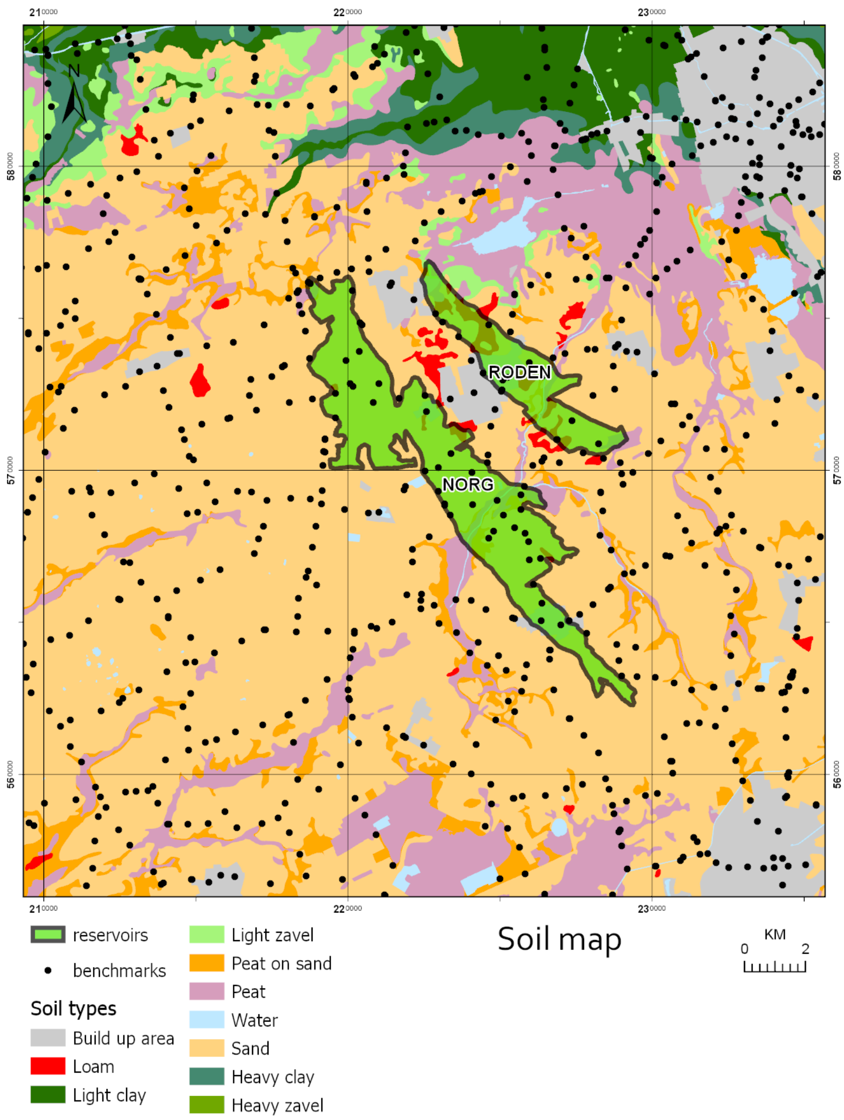

Figure 5.8: Soil types with benchmark locations and reservoirs (with data from WUR [79]).

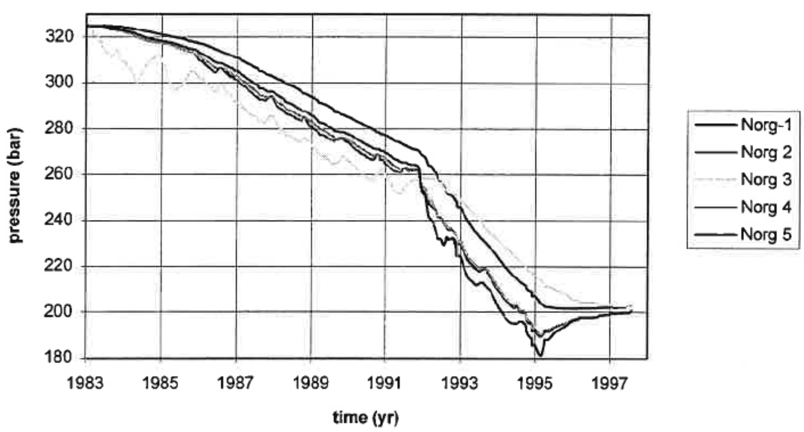

Figure 5.9: Pore pressure development for Norg, based on historic well data (from Nagelhout and Roest [43]).

Roden-201 well was not able longer to contribute and ceased the gas production. As the sand column in the southern block of the Roden field is shallower than in the northern Roden block, the southern block was more sensitive to water breakthrough. The volume connected to the well is also small. While the expanding aquifer was moving into depleted gas zones the reservoir pressure was rising while the well was idle. The pressure at the Roden-201 well declined down to 180 bar and rose to 270 bar. The other two wells (Roden-101 and Roden-102) kept producing until the field was abandoned in 1995.

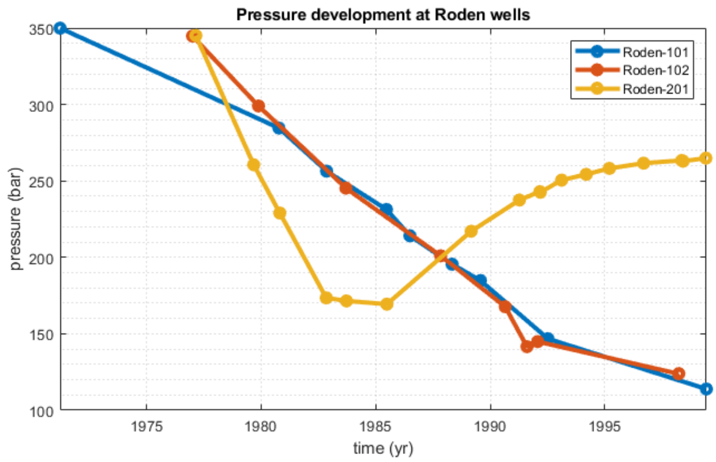

Figure 5.10: Pore pressure development for Roden, based on historic well data. Location of wells can be found on map in A.

The NAM is obliged to comply with legislation and has to report deformation due to the production of hydrocarbons, to retain their license to produce and to safeguard the integrity of infrastructure. Therefore, the NAM frequently publishes reports on subsidence [47]. In 2000, Quadvlieg [55] analyzed optical leveling measurement in the vicinity of Roden and Norg to describe the subsidence due to gas production in Norg and Groningen. For this analysis, leveling measurement from 1975 until 2000 were used. The subsidence analysis was split up into two parts: the period from 1975-1997 and 1997-2000. From 1997 onward the Norg has been used as underground gas storage and the NAM expected a heave. A comparison was made for both periods.

The subsidence model that was used for this analysis is purely geometrical, modeling the subsidence as two overlapping elliptical bowls, one for each gas field. The subsidence z at time t for a point with coordinates x and y is computed with

$$z\{x,y,t\}\begin{cases}0, & \text{if } t \leq t_0\\ \dot{z}(t-t_0)\exp -r^2/2, & \text{if } t_0 < t < t_e\\ \dot{z}(t_e-t_0)\exp -r^2/2, & \text{if } t \geq t_e,\end{cases} \tag{5.15}$$

with

$$\begin{aligned} r^2 &= u^2+v^2\\ u &= ((x-x_0)\sin\alpha+(y-y_0)\cos\alpha)/A\\ v &= ((x-x_0)\cos\alpha+(y-y_0)\sin\alpha)/B, \end{aligned} \tag{5.16}$$

where:

z	: subsidence due to hydrocarbon production
x, y, t	: coordinates surface point and time
t_0,t_e	: start and end time of linear subsidence trend
x_0, y_0	: coordinates of centre of subsidence bowl
A, B	: distance from centre of bowl to steepest slope of bowl, long and short axis of the bowl
α	: angle of long axis of the bowl
$\dot{z}$	: subsidence velocity at centre of bowl

The estimated total subsidence based on this model is visualized in Figure 5.11.

5.5.3. Geodetic data

The NAM has frequently carried out optical leveling survey campaigns in the northern Netherlands, to assess the amount of subsidence due to natural gas production. The survey campaigns are not only carried out above the Groningen gas field but also cover other areas where subsidence is expected due to depletion from smaller gas fields. The first leveling survey for the Groningen gas field was carried out in 1964, only covering the southern part of the field. In 1972 the first leveling survey covering the whole area was conducted [45]. The leveling network of the Groningen field, also covering the Norg and Roden fields in the south is found in Figure 5.12. Since 2010, the PS-InSAR technique has also been used for deformation monitoring. Global Positioning System (GPS) have been placed at 10 locations in Groningen and are recording since 2014 [45].

For this case study, geodetic leveling data in the Norg and Roden area from 1975 until 1993 has been used. Production from the Roden field started in 1976 and gas storage in the Norg field commenced in 1997. This limits the time frame. One leveling campaign before the gas production started has been chosen and the rest should be from the period before gas storage. Five large campaigns have been carried out during this period, the average date and amount of observations per campaign are summarized in Table 5.4. The leveling network in the Norg area from 1993 is visualized in Figure 5.13. The trajectories of all other campaigns (1975, 1978, 1981, 1987 and 1993) can be found in Appendix B.

Table 5.4: Leveling campaigns at Norg and Roden between 1975 and 1993

campaign	average date	number of observations
1975	1-9-1975	316
1978	1-1-1978	320
1981	1-07-1981	351
1987	1-08-1987	632
1993	1-04-1993	686

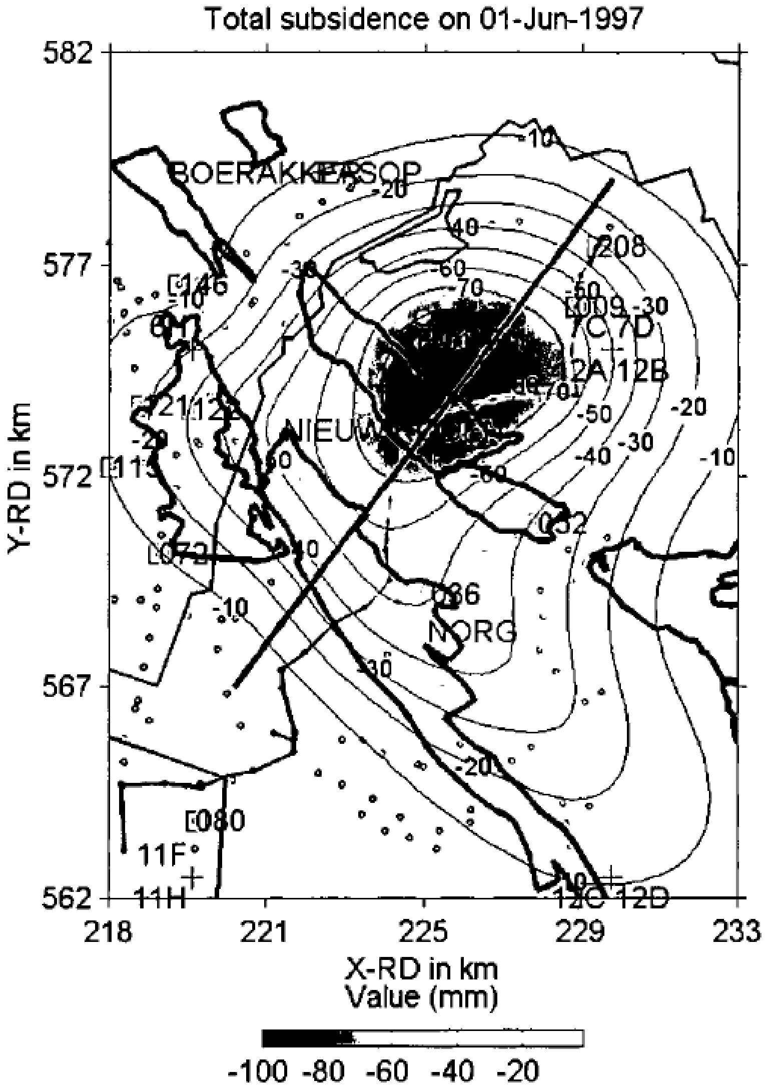

Figure 5.11: Estimated subsidence in 1997 since 1975, by Quadvlieg [55], based on geometrical subsidence model.

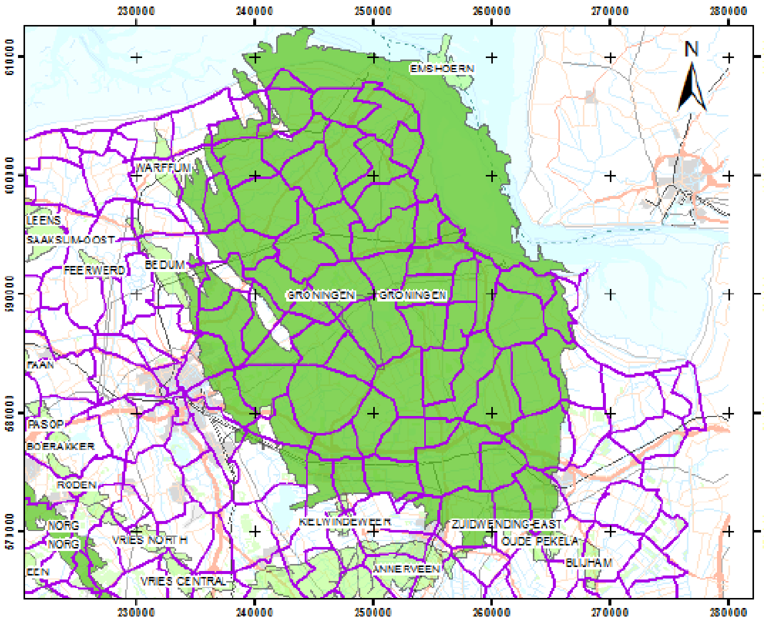

Figure 5.12: Leveling network of the Groningen field as surveyed in 2013, Roden and Norg fields in the south-west (from NAM [45]).

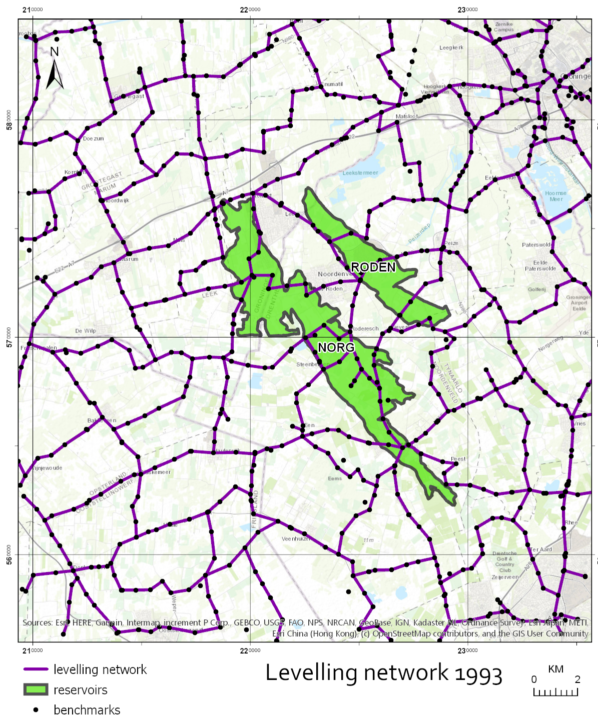

Figure 5.13: leveling network at the Norg and Roden field, as surveyed in 1993.

The data is considered as “raw” measurement data (Level 0 data, see section 2.3.4). When a leveling survey campaign is conducted for the NAM, the data is during the campaign checked for gross errors. If the measurement error of a certain path is too large and falls outside certain error ranges, the trajectory has to be re-measured. The data was collected from 1975 to 1993 and unfortunately, it is therefore not known whether the final dataset consists of single measurements, or whether averaged values of multiple measurements are known. Measurement errors were computed as function of the measurement distance and are assumed known.

6
Results

6.1. Geertsma experiments

The goal of the first synthetic experiments is to assess the influence of different factors in Geertsma's methodology [21] [22]. The experiments start with a simple test set-up: one Geertsma nucleus-of-strain, placed at varying depths. The influence of the depth of the nucleus on the maximum subsidence right above the nucleus is plotted in Figure 6.1. Depths from 2650 to 3050 are chosen because these depths cover the entire depth of both reservoirs. The second result shows the size of the subsidence bowl due to one nucleus. The maximum amount of subsidence is found right above the source at $x = 0$. Figure 6.2 shows at which surface distance from the nucleus center the amount of subsidence is 50% and 10% of the maximum subsidence right above the nucleus. This means that if a nucleus causes 60 mm subsidence right above the nucleus center, one can assess with these plots at which distance 30 mm and 6 mm subsidence are expected. It also indicates the total size of the subsidence bowl. Note that these plots are based on Geertsma's nucleus-of-strain models, as defined in (2.20), not on the analytical solution for a disk-shaped reservoir.

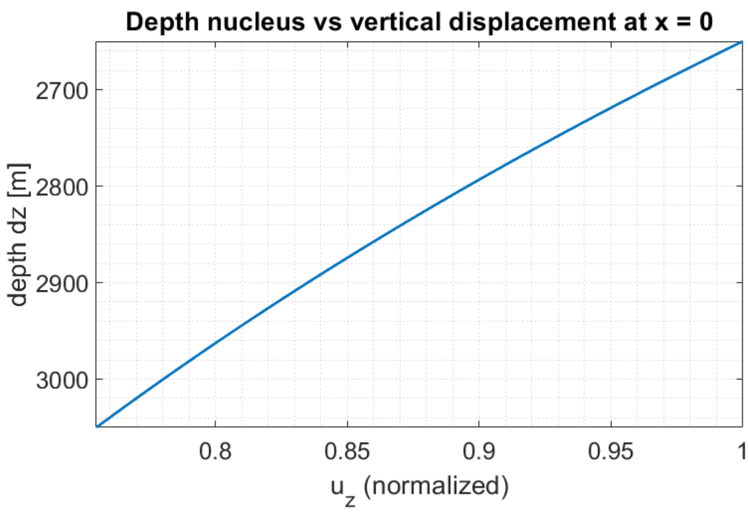

Figure 6.1: Influence of the depth of the nucleus (dz) on subsidence (u_z) at the surface directly above the reservoir (x = 0).

An assessment of the source strength per nucleus for a certain parameterization can be computed. Subsequently, the amount of subsidence that results from these nuclei can be computed. This is a forward model. Figure 6.4 shows the resulting subsidence per year with a centroid parameterization. The centroid parameterization uses 1 nucleus in each reservoir block. The parameters used for this forward model are very roughly estimated and are based on data from Nagelhout and Roest [43], de Kloe et al. [12] and maps from NLOG [51], see Table 6.1. Using the forward Geertsma model

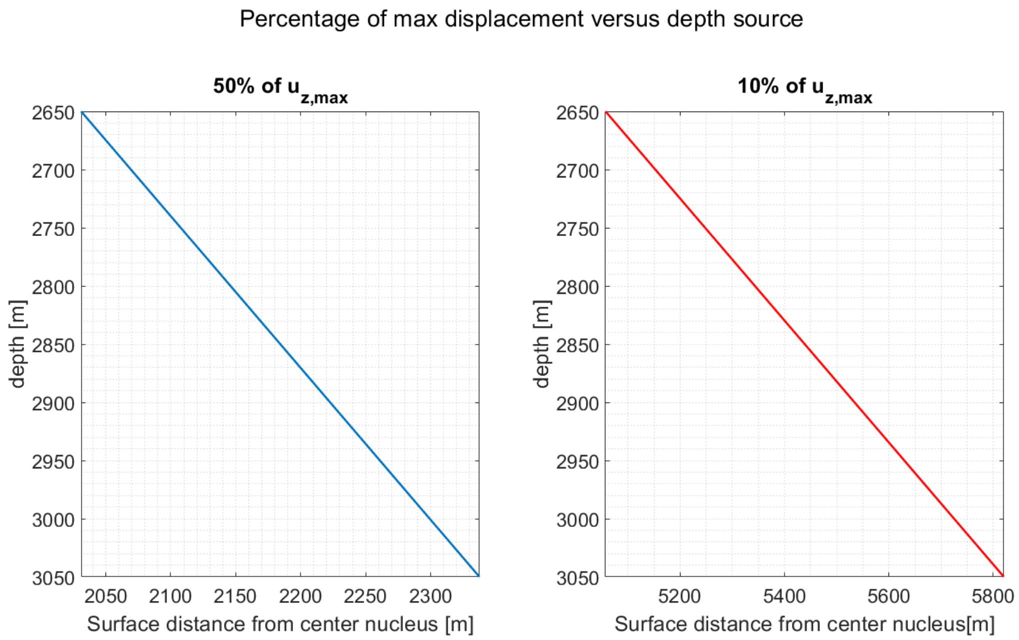

Figure 6.2: Size of subsidence due to one Geertsma nucleus: depth nucleus versus percentage of maximum displacement right above nucleus.

with these approximated parameters gives an estimation of the source strength for 1 nucleus in each reservoir block (see Figure 6.3).

Table 6.1: Parameter assumptions used for forward estimations of source strengths.

Parameter	**Value**
C_m (Roden and Norg)	$6 \cdot 10^{-5}$ bar^{-1}
ν	0.17
α	0.95
ΔP Roden (1978, 1981, 1987, 1993)	50, 80, 145, 210 bar
ΔP Norg (1978, 1981, 1987, 1993)	0, 0, 25, 100 bar
Height Roden	165 m
Height Norg	140 m
Area Roden (block 1, 2)	7.2, 3.2 km^2
Area Norg (block 1, 2a, 2b, 2c, 3, 4)	3.7, 6.2, 1.9, 3.4, 11.7 km^2

These computed source strengths can subsequently be used to forward compute the amount of subsidence, due to these nuclei (see Figure 6.4).

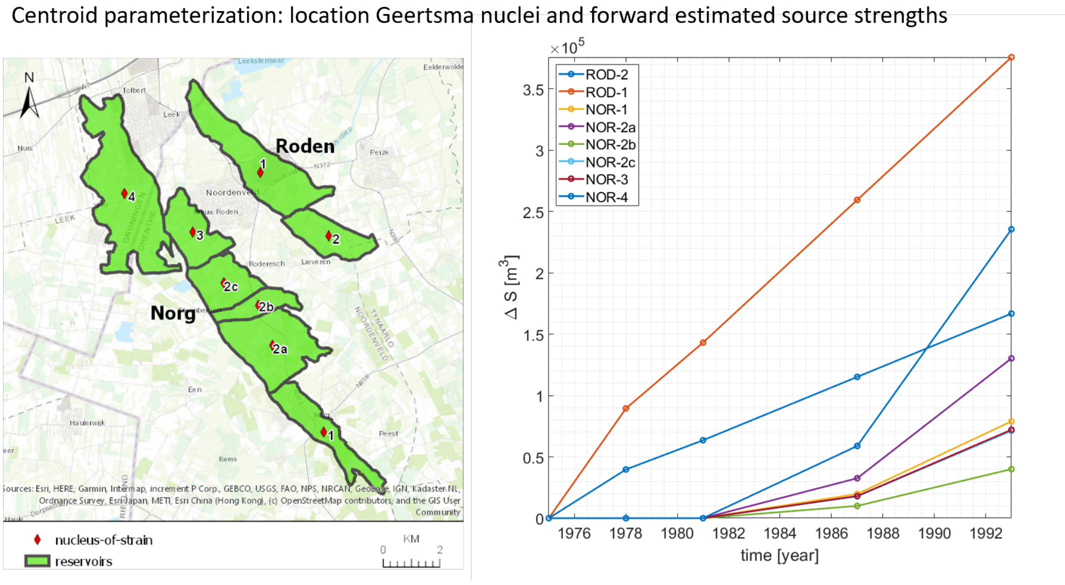

Figure 6.3: Expected Geertsma source strengths per reservoir block centroid parameterization, based on literature parameter assumptions.

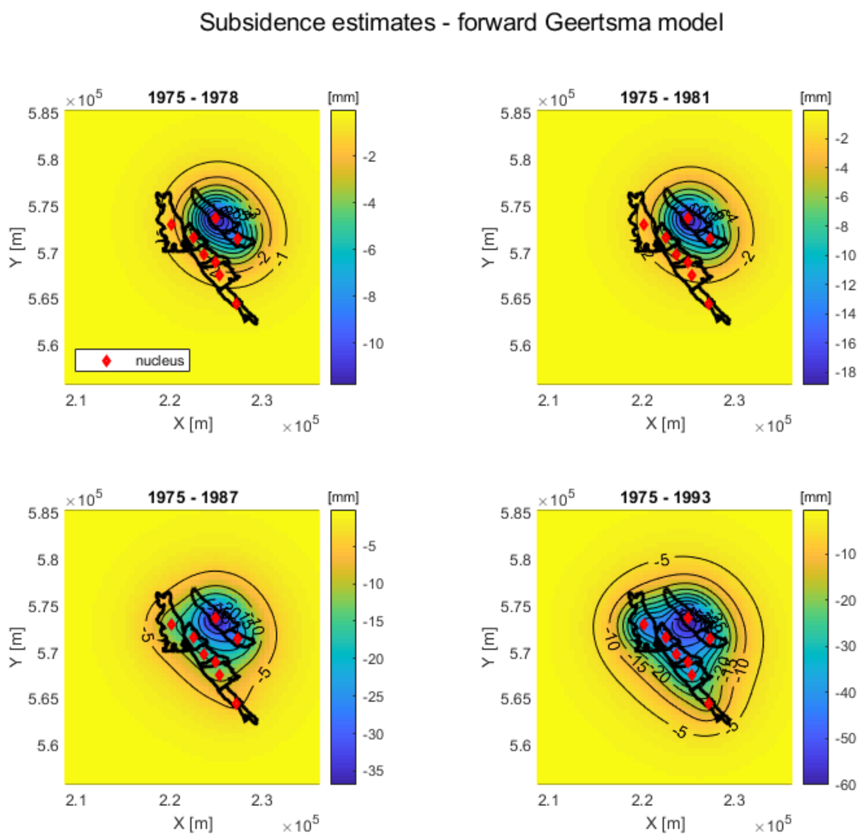

Figure 6.4: Forwardly modelled subsidence with centroid parameterization, literature based parameter assumptions and the Geertsma model

6.1.1. Discussion and conclusion

The Geertsma nucleus-of-strain model can be broken up in two parts: a source strength term ΔS, which consists of $\Delta S_n = \frac{C_m(1-\nu)}{\pi} aV\Delta P$ and of a geometrical term, which consists of the x, y coordinates and depth of the nucleus. The source strength has a linear relationship with the amount of subsidence. The depth of the nucleus has at the depth interval range of the reservoirs of the case study a nearly linear relationship with the amount of subsidence expected right above the source. At 3000 meter depth, the amount of subsidence right above the nucleus is approximately 80% of the amount of subsidence with a source at 2650 meters. The deeper the nucleus, the larger the radius of the subsidence bowl. With a source at 2650 meter, half of $u_{z,max}$ is expected at 2050 surface meters from the source. If the nucleus is placed at 3000 meters, the surface distance increases to 2300 meters. The size of the subsidence bowl can easily be calculated for different percentages of $u_{z,max}$. The size of the subsidence bowl tells us also something about the minimum lateral resolution at which the independent contribution of neighboring nuclei can be estimated. With a burial depth of 2800 meters, 50% of the maximum displacement is expected at 2200 meters from the nucleus. If we place another nucleus at this distance, independent contributions can not be estimated.
Rough assumptions of all parameters in Geertsma's model for the case study are given and these parameters are used to calculate the source strengths with a forward model. The amount of subsidence largely depends on the volume of the reservoir that the nucleus represents and for the chosen parameterization varies in 1993 (the year of the last leveling campaign) between $0.4 \cdot 10^5$ m^3 and $3.7 \cdot 10^5$ m^3. These source strengths can be used to give an estimation of the amount of subsidence at all survey years, which is with this parameterization estimated to be maximally 60 mm in 1993.

A superposition of a limited amount of Geertsma nuclei represents a very simple approximation of the reservoir. Reservoir parameters are assumed equal for the entire half-space. Each Geertsma nucleus-of-strain is assumed to represent an entire reservoir block. There exist many other geomechanical models that might resemble reality more, the Geertsma model, however, does offer a relatively simple, linear methodology to link reservoir compaction and surface deformation.

6.2. SuRe experiments

Multiple runs of the SuRe software are executed to analyze the effect of certain input parameters on the outcomes of the program. The input parameters of the program are:

- the subsidence prognosis grids,
- the parameters of the variance model,
- the test criterion.

,
For each run, the input parameters are varied and the output that SuRe gives will be compared. The output consists of:

- subsidence estimates,
- outliers,
- adjusted variance model.

First a run with default parameters is done and the results are given, such that the outcomes of all runs can be compared with the default settings. The default settings are chosen based on recommendations done by the NAM.

6.2.1. Default run

The default input uses a zero subsidence prognosis at all reference dates (or “0-prognosis”), an initial variance parameter model that was suggested by the NAM and a test criterion α_0 of 0.001. Running the program with these input settings leads to a subsidence estimation for the 4 survey dates (except 1975, because no subsidence due to gas production is expected on that date), see Figure 6.5. The first subfigure shows the subsidence estimates for 1978, where a subsidence bowl with approximately 6 mm of subsidence at the deepest part of the bowl at the southern part of the Roden field can be identified. Production was not yet started in the Norg field, so no subsidence is expected there. In 1981 the amount of subsidence at the deepest part of the bowl has increased to approximately 15 mm, no subsidence is visible at the Norg field still. In 1983 production starts in the Norg field and the subsidence bowl area starts to shift to the Norg field. At the deepest part of the bowl in Roden, now approximately 40 mm of subsidence is computed. During the last survey campaign in 1993, a clear subsidence signal covering both fields can be identified. The deepest part of the subsidence bowl is still located over the Roden field, where now approximately 60 mm of subsidence is estimated.

One of the output files is the geodetic testing results and indicates the identified outliers. All abnormal behaving benchmarks are plotted the soil type map in Figure 6.6, to see whether there is a spatial relation of certain soil types with abnormal behaving benchmarks. The majority of points indicated as benchmarks with abnormal behavior are located in the north-eastern part of the map. This is also the part of the map with a lot of clayey and peat soil. In the most north-eastern corner, the city of Groningen is located. This type of soil is classified as a build-up area in the WUR data but does presumably consist of clayey soil as well.

Other outliers are observation errors and misidentification errors, which occur at specific dates at specific benchmarks. The third type of outlier is a disturbance. Disturbances indicate a jump in the time-series. These three kinds of errors are assumed to not be spatially correlated so these are counted per type, see Table 6.2.

Table 6.2: Outliers per type indicated by geodetic testing SuRe with default input settings.

Type of outlier	Counts
Observation error	13
Disturbance	3
Misidentification error	13
Abnormal behaviour	37

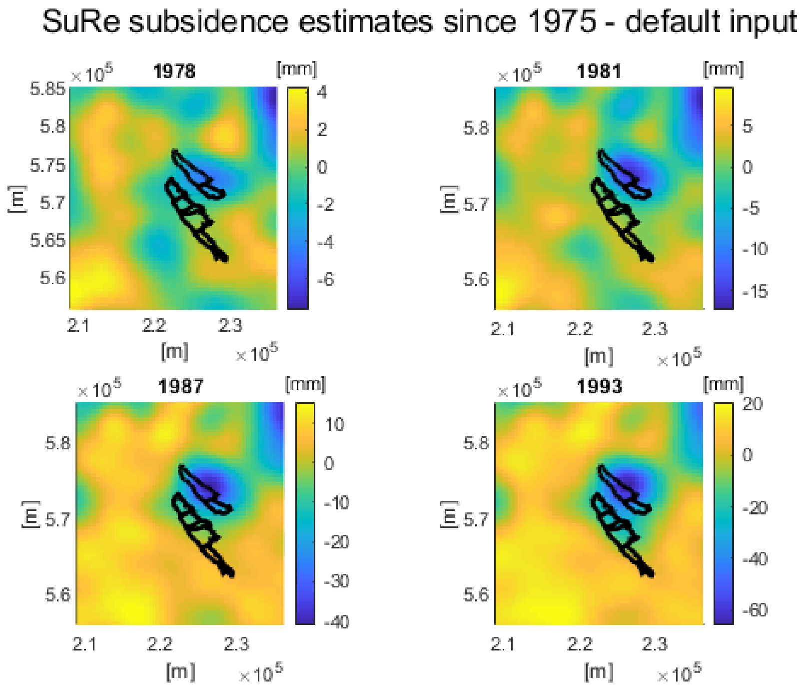

Figure 6.5: SuRe subsidence grids estimates, default input settings

The third outcome of the SuRe run is the adjusted variance model. The parameters of the variance model are adapted until the overall model test is accepted. The initial parameters of the variance model and the outcomes are listed in Table 6.3.

Table 6.3: Initial and adjusted variance model SuRe with default input settings.

Noise type	**Parameter**	**Initial values**	**Adjusted outcome values**
Measurement noise	Standard deviation factor [-]	1.00	1.00
Point noise	Standard deviation [mm/yr^p]	0.33	0.23
	Power (p) [-]	0.75	0.81
Model noise	Standard deviation [mm/yr^q]	2.7	1.35
	Power (q) [-]	0.75	0.82
	Correlation length [m]	4000	4083

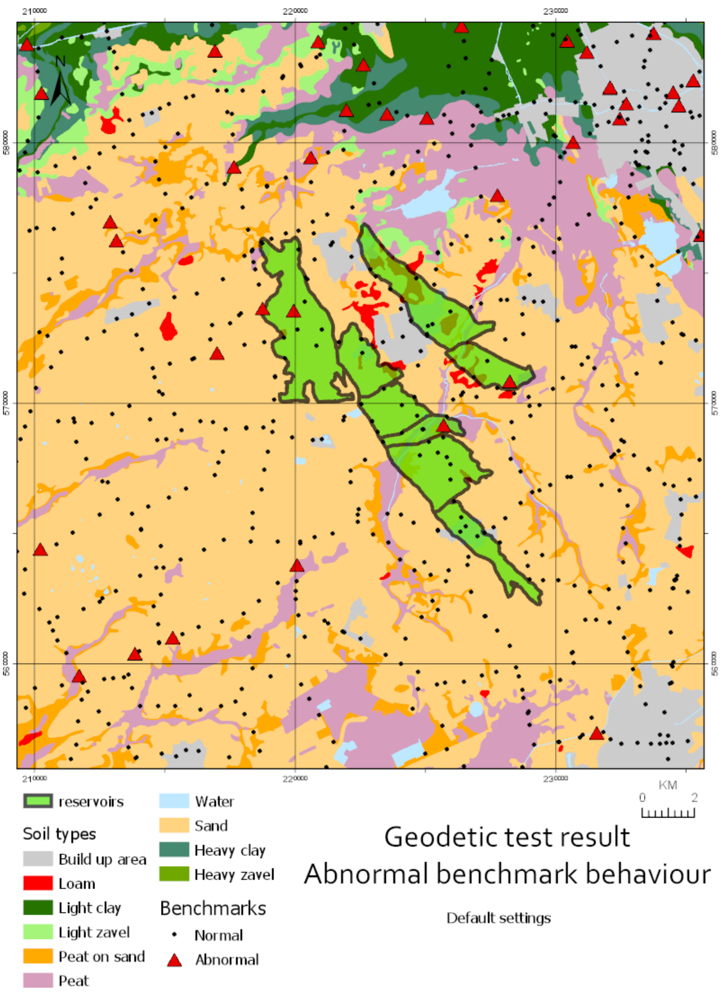

Figure 6.6: Benchmarks flagged with “abnormal behaviour” by SuRe with default input settings on a soil map with data from WUR [79].

6.2.2. Different subsidence prognosis

SuRe was run with a different prognosis grid to see what the influence of the approximate subsidence model input is on the subsidence output and the testing results. As prognosis grids for this run, the subsidence model proposed by Quadvlieg [55] was applied. This model gives a geometrical interpretation of the fields by fitting an ellipsoidal shape through each field. This model is assumed to resemble the real subsidence due to gas production better than a zero subsidence prognosis. The outcome subsidence grid is subtracted from the outcomes from the default settings to see what the differences are between both estimates, see Figure 6.7. The RMSE for the estimates at each reference date and all the output estimates together is computed in Table 6.4.

Table 6.4: RMSE of SuRe subsidence estimates for default input versus input with geometrical prognosis grid

Dataset (survey date)	RMSE [mm]
1978	0.418
1981	0.895
1987	2.342
1993	2.348
all	1.501

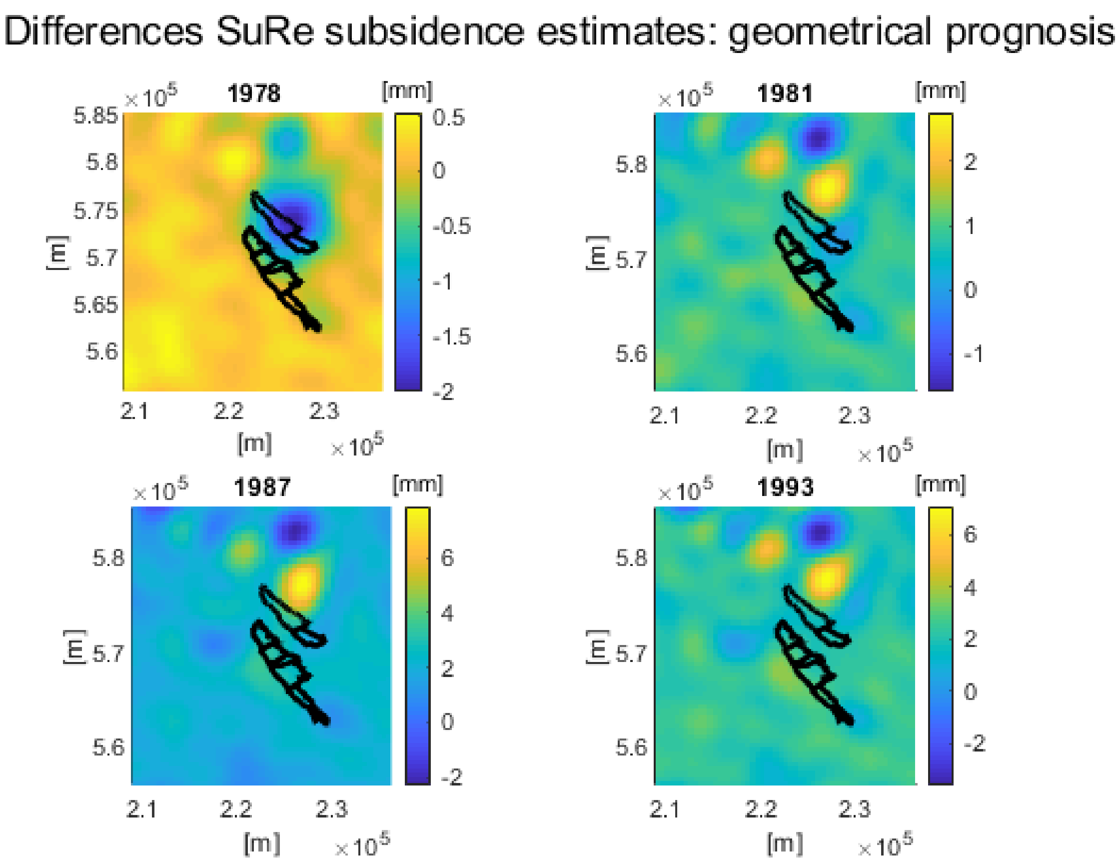

Figure 6.7: Difference in subsidence grids between default run and run with geometric prognosis

The geodetic testing results were analyzed and the different types of outliers counted (see Table 6.5). For this input data, 39 benchmarks were indicated as abnormal behaving benchmarks, of which 37 were similar to the benchmarks indicated with the default settings, adding two extra benchmarks to the list. The same holds for the other outliers, all error list contain the errors of the default settings with the addition of some extra observations/time series.

Table 6.5: Outliers per type indicated by geodetic testing SuRe with geometrical prognosis grid.

Type of outlier	Count geometrical grid	Count default settings	Difference default
Observation error	14	13	+1
Disturbance	4	3	+1
Misidentification error	16	13	+3
Abnormal behaviour	39	37	+2

The output parameters of the variance model are listed in Table 6.6 and vary from the variance model outputted from the default model.

Table 6.6: Initial, adjusted outcome variance model SuRe with geometrical prognosis and outcome of default run.

Noise type	Parameter	Initial	Adjusted	Default	Difference default
Point noise	Standard deviation [mm/yr^p]	0.33	0.19	0.23	-0.04
	Power (p) [-]	0.75	0.84	0.81	+0.03
Model noise	Standard deviation [mm/yr^q]	2.7	1.25	1.35	-0.10
	Power (q) [-]	0.75	0.80	0.82	-0.02
	Correlation length [m]	4000	4334	4083	+251

6.2.3. Different variance model parameters

During the next runs, the parameters of the variance model are changed one by one while the other parameters are kept on the default value. In total, 5 parameters of interest are tested, two in the point noise model and three in the model noise model. The measurement noise is assumed to be known and this factor is thus kept on 1.00. The results are given per noise type.

Point noise The point noise has two parameters: the standard deviation (S.D.) and the power (P). Each run, one of these parameters is changed while the others are kept on the default value. The RMSE per year and in total for the entire subsidence outcome dataset is computed (see Table 6.7).

Table 6.7: RMSE with default input values for changing point noise parameters (S.D. = standard deviation, P = power). Each column represents 1 changed parameter.

dataset	RMSE			
	S.D = 0.1	S.D = 1	P = 0.55	P = 0.95
1978	0.90	0.63	0.31	0.60
1981	1.35	0.96	0.62	0.89
1987	2.17	1.32	1.04	1.21
1993	2.05	1.34	1.25	1.31
all	1.62	1.06	0.80	1.00

The number of outliers indicated by SuRe for these different settings are summarised in Figure 6.8.

For every run with variations in the input variance model, SuRe adjust the final variance model differently to match it to the noise in the data. The results of this adjustment for all different input settings for the point noise parameters are summarised in Table 6.8.

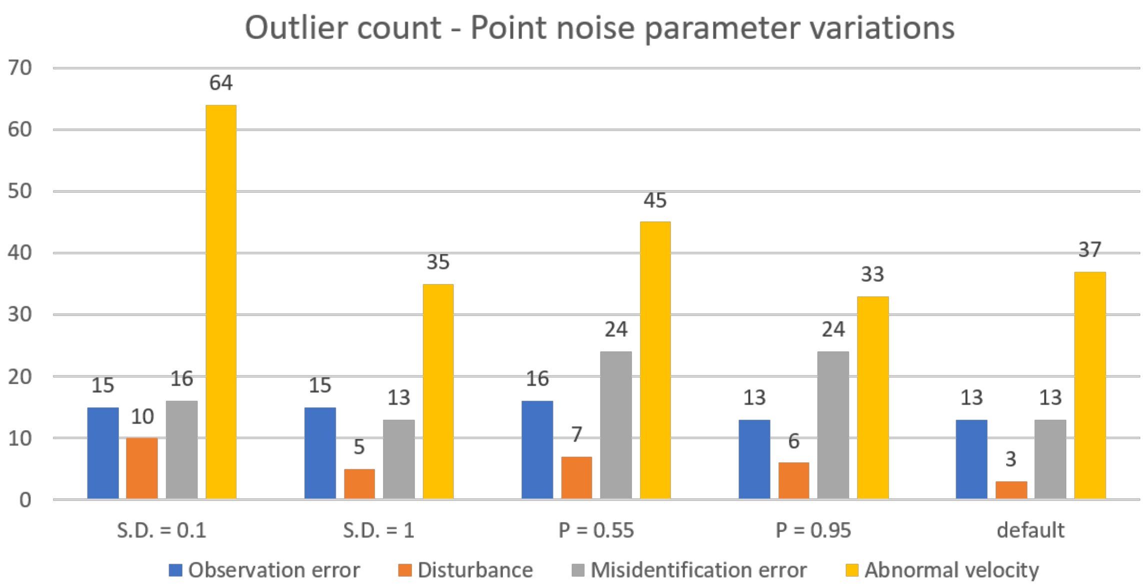

Figure 6.8: Outlier count per type for variation of one parameter of the input point noise variance model

Table 6.8: Initial and adjusted variance model SuRe with variations in the point noise parameters.

Noise type	Parameter	Default	SD = 0.1	SD = 1	P = 0.55	P = 0.95
Point	S.D.[mm/yr^P]	0.23	0.083	0.26	0.17	0.22
	P [-]	0.81	0.83	0.85	0.74	0.92
Model	S.D. [mm/yr^Q]	1.35	1.91	1.18	1.42	1.23
	Q [-]	0.82	0.77	0.88	0.81	0.87
	C.R. [m]	4083	3913	4596	4004	4431

Model noise SuRe uses 3 parameters for the model noise: the standard deviation (S.D.), the power (Q) and the correlation length (C.R.). Each parameter is varied every multiple run while keeping all other parameters on the default value. The RMSE for the model noise variations are listed in Table 6.9, an outlier count in Figure 6.9 and the adjusted variance model after each run in Table 6.10.

Table 6.9: RMSE with default input values for changing model noise parameters (S.D. = standard deviation, P = power, C.R. = correlation length)

dataset	RMSE					
	S.D = 1	S.D = 5	P = 0.55	P = 0.95	C.R. = 3000	C.R. = 5000
1978	0.71	0.13	0.40	0.51	0.47	0.25
1981	1.06	0.18	0.62	0.69	0.61	0.51
1987	1.36	0.26	0.96	0.94	0.91	1.10
1993	1.44	0.36	1.05	1.26	1.10	1.20
all	1.14	0.23	0.76	0.85	0.77	0.76

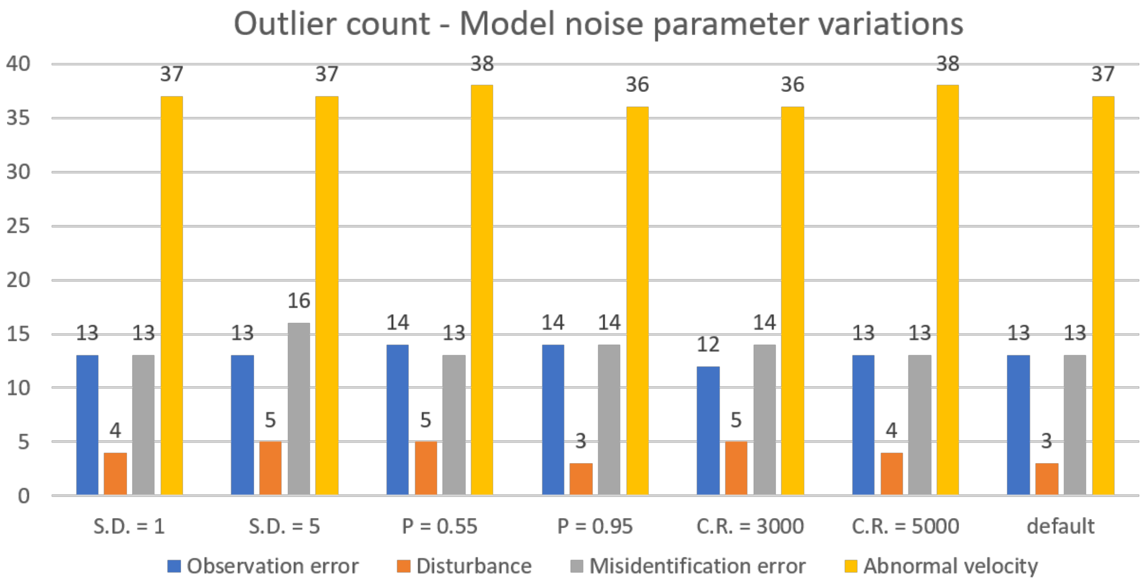

Figure 6.9: Outlier count per type of SuRe outcomes for variations in the input model noise variance model

Table 6.10: Initial and adjusted variance model SuRe with variations in the model noise parameters.

Noise type	Parameter	default	SD = 1	SD = 5	P = 0.55	P = 0.95	CR = 3000	CR = 5000
Point	S.D.	0.23	0.26	0.20	0.21	0.23	0.20	0.23
	P	0.81	0.78	0.85	0.83	0.80	0.83	0.81
Model	S.D.	1.35	1.12	1.32	1.15	1.35	1.10	1.35
	Q	0.82	0.94	0.84	0.88	0.94	0.88	0.82
	C.R.	4083	4716	4037	4523	3992	3474	4678

6.2.4. Different test criterion

The last input parameter analyzed in this sensitivity study is the test criterion α. α is increased and decreased by a factor 10, to see what the effects on both the subsidence grids and outlier testing is. For $\alpha = 0.01$, the program keeps on iterating, because it cannot find a hypothesis that gets accepted. This means that the test criterion is set too high, SuRe cannot find a model within the set acceptance criterion. For $\alpha = 0.0001$, SuRe can find a solution within the acceptance bounds. All results are summarised in Tables 6.11, 6.12 and 6.13.

Table 6.11: RMSE of SuRe subsidence estimates for default input versus input with test criterion of $\alpha = 0.0001$.

Dataset (survey date)	RMSE [mm]
1978	0.181
1981	0.381
1987	0.651
1993	0.855
all	0.501

Table 6.12: Outliers per type indicated by geodetic testing SuRe with test criterion of $\alpha = 0.0001$.

Type of outlier	Count adapted α	Count default	Difference default
Observation error	9	13	-4
Disturbance	2	3	-1
Misidentification error	13	13	+0
Abnormal behaviour	32	37	-5

Table 6.13: Initial and adjusted variance model SuRe with geometrical prognosis.

Noise type	Parameter	Initial	Default	Adjusted	Difference default
Point noise	Standard deviation [mm/yr^p]	0.33	0.24	0.23	+0.01
	Power (p) [-]	0.75	0.82	0.81	+0.01
Model noise	Standard deviation [mm/yr^q]	2.7	1.4	1.35	+0.05
	Power (q) [-]	0.75	0.82	0.82	+0.00
	Correlation length [m]	4000	4058	4083	-25

6.2.5. Discussion and conclusion

For this thesis, a workflow is developed in which geomechanical parameters are directly estimated from survey observations. Part of this workflow consists of a geodetic testing procedure of these survey observations, which is carried out by SuRe, the subsidence estimation program currently being used by the NAM. Part of this program is an extensive geodetic testing procedure. To assess the influence of different input parameters, multiple runs with the program were performed and the outcomes are compared. The input of SuRe consists of “raw” measured height differences from different optical leveling campaigns, a subsidence prognosis model, an initial variance model, and a test criterion. Experts at the NAM recommended certain input parameters that they would use for this project, based on their experience. These input settings serve as a default model, against which all other settings were tested. The influence of the subsidence prognosis grid, the initial variance model and the test criterion is assessed.

Default run The subsidence estimates of the default run in Figure 6.5 show a subsidence pattern that is expected with the production numbers from the NAM. Subsidence starts at the Roden field and the subsidence bowl progressively moves to the Norg field. In the area of interest are 751 benchmarks located which have been measured at least once, SuRe indicates that with default settings 37 of these benchmarks show abnormal behavior. The majority of these benchmarks are located on clayey, peat or build-up soils, which are areas that are expected to lead to for example compaction or benchmark settling. The other outliers are assumed to have no spatial relation. When all 1D errors are solved, SuRe adjusts the variance model until the overall model test gets accepted. The biggest adjustment is done to the standard deviation of the model noise, this means that the standard deviation of the prognosed subsidence model is decreased.

Influence of prognosis grid The default settings use a zero subsidence grid ("0 prognoses"). This setting was tested against a run with a geometrical prognosis, which was based on a subsidence model earlier developed by the NAM [55] for this field. The subsidence estimates per grid cell show a difference up to 6 mm with the 0 prognoses, this is however on local spots. The RMSE for the total dataset is 1.501 mm. The amount of outliers indicated by the program has slightly increased compared with default settings, whilst the standard deviation of the subsidence model has decreased by -0.1. A possible explanation could be that by using a more realistic subsidence prognosis model, the model uncertainty decreases, leading to the indication of slightly more outliers. The differences are however not significant enough for a statement to be made with certainty. The adjusted variance matrix does not show significant changes. The influence of the prognosis grid is thus limited to the outcomes of the geodetic testing procedure and on the adjusted variance model.

Influence of initial variance model By varying all parameters of the variance model, both point and model noise, an assessment can be made on what influence these parameters have on the geodetic testing outcome and the subsidence estimates. Changing the point noise parameters has the most significant effect on the amount of detected abnormal velocity outliers. This is because decreasing the point noise standard deviation for all points allows for more points to be indicated as outlier because their behavior does not fall under the uncertainty ranges of the point behavior. Increasing the standard deviation does however not make a big difference compared to the default settings, which means that the majority of abnormal behaving benchmarks are captured within an uncertainty range standard deviation of 0.55. The power of the point noise is related to the expected smoothness of the benchmark displacement. A lower value of p leads to frequent misfits of the surveyed sections, whereas a higher value implies a constant displacement rate, leading to less abnormal behaving errors. Changing the model noise parameter has no significant effect on the detected outliers nor the adjusted variance model. The most significant changes are visible when the parameters of the point noise model are adjusted, which could lead to a larger outlier count. To prevent the program from detecting too many false positive abnormal behaving outliers, the point noise standard deviation should not be set too low.

Influence of test criterion Setting the test criterion to $\alpha = 0.01$ does not lead to convergence of the program. The 1D tests get never accepted because the test criterion is set too tight. Decreasing the test criterion leads to relaxing of the overall model test and the test is thus faster accepted. This means that fewer outliers are indicated. By varying the test criterion, one can manage the number of outliers identified. This value should neither be set too conservative because this will not lead to acceptance of the overall model test nor too loose, because that will cause to acceptance of too many outliers.

Overall conclusion SuRe has an extensive geodetic testing procedure, by testing alternative hypotheses are outliers detected in the data. The program makes use of a prior subsidence model ("prognosis grid"), which could lead to biased outlier detection. Changing the prognosis grid however does not have a significant influence on the outcomes of SuRe for the case study, neither has changing the model noise parameters. The most significant effect is visible when the point noise parameters are changed, because more benchmarks are flagged as abnormal behaving benchmark, due to the decreased point noise standard deviation. For the remainder of the experiments, the default settings are kept. These settings are recommended by experts and changing these parameters has proven not to result in significantly different results.

6.3. Inversion experiments

For the third group of experiments, the proposed methodology is applied to the case study data. First, data testing and processing are applied to data in the area of interest. The area of interest is defined by looking at the results from the Geertsma experiments. Subsequently, regularized inversion is performed by selecting a parameterization, a regularization parameter and then applying the actual inversion. This eventually leads to estimates for the source strengths for all nuclei and initial height estimates for all benchmarks. These source strengths estimates are subsequently used in a forward model to determine the amount of subsidence in the area of interest.

6.3.1. Processing of raw data

The area of interest is determined based on the outcomes of the previous experiments. The Geertsma experiments showed that at approximately 5 km from the source, 10% of the maximum deformation signal is found. Therefore, the area of interest is limited to approximately 5 km from the outlines of the reservoir. The area of interest is chosen to be: $x = [2.15 \cdot 10^5\text{m} - 2.35 \cdot 10^5\text{m}]$ and $y = [5.60 \cdot 10^5\text{m} - 5.80 \cdot 10^5\text{m}]$. The raw measurements are imported from the database and used as input for a SuRe run. The outcome of the SuRe run can be found in Table 6.14.

Table 6.14: Outcomes SuRe run for chosen area of interest (outliers and variance model).

Noise type	Count	Variance model parameter	Adjusted value
Observation error	2	Point noise s.d.	0.18
Misidentification error	6	Point noise power	0.86
Disturbance	2	Model noise s.d.	1.35
Abnormal benchmark behaviour	12	Model noise power	0.81
		Model noise correlation length	4133

Knowing which measurements represent outliers, the raw data is processed and with the adjusted variance model, the corresponding uncertainty model is adjusted. A reference benchmark that is present in all survey campaigns is selected and all measurements that are disconnected from this reference benchmark are removed (this reference benchmark is indicated in Figure 6.14. Points with similar “same” and “to” coordinates were removed. Table 6.15 gives an overview of the number of observations before and after the processing of the raw measurements.

Table 6.15: Amount of observations in area of interest before and after raw measurement processing.

Average date campaign	Number of measurements before processing	after processing
01-Sep-1975	120	114
01-Jan-1978	125	121
01-Jul-1981	143	132
01-Aug-1987	293	285
28-Mar-1993	298	296

6.3.2. Centroid parameterization

The optimal regularization parameter λ is computed with a 4-fold cross-validation scheme, where the data is partitioned into 4 subsets by overlaying the area of interest with a 4 quadrant grid. The variance of the prediction error S_{tot} for a range of candidate λ is depicted in Figure 6.10. The partitioning of the data for the 1993 campaign is depicted in Figure 6.11, the same grid partitioning holds for data from the other survey campaigns.

The optimal regularization parameter is found to be $\lambda_{optim} = 10^{-6}$. With this λ_{optim} an estimation of the source strengths and initial heights is made. The estimated source strengths are depicted in Figures 6.12 and 6.13. The other group of estimated parameters is the initial benchmark heights (the heights in 1975). These are plotted and compared with a (relative) height map derived with laser-altimetry

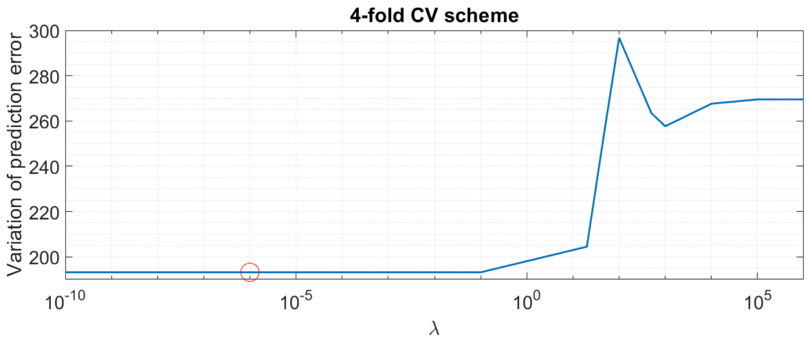

Figure 6.10: Estimated optimum regularization parameter λ for the 4-fold cross-validation scheme. λ_{optim} is indicated by a red circle on the graph.

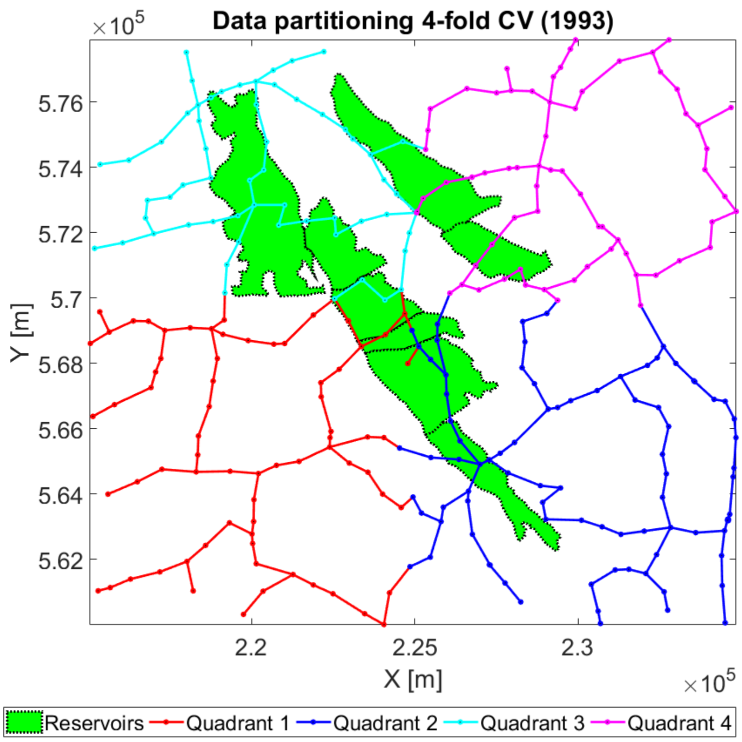

Figure 6.11: Data in the area of interest is split up into four quadrants, to be used in the 4-fold cross validation scheme. This figure depicts 1993, same partitioning scheme holds for other survey campaigns.

derived data from PDOK [53] (see Figure 6.14). This AHN map serves as a visual way of comparing the height estimates and height data roughly. The benchmarks are usually not found at ground level, but rather in walls on arbitrary heights. The AHN-3 data was collected from 2014 until 2019 and thus does not reflect ground heights in 1975. The estimated initial heights and the AHN-3 data do show a good spatial correlation.

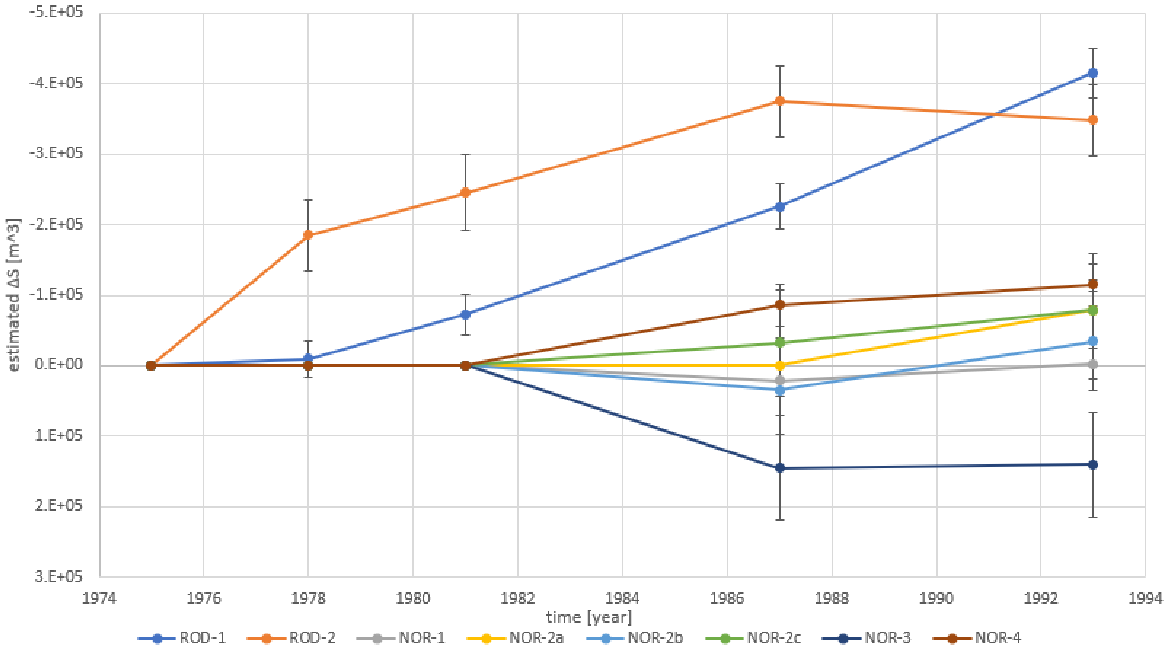

Figure 6.12: Graph of estimated source strength, for the centroid parameterization. Error bars indicate 1 standard deviation.

The RMSE for the entire dataset is 0.0077m. The RMSE can also be computed for each survey campaign, results are summarised in Table 6.17. The overall model test for these estimates gets accepted, see Table 6.16 after removal of 9 observations with a w-test procedure.

Table 6.16: Test statistic and K ($\alpha = 0.01$) for the centroid parameterization.

T	**K**
629.61	695.33

Table 6.17: Root-mean-square errors (RMSE) for the centroid parameterization, for entire dataset and per campaign

Campaign	RMSE [m]
1975	0.00086
1978	0.0016
1981	0.0015
1987	0.0029
1993	0.0043
total	0.0030

The source estimates can be used in a forward model to give an estimation of the amount of subsidence due to these sources, see Figure 6.15.

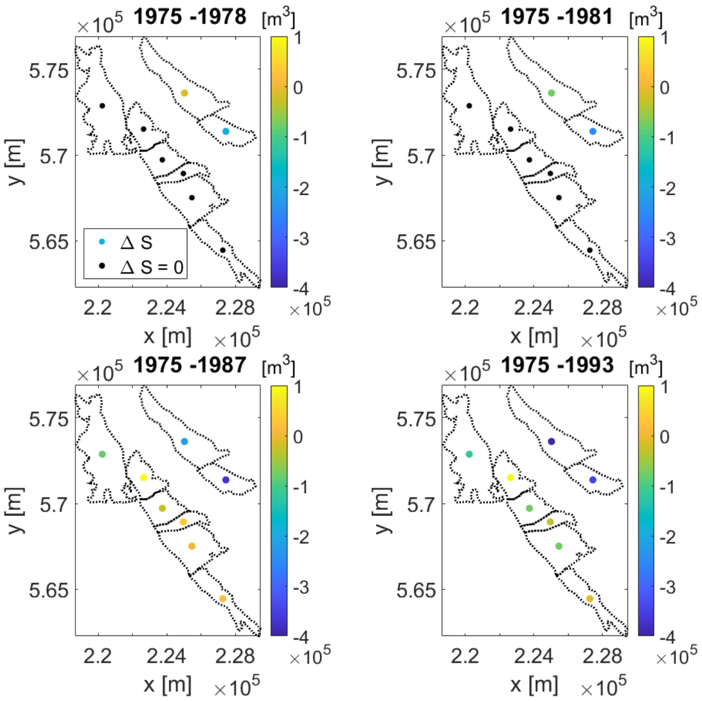

Figure 6.13: Plot of estimated source strengths in reservoir blocks for the centroid paramterization. At 1978 and 1981, the Norg reservoir is not yet producing and thus ΔS is assumed to be 0 for the nuclei of this field.

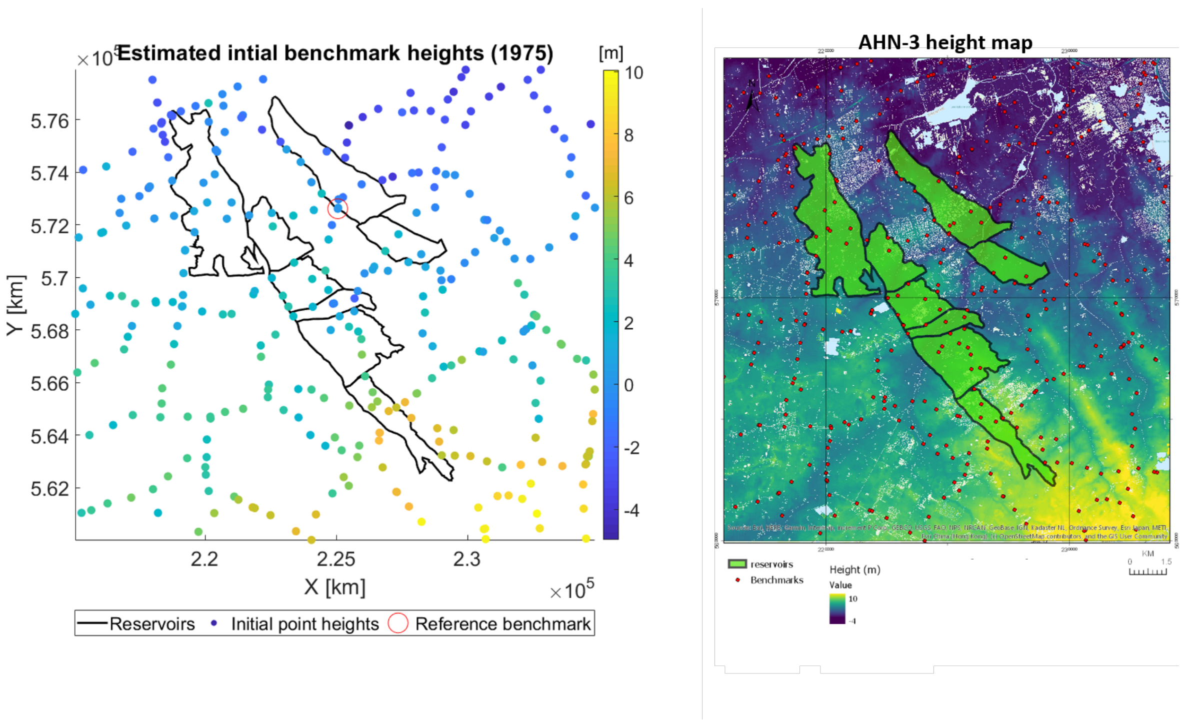

Figure 6.14: Estimated initial benchmark heights estimates (1975) with a height map derived from AHN data, for visual comparison (from PDOK [53]).

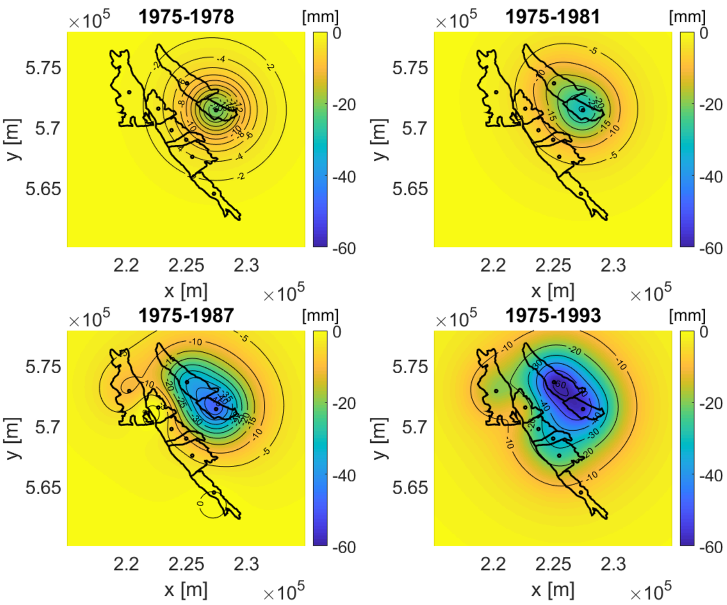

Figure 6.15: Estimated subsidence based on source strengths estimates from Figure 6.13.

6.3.3. Other parameterizations

Three nuclei in Norg reservoir, 2 in Roden The centroid parameterization is chosen because each nucleus represents one reservoir block. The Norg reservoir blocks are separated by non-sealing faults, which means that pressure decline is assumed to be equal in each block. The nuclei in the 2a, 2b, 2c and 3 blocks are in the proximity of each other and the minimum lateral resolution at which independent contribution of neighboring nuclei can be detected is probably exceeded. It is therefore that for the next parameterization, the nuclei representing blocks 2a, 2b and 3 were deleted. A new regularised inversion was run with this new parameterization. The source strengths for the Norg field are again assumed to be 0 for 1975 and 1981. The results are plotted in Figure 6.16 and visualized in Figure 6.17. The overall model test for this test was accepted after the removal of 5 observations. The test statistic and the critical value are listed in Table 6.18. The RMSE per campaign and the RMSE for all data is found in Table 6.19. Expected subsidence is again estimated for this parameterization, results are visualized in Figure 6.18.

Table 6.18: Test statistic and K ($\alpha = 0.01$) for lesser nuclei in Norg reservoir (3).

T	**K**
670.10	706.23

Table 6.19: Root-mean-square errors (RMSE) of the estimated model, for all data and data per campaign, for lesser nuclei in Norg reservoir (3).

Campaign	RMSE [m]
1975	0.0010
1978	0.0068
1981	0.0061
1987	0.011
1993	0.0063
total	0.0077

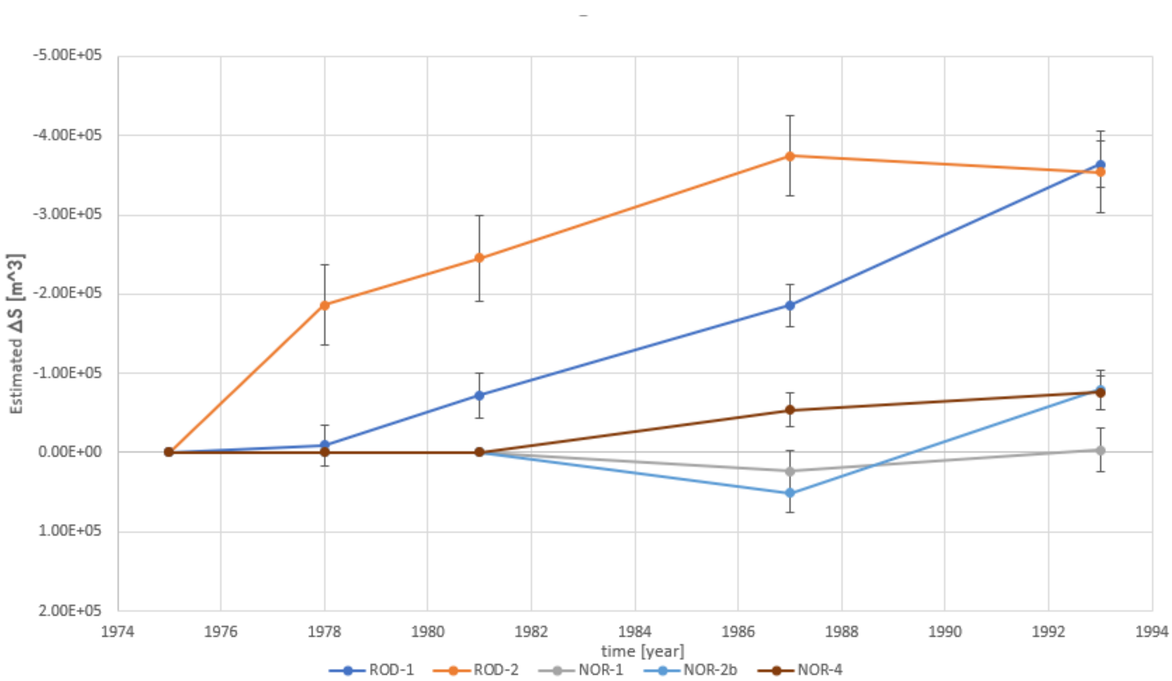

Figure 6.16: Graph of estimated source strengths with 5 nuclei: 3 in Norg field and 2 in Roden. Error bars indicate 1 standard deviation.

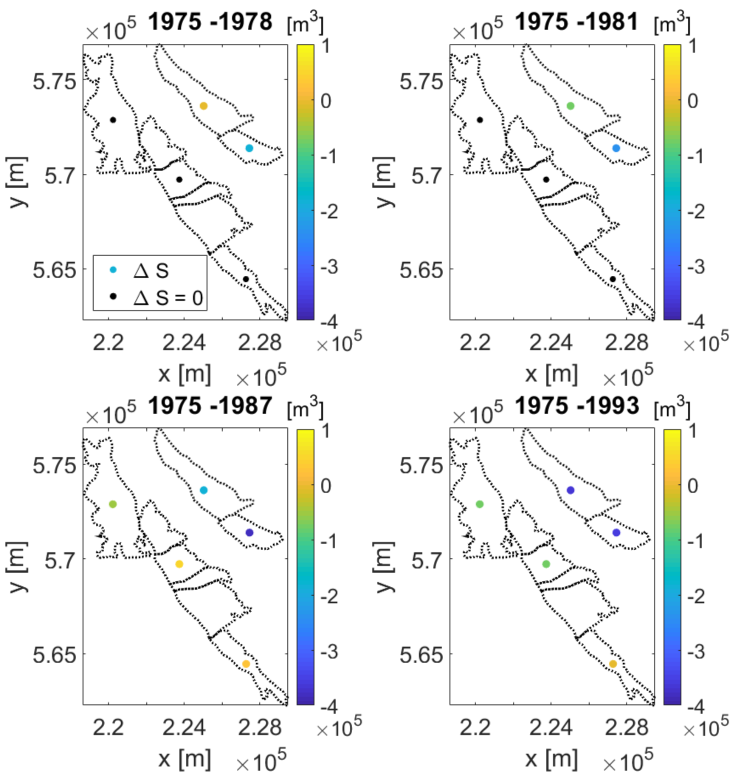

Figure 6.17: Plot of source strengths in reservoir blocks for 5 nuclei: 3 in Norg field and 2 in Roden field.

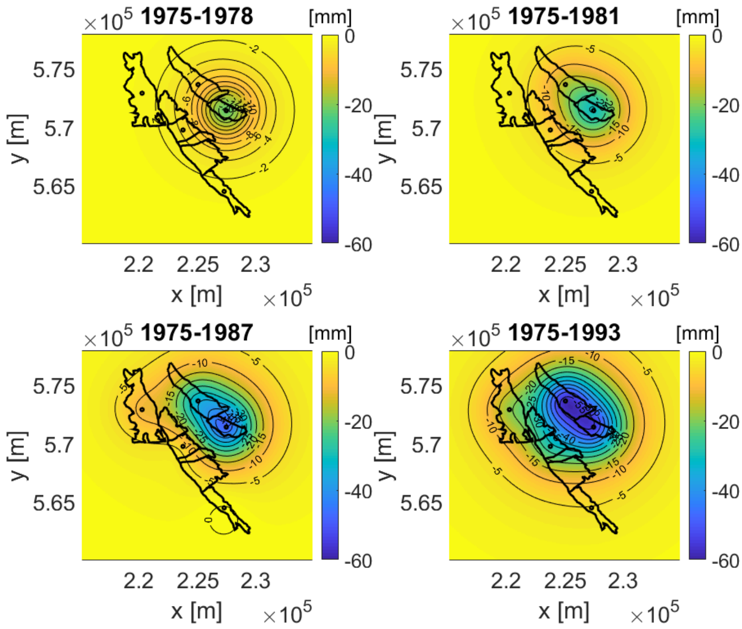

Figure 6.18: Estimated subsidence based on the source strengths estimates from Figure 6.13 (for the 5 nuclei parameterization).

1 nucleus per reservoir The next inversion is performed on a parameterization with 1 nucleus representing an entire reservoir. The position of the nucleus is determined by taking the center of mass of each reservoir. The source strengths are assumed for the Norg field are again assumed to be active after 1983. During processing, now 4 observations are removed after the w-test. The source strengths estimates are plotted in a graph in Figure 6.19 and on the reservoir maps in Figure 6.19.

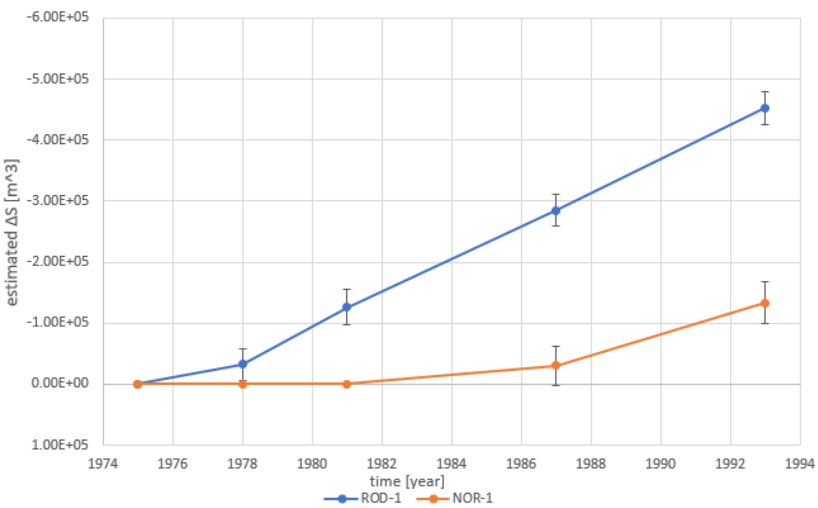

Figure 6.19: Graph of estimated source strengths if only 1 source strength per reservoir is estimated. Error bars indicate 1 standard deiation.

The overall model test for this parameterization is accepted, the test statistic and critical value are given in Table 6.20. The root-mean-square-error is given in Table 6.21, note that for this parameterization more observations were removed, possibly leading to a relatively lower RMSE. The estimated source strengths are used to forward model subsidence (see Figure 6.21.

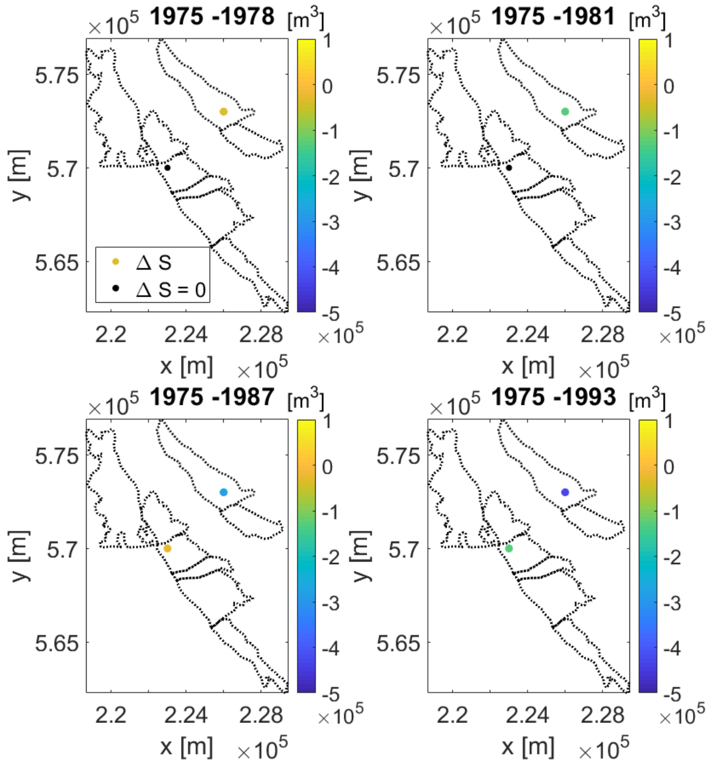

Figure 6.20: Plot of estimated source strengths in reservoirs, if only 1 source strength per reservoir is estimated.

Table 6.20: Test statistic and K ($\alpha = 0.01$), for parameterization with 1 source strength estimated for each reservoir.

T	**K**
704.32	709.50

Table 6.21: Root-mean-square errors (RMSE) of the estimated model for one source strength estimated in each reservoir, for data per campaign and entire dataset

Campaign	RMSE [m]
1975	0.00095
1978	0.0014
1981	0.0015
1987	0.00312
1993	0.0045
total	0.0031

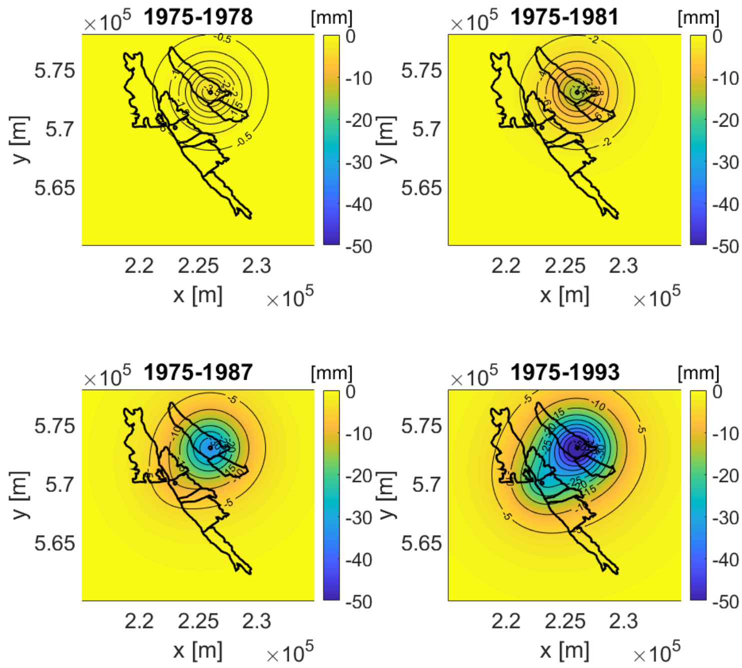

Figure 6.21: Estimated subsidence based on source strengths estimates from Figure 6.20, if the parameterization consist of two sources, one in each reservoir.

Grid parameterization Finally, an inversion is performed with a so-called “grid parameterization”. This means that the entire reservoir outlines are filled with nuclei, with a grid spacing of 1 km. This distance is smaller than the minimum lateral resolution at which the contribution of a nucleus can be detected. After a w-test, 2 observations were removed. The estimated sources are visualized in Figure 6.22.

Another tested parameterization is the grid parameterization. Both reservoirs are filled with nuclei with a grid spacing of 1 km. The estimated sources are visualised in Figure 6.22. The RMSE per campaign and for the total dataset can be found in Table 6.23. The critical value and test statistic are stated in Table 6.22

Table 6.22: Test statistic and K ($\alpha = 0.01$) for grid parameterization.

T	**K**
433.66	594.66

These results are used to forward model the amount of subsidence expected with these compaction estimates, see Figure 6.23.

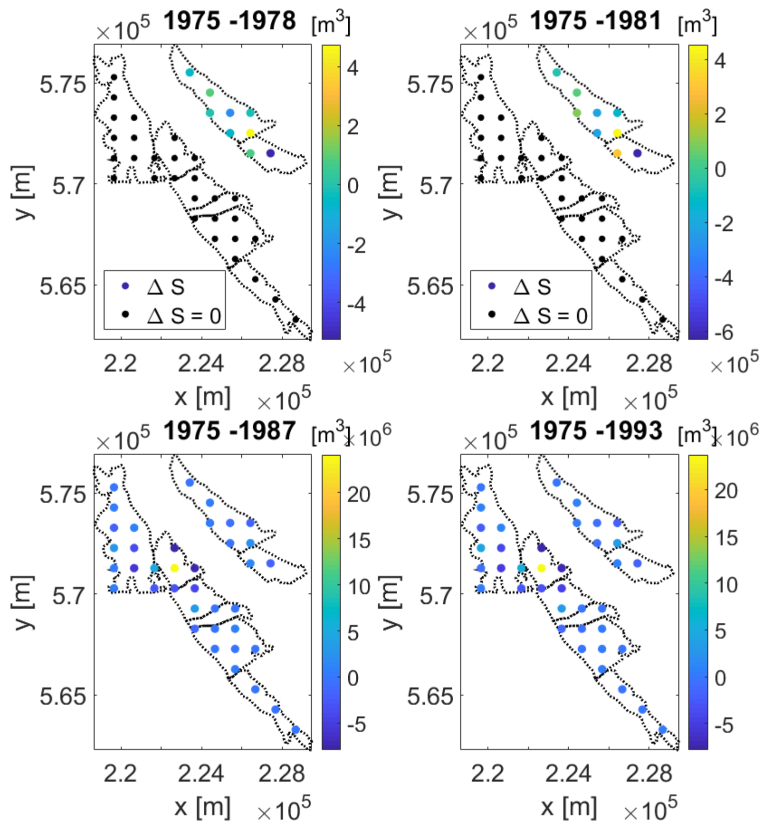

Figure 6.22: Plot of source strengths in reservoir blocks for grid parameterization.

Table 6.23: Root-mean-square errors (RMSE) of the estimated model with one source in each reservoir, for all data and data per campaign

Campaign	RMSE [m]
1975	0.00067
1978	0.0011
1981	0.0013
1987	0.0028
1993	0.0021
total	0.0020

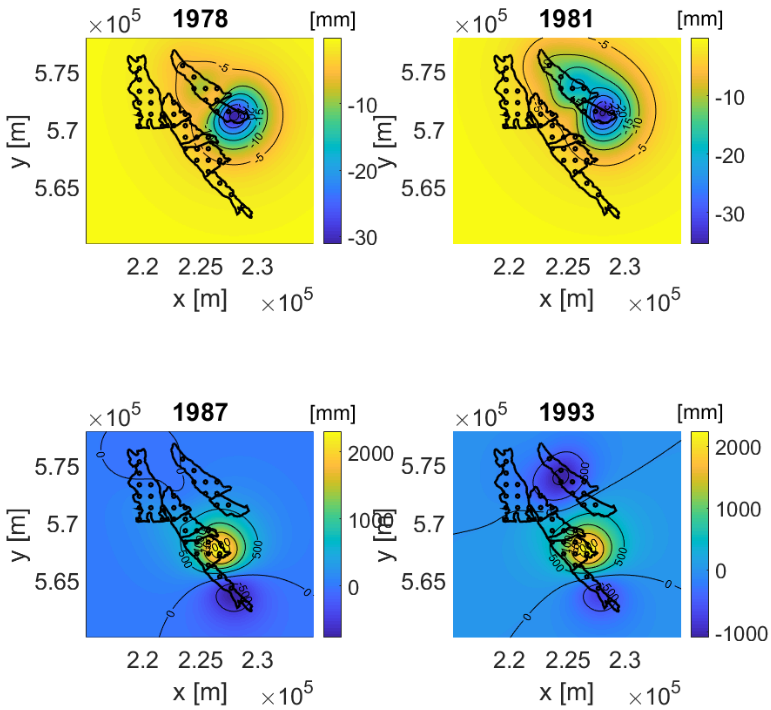

Figure 6.23: Estimated subsidence based on source strengths estimates from Figure 6.22, if the parameterization consist of a 1 km grid.

6.3.4. Discussion and conclusion

The proposed methodology was applied to a dataset that consists of measurements from five leveling campaigns in the period 1975-1993. The dataset was tested with SuRe and subsequently the observations were adjusted if necessary and the covariance model of the data was adapted, by including a term for the point noise. A regularized inversion was performed on different parameterizations, where each time the location and depth of the nuclei are considered known. The experiments lead to mixed results. On parameterization with few sources, where the distance between sources was large enough for independent contributions of u nuclei to be estimated ("the minimum lateral resolution"), the inversion led to estimates that reflect the expected behavior for the reservoir blocks that the nuclei represent. The amount of compaction grows for each time step. When considering the Roden field, it is visible that during the first three time steps maximum compaction takes place for the southern block (block 2). If this is compared with the pressure depletion graphs for the ROD-201 well that was drilled in this block, it becomes clear that pressure depletion in this block is faster than in the other block that was drilled by ROD-101 and ROD-102. In 1993, the maximum amount of compaction is at the Northern block. It is known that the southern field was producing water after 1987 and that pressure as a result increased. The source estimates for the Norg field are assumed 0 for the first two time steps since the Norg field has not been producing during these survey campaigns. In 1987, negative compaction is estimated for some reservoir blocks, but not for all. Two reasons could explain this behavior, the first one being the lateral resolution at which individual contributions of nuclei can be detected. It could be that the sources are too close to be properly detected and another form of regularization could be applied to constrain the outcome space for these sources. The second reason for the unexpected outcomes is the signal to noise ratio. In 1987, the Norg has field has only been producing a limited time with small pressure decline. It could be that the signal to noise ratio is too small to properly detect the compaction for this field.

Using other parameterizations leads to mixed outcomes. By using only 3 nuclei for the Norg field, the problem of negative compaction estimates is again visible in 1987. Using only 1 nucleus for each reservoir leads to only compaction estimates The downside of using 1 nucleus is however that only 1 reservoir compaction parameter is estimated and that the forward modeled subsidence due to 1 source can not account for the overall subsidence.

Estimating compaction for multiple nuclei in a grid formation leads to unrealistic results, with sometimes alternating high and low values. The main reason for the results is probably the lateral resolution at which individual contribution for independent nuclei can be detected. Again, feeding the problem more information, by for instance another form of regularisation, might help to constrain the outcome such that better estimates can be made.

RMSE differs for different datasets, but it is impossible to compare these figures for different parameterizations. Some parameterizations lead to a decline of the w-test and a few observations are removed. Other parameterizations lead to immediate acceptance of the w-test. Removal of more outliers generally leads to lower RMSE.

The used inversion methodology together with data testing and processing leads overall to acceptance of the overall model test. The geomechanical estimates lead to mixed results. For some parameterizations, results follow expected trends. Other parameterizations lead to positive source terms, which would indicate a pressure increase. This is not expected and is probably caused by the minimum lateral resolution at which the contribution of an independent nucleus can be detected.

7
Conclusions

This research aims to assess whether optical leveling measurements can directly be used to derive information about geomechanical subsurface processes, with a direct geomechanical inversion. This means that a direct relation was sought between optical leveling measurements and geomechanical parameters. The biggest advantage of this direct relationship would be the ability to relatively easily propagate uncertainties from the geodetic data to the geomechanical estimates. In previous research, direct relationships between geodetic data and geomechanical data have been defined, but never directly with measurements. The data in previous research is always temporal differenced, such that double-differences are formed, or even an absolute height difference, by defining a stable reference point. The downside is of this methodology is that correlation is introduced into the covariance of the data. Other previous studies define non-linear relationships between data and geomechanical estimates. The goal of this thesis is thus to assess to what extent a direct relationship between geomechanical parameter estimates and optical leveling measurements can be defined.

7.1. Conclusions

To answer the main research question of this thesis, a few subquestions were drawn up. First, the subquestions will be answered, after which the main question will be answered.

1. **What are the current methods used for geomechanical inversion?**
   First, it is important to have a clear definition of what "geomechanical inversion" means. In this thesis, a direct geomechanical inversion is defined as the process in which subsurface information is estimated with surface deformation data, by inverting a direct relation between measurements and data. Previous researches can be split up into three groups: data assimilation methods, methods that use geodetic surface deformation data as a way to validate their subsurface estimates and methods that use geodetic data as input for a direct inversion. No research is found where optical leveling measurements are directly used as input for an inversion, all researches perform a form of differencing. This can be double-differencing, where spatio-temporal differences are computed, or estimated spatial displacements at point or grid level. The disadvantage of using estimated spatial displacements is that an assumption regarding a stable reference point should be done, which could include bias. This disadvantage does not hold for double-difference data, because double-differences are relative. When double-differences or spatial displacements are estimated, correlations are included in the covariance matrix of the estimates. The disadvantage of having correlations into the covariance matrix of the data is that error propagation becomes more complex, especially when a non-linear inversion is performed on the data. Error propagation is therefore often omitted in previous work, making the quality assessment of the geomechanical estimates impossible. A positive exception is the LTS-II study, where extensive geodetic processing is applied to the data and uncertainties of the data are quantified in a complete covariance matrix.

2. **How are geomechanical parameters directly expressed in terms of geodetic leveling measurements?**
The relation between subsidence and geomechanical parameters is expressed in a geomechanical model, such as the Mogi model or Geertsma's model. These models are so-called nucleus-of-strain models. These models relate subsurface compaction to deformation at the surface. The deformation terms in these models consist of vertical displacements of points on the surface, or "temporal differences". Optical leveling measurements are "spatial differences", which means that they express a height difference between two points at a specific point in time. To relate subsurface compaction to leveling measurements, a temporal component should be introduced into the equation. This is done by not only estimating compaction terms but also initial height parameters. The introduction of these initial heights makes it possible to estimate temporal compaction parameters from spatial measurements. If these models are used for linear inversion, a-priori information should be fed to the problem, such as the location of the sources. If only the location of the sources is considered known, a lumped parameter is estimated in the inversion, which we call the "source term". In this "source term", we find a pressure term, a volume term, and several elastic rock parameters. To estimate a specific term, such as the compaction coefficient, assumptions regarding all other terms in the source term should be made.

3. **Why and how can the optical leveling measurements be geodetically tested, before being used as input for the geomechanical inversion?**
Optical leveling measurements should be tested and adjusted before they are used as input data for a geomechanical inversion, to detect outliers in the data and to account for idealization noise. Outliers can consist of observations errors, benchmark misidentification errors, benchmark disturbances, and abnormally fast benchmark displacement. Idealization noise is considered as all surface deformation signals caused by other sources than hydrocarbon production. During geodetic leveling measurement campaigns, geodetic testing on gross outliers has taken place and trajectories with obvious outliers were remeasured. Other testing than that is not yet applied to the data used for this thesis. For further geodetic testing, we used a software program called Subsidence Residual Modelling (SuRe), because this program has an extensive build-in geodetic testing procedure. Based on several input parameters, a subsidence prognosis, and raw optical leveling measurements, the program tests the measurements and estimates a subsidence model. The outcomes of the testing procedure are used for this thesis, to detect outliers and subsequently appropriately act on these outliers. Observation errors are deleted, misidentification errors are bypassed, time-series with benchmark disturbances are split and the idealization noise of benchmarks with abnormally fast displacement is increased. Another outcome of SuRe is are parameters that describe a variance model for the point noise. These parameters are used to estimate the idealization noise of each measurement, which is added to the measurement noise of the raw measurements.

4. **How could a geomechanical inversion, with correct uncertainty handling and uncertainty propagation look like?**
For this thesis, it is chosen to use the nucleus-of-strain model of Geertsma to define the relationship between geodetic measurements and geomechanical parameters. If the location of the nuclei is considered known and the principle of superposition is used, the problem becomes linear. A system of equations is set up, with a design matrix and a data vector. The data vector consists of leveling measurements. These leveling measurements are geodetic tested and, if necessary, adjusted. The covariance matrix of the data is constructed by including measurement noise and idealization noise for each measurement. This inversion problem is ill-conditioned, like many geophysical inversion problems with limited information, which means that a form of regularization should be applied. Regularization can be achieved in many ways, for this thesis we used Tikhonov regularization that penalizes spatial differences for source estimates of neighboring reservoir blocks. The amount of spatial smoothness is controlled by the regularization parameter, which is determined by a cross-validation scheme. The uncertainty of the geodetic measurements is propagated by following linear variation propagation laws.

5. **How do the proposed inversion methodology and error propagation perform on actual geodetic measurements?**
   To test the validity of the proposed methodology, a case study was defined. The Norg and Roden gas fields are located in the northern Netherlands, just south of the Groningen field. Several optical leveling campaigns were organized here while these fields were producing. The first data results from a leveling campaign from 1975 and the most recent data used stems from 1993 because one of the fields was turned into a gas storage field in 1995, to only capture subsidence in the measurements. The undeep underground surrounding these gas fields consist of mainly sandy soils, which means that a limited amount of subsidence due to undeep compaction is expected. This means that the signal-noise ratio for this field is probably relatively good. The geodetic testing procedure was applied to the data and the data was subsequently adapted. Subsequently, the actual regularized inversion was applied. The RMSE on the total dataset is 3.0 mm. The resulting compaction estimates follow the trends expected from the corresponding reservoir blocks. However, some results are not exactly what is expected. Some reservoir blocks show negative compaction, or expansion, which is not expected from these fields. This is due to the minimum lateral resolution at which the independent contribution of the neighboring section in the reservoir can be estimated, which is about the burial depth of the reservoir. For the Norg and Roden fields, this is approximately 2800m. This means that sources should be placed with a spacing of least 2800m, which is not the case when placing sources in all reservoir blocks. The overall conclusion after the experiments is that the proposed inversion is likely improved when more information is added to the inversion.

6. **What are the limitations of a regularised direct linear geomechanical inversion?**
   The main limitation of the proposed inversion methodology is that a lumped parameter term is estimated, the “source term”. This term includes pressure, volume, and elastic rock property parameters and without additional information, it is not possible to differentiate between these different terms.
   When using a regularisation for an inversion, extra information is added to the problem. This means that regularised inversion will result in biased estimates of parameters. The estimates will vary with the choice of cross-validation scheme, regularization matrix, and regularization matrix. The choice for certain epochs or survey campaigns used for the inversion is important too. If little subsidence has taken place during between survey campaigns, the signal-noise ratio will be low, due to measurement errors or idealization noise (subsidence caused by other processes than reservoir compaction.
   The proposed methodology assumes a linear relationship between compaction estimates and observational data. This means that a linear inversion can be applied and linear variance propagation. If a more complex model like a finite element model is used, this kind of inversion and error propagation does not work.

These subquestions lead to the main question:

To what extent can results from optical leveling campaigns be used as input for a direct inversion to estimate a simplified set of geomechanical parameters?

To answer this question, a methodology is proposed that uses optical leveling measurements as input data and estimates geomechanical compaction parameters, by defining a direct relationship between leveling measurements and a simplified set of geomechanical parameters. The main advantage of this methodology is that the uncertainties that are tied to optical leveling measurements can be relatively easily propagated into the geomechanical parameter estimates. The biggest limitation is that only a lumped parameter can be estimated, which consists of volume, pressure and rock elastic properties. If one would want to know one specific parameter, such as the compaction coefficient, assumptions regarding all other parameters should be made. Another limitation is that regularization should be imposed to solve the inversion. Regularization imposes extra information on the problem and will inevitably result in biased parameter estimates. The parameter estimates will vary depending on the form of regularization imposed.

7.2. Recommendations

The following topics have been identified for further research:

- Feed the inversion more information, such as reservoir pressure models or compaction models. This might relax the need for regularization and thus lead to better geomechanical estimates. More information could also lead to the differentiation of parameters in the lumped source term.
- Implement the methodology on data from other reservoirs, to assess whether the methodology is applicable for other case studies.
- Find ways of implementing a geodetic test procedure iteratively in the inversion methodology. Within this research, geodetic testing is applied once before the inversion, but including testing in the workflow might improve consistency.
- Implement more complex reservoir models that describe the subsidence signal more realistic. The Geertsma model used for this thesis is a relatively simple geomechanical model and will within the limitations of a linear inversion never be able to describe the subsidence signal perfectly. A more complex geomechanical model might be able to describe the signal closer to reality and give more insight into the subsurface.
- Further investigate the effects of regularization, the effect of the choice of CV scheme, the design of the regularisation matrix and the regularization parameter. More regularization could be added, for example by restricting the compaction estimates to be only positive, such that no volume expansion is allowed. Also, a penalty on temporal smoothness could be added, if pressure decline is smooth over a reservoir. Adding more information on the reservoir characteristics and pressure declines could constrain the outcome space and lead to better estimates.
- Modify the workflow such that observational data can also be used as input for non-linear inversions, as used by for example finite-element methods.
- Use other kinds of geodetic observation data as input for the inversion, such as InSAR or GPS data. This data has other characteristics than optical leveling data, so parts of the methodology should be adapted. The geodetic testing procedure should be adjusted to InSAR and/or GPS data and the inversion design. For the uniformization of different kinds of geodetic data, we refer to van Leijen et al. [72].

Bibliography

[1] J.E. Alberda and J.B. Ebbinge. *Inleiding Landmeetkunde*. Delft University Press, 7th edition, 2003.

[2] E.M. Anderson. The Dynamics of the Formation of Cone-sheets, Ring-dykes, and Caldron-subsidences. *Proceedings of the Royal Society of Edinburgh*, 56:128–163, 1936.

[3] R.C. Aster, B. Borchers, and C.H. Thurber. *Parameter estimation and inverse problems*. Elsevier, third edition, 2018.

[4] D. Baù, M. Ferronato, G. Gambolati, P. Teatini, and A. Alzraiee. Ensemble smoothing of land subsidence measurements for reservoir geomechanical characterization. *International Journal for Numerical and Analytical Methods in Geomechanics*, 39:207–228, 2015.

[5] J. Besag, J. York, and A. Mollie. Bayesian image restoration, with two applications in spatial statistics. *Annals of the Institute of Statistical Mathematics*, 43:1–20, March 1991.

[6] S.M. Bierman, F. Kraaijeveld, and S.J. Bourne. Regularised direct inversion to compaction in the Groningen reservoir using measurements from optical leveling campaigns. Technical Report SR.15.11194, NAM, 2015.

[7] M.A. Biot. General Theory of Three-Dimensional Consolidation. *Journal of Applied Physics*, 12: 155–164, 1941.

[8] M.A. Biot. Mechanics of Deformation and Acoustic Propagation in Porous Media. *Journal of Applied Physics*, 33:1482–1498, 1962.

[9] K. Bisdom, M. Cid Alfaro, K. Hindriks, and A. Kudarova, editors. *Robust non-linear inversion for reservoir deformation from surface displacement data*, 2018. 80th EAGE Conference and Exhibition.

[10] L. Chang and R.F. Hanssen. Detection of cavity migration and sinkhole risk using radar interferometric time series. *Remote Sensing of Environment*, 147:56–64, 2014.

[11] H.M de Heus, P. Joosten, M.H.F. Martens, and H.M.E. Verhoef. Geodetische deformatie analyse: 1D-deformatieanalyse uit waterpasnetwerken. LGR-Series 5, Delft Geodetic Computing Centre, 1994.

[12] K.P. de Kloe, A.J. van der Linden, and J.W. Dudley. Cyclic Compaction Experiments on Samples from Norg-5. Technical Report EP 2008-5189, Shell International Exploration and Production B.V., 2008.

[13] E. Detournay and A.H.D. Cheng. Fundamentals of poroelasticity. In C. Fairhust, editor, *Comprehensive Rock Engineering: Principles, Practice and Projects, Vol. II, Analysis and Design Method*, chapter 5, pages 113–171. Pergamon Press, 1993.

[14] D. Dzurisin and M. Lisowski. *Volcano Deformation*. Springer, Berlin, Heidelberg, 2007.

[15] E. Fjaer, R.M. Holt, P. Horsrud, A.M. Raaen, and P. Risnes. *Petroleum Related Rock Mechanics*. Developments in Petroleum Science. Elsevier, 2nd edition, 2008.

[16] P.A. Fokker and B. Orlic. Semi-analytic modeling of subsidence. *Math Geol*, 38:565–589, 2006.

[17] P.A. Fokker and K. van Thienen-Visser. Inversion of double-difference measurements from optical levelling for the Groningen gas field. In *Proc. IAHS*, volume 372, pages 375–378, 2015.

[18] P.A. Fokker, F.J. van Leijen, B. Orlic, H. van der Marel, and R.F. Hanssen. Subsidence in the Dutch Wadden Sea. *Netherlands Journal of Geosciences - Geologie en Mijnbouw*, 97-3:129–181, 2018.

[19] H.W. Frikken. Wrench tectonic signatures: prediction of open fracture systems and prospectivity in the Zechstein gas reservoirs, NE Netherlands. *Geologie en mijnbouw/Netherlands Journal of Geosciences*, 76-3, 1997.

[20] B. Gambolati. Numerical models in land subsidence control. *Computer Methods in Applied Mechanics and Engineering*, 5:227–237, March 1975.

[21] J. Geertsma. Land subsidence above compacting oil and gas reservoirs. *Journal of Petroleum Technology*, 25:734–744, 1973.

[22] J. Geertsma. A basic theory of subsidence due to reservoir compaction: the homogeneous case. *Transactions of Royal Dutch Society of Geologists and Mining Engineers*, 28:43–62, 1973.

[23] J. Geertsma and G. van Opstal. A Numerical Technique for Predicting Subsidence Above Compacting Reservoirs, Based on the Nucleus of Strain Concept. *Verh. Kon. Ned. Geol. Mijnbouwk. Gen.*, 28:63–78, 1973.

[24] G.H. Golub and C.F van Loan. *Matrix Computations*. John Hopkins University Press, 4th edition, 2012.

[25] G.H. Golub, M. Heath, and G. Wahba. Generalized Cross-Validation as a Method for Choosing a Good Ridge Parameter. *Technometrics*, 21-2:215–223, 1979.

[26] P.C. Hansen. *Rank-Deficient and Discrete Ill-Posed Problems: Numerical Aspects of Linear Inversion*. Society for Industrial and Applied Mathematics, 1998.

[27] P.C. Hansen. The L-Curve and Its Use in the Numerical Treatment of Inverse Problems. In P.R. Johnstonn, editor, *Computational Inverse Problems in Electrocardiology*, pages 119–142. WIT Press, 2001.

[28] P.C. Hansen. Regularization Tools: A Matlab Package for Analysis and Solution of Discrete Ill-Posed Problems. Technical Report 4.1, Informatics and Mathematical Modelling, Technical University of Denmark, March 2008.

[29] R.F. Hanssen, R. Kremers, and H. van der Marel. Bodembeweging langs de kust: 'Wat kun je meten?'. In F. Barends, D. Dillingh, R.F. Hanssen, and K. van Onselen, editors, *Bodemdaling langs de Nederlandse kust; Case Hondsbossche en Pettemer zeewering*. IOS Press (Amsterdam), 2008.

[30] R.F. Hanssen, F.J. van Leijen, G.J. van Zwieten, S. Dortland, C.N. Bremmer, and M. Kleuskens. Validation of PSI results of Alkmaar and Amsterdam withing the Terrafirma Validation Project. In *Proc. of FRINGE 2007 Workshop, Frascati, Italy, 26-30 November 2007*, ESA SP-649, February 2008.

[31] A.P.E.M. Houtenbos. *Subsidence Residual Modelling*. A.P.E.M. Houtenbos Geodetic Consultancy, De Esstukken 18, 9751 HB Haren, 1st edition, February 2007.

[32] R. E. Kalman. A New Approach to Linear Filtering and Prediction Problems. *ASME – Journal of Basic Engineering*, 82:35–45, 1960.

[33] H. Kooi, P. Johnston, K. Lambeck, C. Smither, and R. Molendijk. Geological causes of recent (~100 yr) vertical land movement in the Netherlands. *Tectonophysics*, 299:297–316, 1998.

[34] K. Koutroumbas and S. Theodoridis. *Pattern Recognition*. Academic Press, 4th edition, 2008.

[35] K. Lambeck and J. Chappell. Sea Level Change Through the Last Glacial Cycle. *Science*, 292: 679–686, April 2001.

[36] J.G. Leusink. Wat waterpasgegevens vertellen over geologische bodembeweging. Master thesis, Delft University of Technology, 2003.

[37] V.M.R. Maury, J.R. Grasso, and G. Wittlinger. Monitoring of subsidence and induced seismiticity in the Lacq Gas Field (France): the consequences on gas production and field operation. *Engineering Geology*, 32:123–135, 1992.

[38] W. Menke. *Geophysical data analysis: discrete inverse theory*, volume 45 of *International Geophysics Series*. Academic Press, Revised edition, 1989.

[39] R.D. Mindlin. Force at a point in the interior of a semi-infinite solid. *Physics*, 7:195–202, 1936.

[40] R.D. Mindlin and D.H Cheng. Nuclei of Strain in the Semi-Infinite Solid. *Journal of Applied Physics*, 21:926–930, 1950.

[41] K. Mogi. Relations between eruptions of various vulcanoes and the deformations of the ground surface around them. *Bulletin of the Earthquake Research Institute*, 36:99–134, 1958.

[42] A.G. Muntendam-Bos, I.C. Kroon, and P.A. Fokker. Time-dependent Inversion of Surface Subsidence due to Dynamic Reservoir Compaction. *Math Geosci*, 40:159–177, 2008.

[43] A.C.G. Nagelhout and J.P.A. Roest. Geomechanical modelling of the Norg gasfield. Technical Report TA/IG/97.51, TU Delft, 1997.

[44] NAM. Norg UGS fault reactivitation study and implications for seismic threat, October 2016.

[45] NAM. Technical addendum to the Winningsplan Groningen. Production, subsidence, induced earthquakes and seismic hazard and risk assessment in the Groningen Field., 2016.

[46] NAM. Ensemble Based Subsidence application to the Ameland gas field – long term subsidence study part two (LTS-II) continued study, October 2017.

[47] NAM. Bodemdaling noord-nl, December 2019. URL `https://www.nam.nl/feiten-en-cijfers/bodemdaling.html#iframe=L2VtYmVkL2NvbXBvbmVudC8_aWQ9Ym9kZW1kYWxpbmc`.

[48] NAM. Gasopslag locaties, September 2019. URL `https://www.nam.nl/gas-en-oliewinning/ondergrondse-gasopslag/gasopslag-locaties.html#iframe=L21hcHMvb25kZXJncm9uZHNlLWdhc29wc2xhZy1rYWFydC8`.

[49] NCG. Actuele Bodemdalingskaart Nederland, March 2020. URL `https://bodemdalingskaart.nl/`.

[50] NLOG. Map of boreholes, September 2019. URL `https://www.nlog.nl/en/map-boreholes`.

[51] NLOG. Interactive map, December 2019. URL `https://www.nlog.nl/kaart-boringen`.

[52] NOAA. What is subsidence?, February 2020. URL `https://oceanservice.noaa.gov/facts/subsidence.html`.

[53] PDOK. PDOK - AHN3 downloads, March 2020. URL `https://www.pdok.nl/introductie/-/article/actueel-hoogtebestand-nederland-ahn3-`.

[54] J.P. Pruiksma, J.N. Breunese, K. van Thienen-Visser, and H. De Waal. Isotach formulation of the rate type compaction model for sandstone. *International Journal of Rock Mechanics and Mining Sciences*, 78:127–132, 2015.

[55] R.C.H. Quadvlieg. Bodembeweging nabij Roden en Norg. NAM rapport 200111001160, NAM, 2001.

[56] L. Ryan, K. Mengersen, G. Morgan, A. Earnest, R. Summerhayes, and J. Beard. Evaluating the effect of neighbourhood weight matrices on smoothing properties of Conditional Autoregressive (CAR) models. *International Journal of Health Geographics*, 6, 2007.

[57] S. Samiei-Esfehany and H. Bähr. Research and Development Project for Geodetic Deformation Monitoring. Contribution to the research project: “Long-term study on the anomalous time-dependent subsidence in the Wadden Sea Region”. NAM rapport EP201505216980, Delft University of Technology and Nederlandse Aardolie Maatschappij B.V., 2015.

[58] S. Samiei-Esfehany and H. Bähr. Erratum to the report: ”Research and Development project for Geodetic Deformation Monitoring” – Revision of recommendations from the project: “Long-term study on anomalous time-dependent subsidence in the Wadden sea region”. NAM rapport EP201701215912, Delft University of Technology and Nederlandse Aardolie Maatschappij B.V., 2017.

[59] Schlumberger. Oilfield glossary: geomechanics, 2019. URL `https://www.nam.nl/gas-en-oliewinning/ondergrondse-gasopslag/gasopslag-locaties.html#iframe=L21hcHMvb25kZXJncm9uZHNlLWdhc29wc2xhZy1rYWFydC8`.

[60] M.C. Schomaker and R.M. Berry. *Geodetic Leveling Manual*. National Oceanic and and Atmospheric Administration (NOAA), 1981.

[61] P. Segall, J.R. Grass, and A. Mossop. Poroelastic stressing and induced seismicity near the Lacq gas field, southwestern France. *Journal of Geophysical Research: Solid Earth*, 99:15,423–15,438, 1994.

[62] A. Tarantola. *Inverse Problem Theory: Methods for Data Fitting and Model Parameter Estimation*. Elsevier, first edition, 1987.

[63] P. Teatini, G. Gambolati, M. Ferronato, A. Settari, and D. Walters. Land uplift due to subsurface fluid injection. *Journal of Geodynamics*, 51:1–16, January 2011.

[64] K. Terzaghi. Die berechnung der durchlassigkeitzifer des tones aus dem verlauf der hydrodynamischen spannungserscheinungen. *Mathematish-naturwissenschaftliche, Klasse. Akademie der Wissenschaften,s*, pages 125–138, 1923.

[65] P.J.G. Teunissen. *Testing theory: An Introduction*. Delft University Press, 1st edition, 2000.

[66] P.J.G. Teunissen. *Reader Probability and Observation Theory*. TU Delft, December 2009.

[67] A.N. Tikhonov. Solution of incorrectly formulated problems and the regularization method. *Soviet Mathematics*, 4:1035–1038, 1963. English translation.

[68] W. Torge and J. Müller. *Geodesy*. De Gruyter, 4th edition, 2012.

[69] S. van Asselen, G. Erkens, E. Stoughamer, H.A.G. Woolderink, R.E.E. Geeraert, and M.M. Hefting. The relative contribution of peat-compaction and oxidation to subsidence in built-up areas in the Rhine-Meuse delta, the Netherlands. *Science of the Total Environment*, 636:177–191, 2018.

[70] R.M.H.E. van Eijs and O. van der Wal. Field-wide reservoir compressibility estimation through inversion of subsidence data above the Groningen gas field. *Netherlands Journal of Geosciences*, 96-5:s117–s129, 2017.

[71] P.J. van Leeuwen, H. R. Künsch, L. Nerger, R. Potthast, and S. Reich. Particle filters for high□dimensional geoscience applications: A review. *Quaterly Journal of the Royal Meteorological Society*, 145:2335–2365, 2019.

[72] F. van Leijen, S. Samiei-Esfahany, H. van der Marel, and R.F. Hanssen. Uniformization of Geodetic data for deformation analysis – Contribution to the research project: Second phase of the long-term subsidence study in the Wadden Sea Region (LTS2). Technical report, Delft University of Technology, 2017.

[73] H. van Oeveren, P. Valvatne, L. Geurtsen, and J. van Elk. History match of the Groningen field dynamic reservoir model to subsidence data and conventional subsurface data. *Netherlands Journal of Geosciences*, 96-5:s47–s54, 2017.

[74] G.H.C. van Opstal. The effect of base-rock rigidity on subsidence due to reservoir compaction. In *Proceedings of 3rd Congress of International Society for Rock Mechanics, Denver, CO, USA*, volume 2, pages 1102–1111, 1974.

[75] K. van Thienen-Visser and P.A. Fokker. The future of subsidence modelling: compaction ans subsidence due to gas depletion of the Groningen gas field in the Netherlands. *Netherlands Journal of Geosciences - Geologie en Mijnbouw*, 96-5:105–116, 2017.

[76] V.B.H.Ketelaar. *Satellite Radar Interferometry: Subsidence Monitoring Techniques*. Springer, 2009.

[77] S. Vetra-Carvalho, P.J. van Leeuwen, L. Nerger, A. Barth, U. Altaf, P. Brasseur, P. Kirchgessner, and J-M. Beckers. State-of-the-art stochastic data assimilation methods for high-dimensional non-Gaussian problems. *Tellus A: Dynamic Meteorology and Oceanography*, 70:1–43, 2018.

[78] H. Wang. *Theory of Linear Poroelasticity*. Princeton University Press, 2000.

[79] WUR. Grondsoortenkaart, December 2019. URL `https://www.wur.nl/nl/show/Grondsoortenkaart.htm`.

[80] Z. Zhang and J. C. Moore. *Mathematical and Physical Fundamentals of Climate Change*. Elsevier, 2005.

[81] M.S. Zhdanov. *Geophysical Inverse Theory and Regularization Problems*. Elsevier, 2002.

[82] M.D. Zoback. *Reservoir Geomechanics*. Cambridge University Press, 2007.

A

Top Rotliegend maps of reservoirs

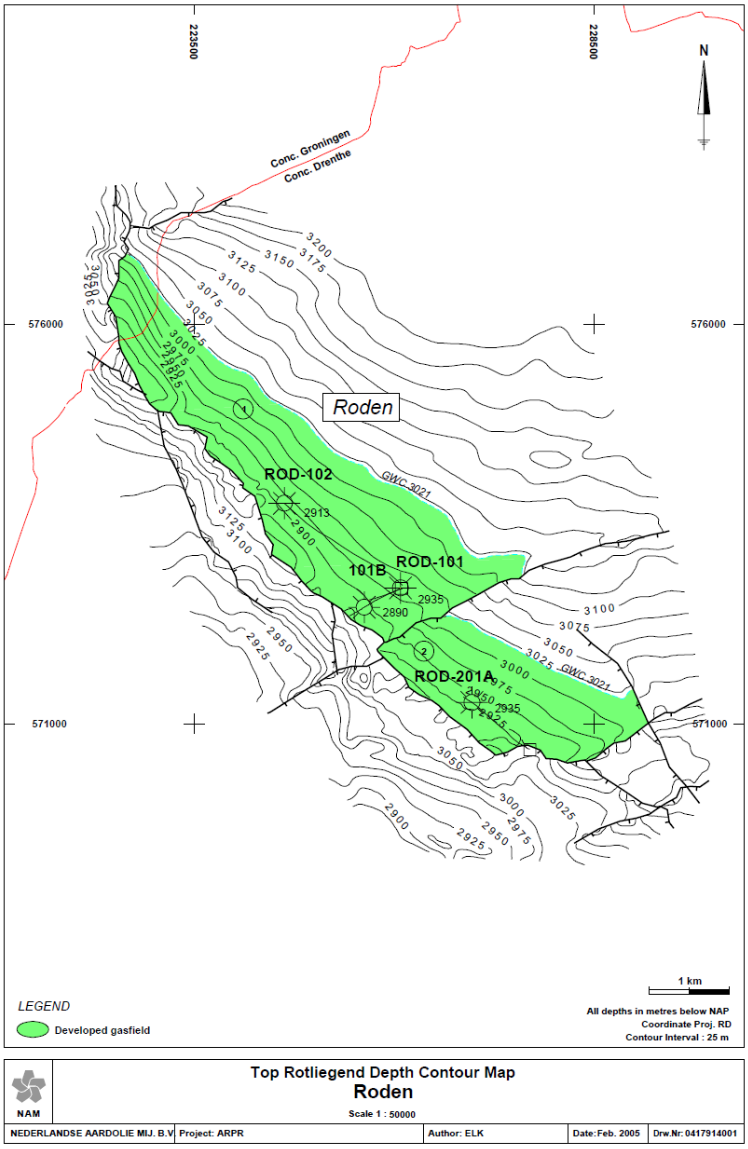

Figure A.1: Roden top Rotliegend depth contour map with faults and well locations (from NLOG [51]).

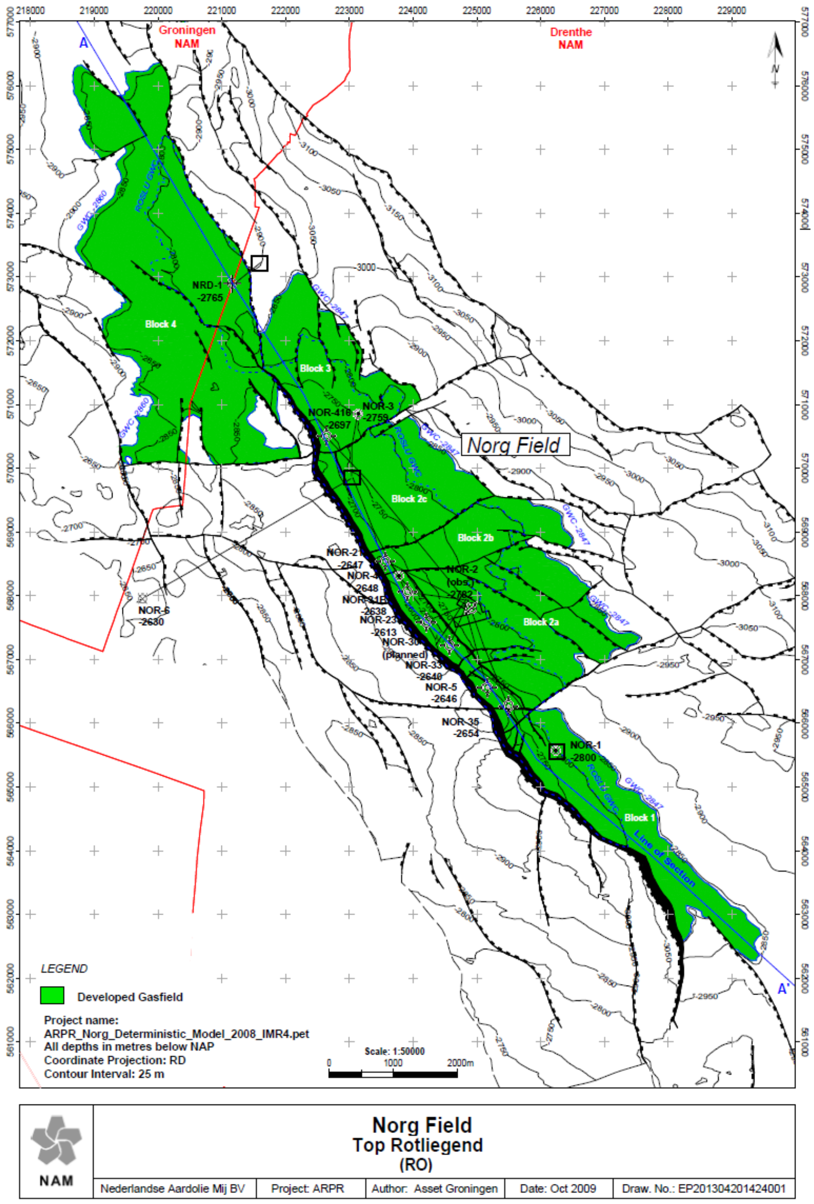

Figure A.2: Norg top Rotliegend depth contour map with faults and well locations (from NLOG [51]).

B

Surveyed levelling networks

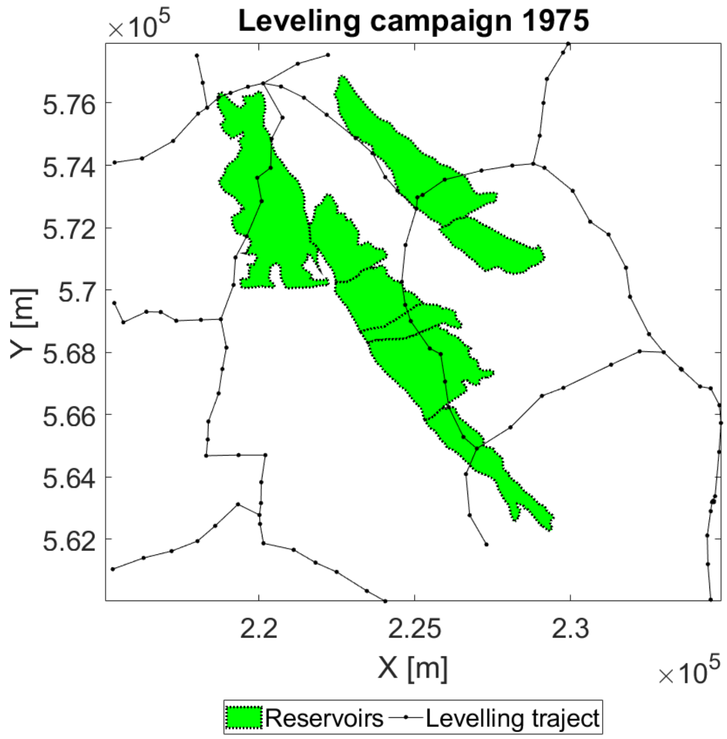

Figure B.1: Levelling network at the Norg and Roden field, as surveyed in 1975.

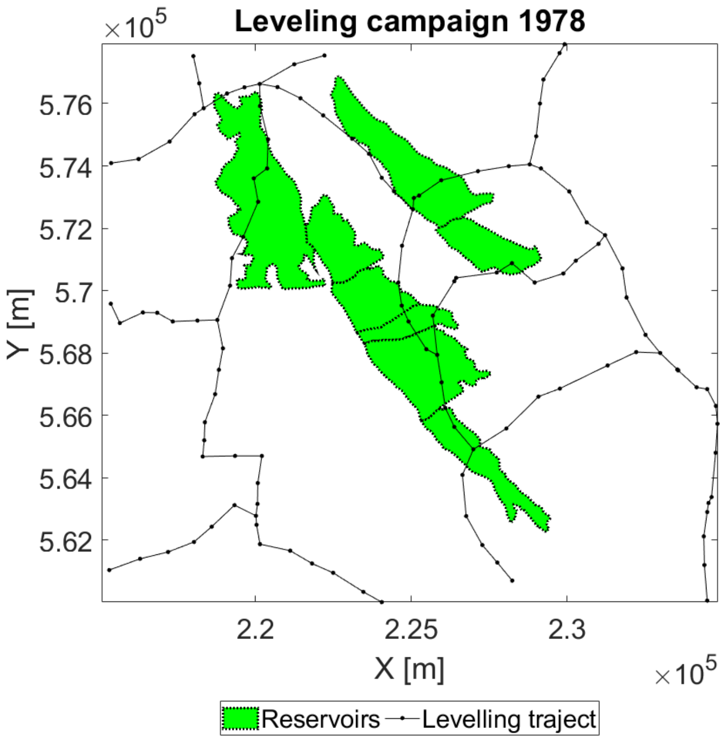

Figure B.2: Levelling network at the Norg and Roden field, as surveyed in 1978.

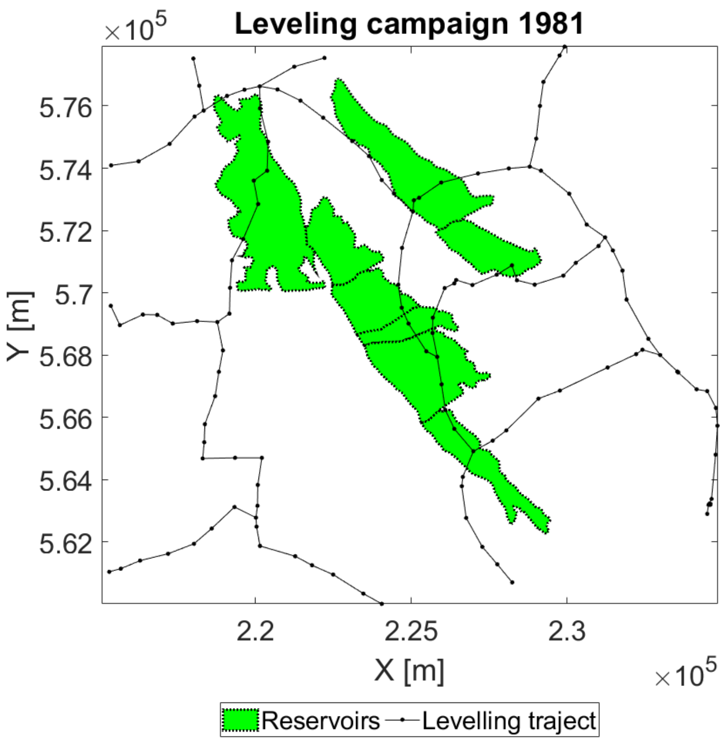

Figure B.3: Levelling network at the Norg and Roden field, as surveyed in 1981.

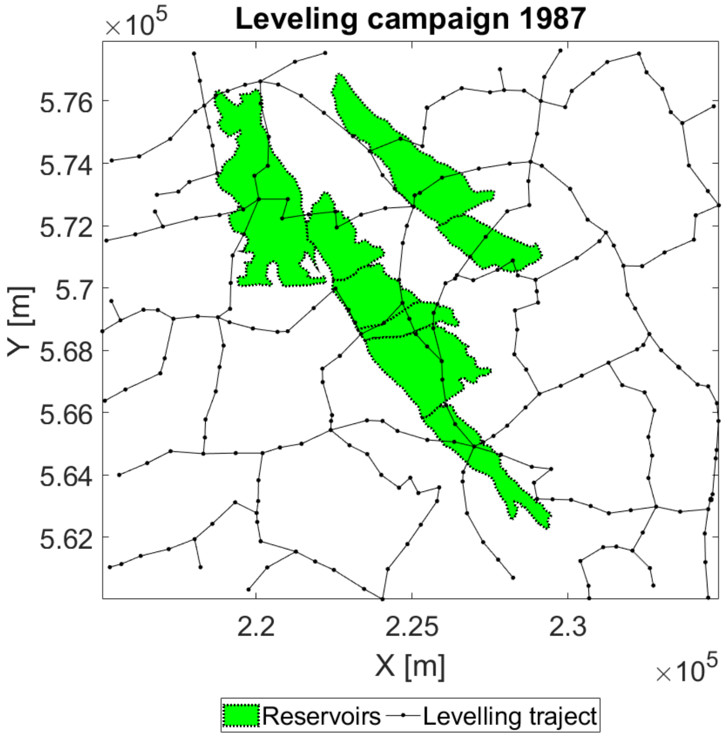

Figure B.4: Levelling network at the Norg and Roden field, as surveyed in 1987.

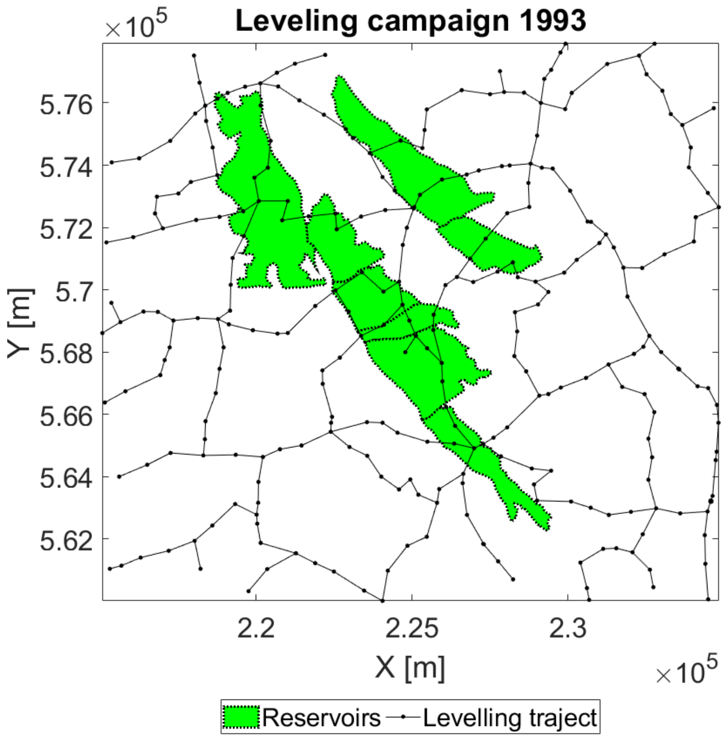

Figure B.5: Levelling network at the Norg and Roden field, as surveyed in 1993.